ORNL
MASTER COPY

JAN 21 1994

NUREG/CR-6117
ORNL/TM-12484

Neutron Spectra at Different High Flux Isotope Reactor (HFIR) Pressure Vessel Surveillance Locations

Prepared by
I. Remec, F. B. Kam

Oak Ridge National Laboratory

Prepared for
U.S. Nuclear Regulatory Commission

AVAILABILITY NOTICE

Availability of Reference Materials Cited in NRC Publications

Most documents cited in NRC publications will be available from one of the following sources:

1. The NRC Public Document Room, 2120 L Street, NW, Lower Level, Washington, DC 20555-0001

2. The Superintendent of Documents, U.S. Government Printing Office, Mail Stop SSOP, Washington, DC 20402-9328

3. The National Technical Information Service, Springfield, VA 22161

Although the listing that follows represents the majority of documents cited in NRC publications, it is not intended to be exhaustive.

Referenced documents available for inspection and copying for a fee from the NRC Public Document Room include NRC correspondence and internal NRC memoranda; NRC Office of Inspection and Enforcement bulletins, circulars, information notices, inspection and investigation notices; Licensee Event Reports; vendor reports and correspondence; Commission papers; and applicant and licensee documents and correspondence.

The following documents in the NUREG series are available for purchase from the GPO Sales Program: formal NRC staff and contractor reports, NRC-sponsored conference proceedings, and NRC booklets and brochures. Also available are Regulatory Guides, NRC regulations in the *Code of Federal Regulations,* and *Nuclear Regulatory Commission Issuances.*

Documents available from the National Technical Information Service include NUREG series reports and technical reports prepared by other federal agencies and reports prepared by the Atomic Energy Commission, forerunner agency to the Nuclear Regulatory Commission.

Documents available from public and special technical libraries include all open literature items, such as books, journal and periodical articles, and transactions. *Federal Register* notices, federal and state legislation, and congressional reports can usually be obtained from these libraries.

Documents such as theses, dissertations, foreign reports and translations, and non-NRC conference proceedings are available for purchase from the organization sponsoring the publication cited.

Single copies of NRC draft reports are available free, to the extent of supply, upon written request to the Office of Information Resources Management, Distribution Section, U.S. Nuclear Regulatory Commission, Washington, DC 20555-0001.

Copies of industry codes and standards used in a substantive manner in the NRC regulatory process are maintained at the NRC Library, 7920 Norfolk Avenue, Bethesda, Maryland, and are available there for reference use by the public. Codes and standards are usually copyrighted and may be purchased from the originating organization or, if they are American National Standards, from the American National Standards Institute, 1430 Broadway, New York, NY 10018.

DISCLAIMER NOTICE

This report was prepared as an account of work sponsored by an agency of the United States Government. Neither the United States Government nor any agency thereof, or any of their employees, makes any warranty, expressed or implied, or assumes any legal liability of responsibility for any third party's use, or the results of such use, of any information, apparatus, product or process disclosed in this report, or represents that its use by such third party would not infringe privately owned rights.

NUREG/CR-6117
ORNL/TM-12484
RF, R5, 9L

Neutron Spectra at Different High Flux Isotope Reactor (HFIR) Pressure Vessel Surveillance Locations

Manuscript Completed: November 1993
Date Published: December 1993

Prepared by
I. Remec,* F. B. Kam

Oak Ridge National Laboratory
Managed by Martin Marietta Energy Systems, Inc.

Oak Ridge National Laboratory
Oak Ridge, TN 37831-6285

Prepared for
Division of Safety Issue Resolution
Office of Nuclear Regulatory Research
U.S. Nuclear Regulatory Commission
Washington, DC 20555-0001
NRC FIN L2552
Under Contract No. DE-AC05-84OR21400

*Josef Sefan Institute, Ljubljana, Slovenia

ABSTRACT

This project addresses the potential problem of radiation embrittlement of reactor pressure vessel (RPV) supports. Surveillance specimens irradiated at the High Flux Isotope Reactor (HFIR) at relatively low neutron flux levels (about 1.5E+8 $cm^{-2}. s^{-1}$) and low temperature (about 50°C) showed embrittlement more rapidly than expected[1]. Commercial power reactors have similar flux levels and temperatures at the vessel support structures. The purposes of this work are to provide the neutron fluence spectra data that are needed to evaluate previously measured mechanical property changes in the HFIR, to explain the discrepancies in neutron flux levels between the nickel dosimeters and two other dosimeters, neptunium and beryllium, and to address any questions or peculiarities of the HFIR reactor environment.

The current work consists of neutron and gamma transport calculations, dosimetry measurements, and least-squares logarithmic adjustment to obtain the best estimates for the neutron spectra and the related neutron exposure parameters. The results indicate that the fission rates in neptunium-237 (Np-237) and uranium-238 (U-238) and the helium production rates in beryllium-9 (Be-9) are dominated by photo-induced reactions. The displacements per atom rate for iron (dpa/s) from gamma rays is five times higher than the dpa/s from neutrons. The neutron fluxes in key 7, position 5 do not show any significant gradient in the surveillance capsule, but key 4 and key 2 showed differences in magnitude as well as in the shape of the spectrum. The stainless steel monitor in the V-notch of the Charpy specimens of the surveillance capsules is adequate to determine the neutron flux above 1.0 MeV at the desired V-notch location. Simultaneous adjustment of neutron and gamma fluxes with the measurements has been demonstrated and should avoid future problems with photo-induced reactions.

CONTENTS

	Page
ABSTRACT	iii
LIST OF FIGURES	vii
LIST OF TABLES	viii
EXECUTIVE SUMMARY	ix
ACKNOWLEDGMENTS	xi
ABBREVIATIONS	xiii
1. INTRODUCTION	1
2. EXPERIMENTAL PROGRAM	2
2.1 Experimental Locations	2
2.2 Dosimetry Capsules	2
2.3 Radiometric Measurements	2
3. METHODOLOGY	4
3.1 Background	4
3.2 Gamma-Induced Reactions	6
3.3 Photon-Induced Reaction-Rate Correction Factor	10
3.4 Adjustment Options	12
3.5 Adjustment Procedure	12
4. RESULTS AND DISCUSSION	16
5. CONCLUSIONS AND RECOMMENDATIONS	28
6. REFERENCES	29
APPENDIX A. LETTER REPORT ON NIST SUPPORT	31
APPENDIX B. HELIUM ANALYSES OF BERYLLIUM HAFMs FROM HFIR: DOS-2/3	41
APPENDIX C. RESULTS FOR SOLID STATE TRACK RECORDERS	49
APPENDIX D. NEUTRON TRANSPORT CALCULATIONS FOR HFIR	69
APPENDIX E. RESULTS FOR KEY 7, POSITION 5	77
APPENDIX F. RESULTS FOR KEY 2, POSITION 9	87

CONTENTS
(continued)

APPENDIX G. RESULTS FOR KEY 4, POSITION 2 97

APPENDIX H. RESULTS FOR KEY 4, POSITION 10 107

APPENDIX I. SCHEMATIC OF DOSIMETRY CAPSULE WITH SLOT LOCATIONS 117

LIST OF FIGURES

Page

1. Horizontal cross section through the HFIR at the core midplane, showing locations of the surveillance keys and the DOS 1 experiment 3

2. Calculated (1D) distribution of Np(n,f) and Np(gamma,f) reaction rates 7

3. Calculated (1D) distribution of fast (E > 1 MeV) neutron flux 8

4. Calculated (1D) distribution of absorbed gamma dose rate in Si 9

5. Calculated and adjusted neutron spectrum, key 7, position 5, J 23

6. Calculated and adjusted neutron spectrum, key 2, position 9, J 24

7. Calculated and adjusted neutron spectrum, key 4, position 2, J 25

8. Calculated and adjusted neutron spectrum, key 4, position 10, J 26

E.1 Calculated and adjusted neutron spectrum, key 7, position 5, D 85

E.2 Calculated and adjusted neutron spectrum, key 7, position 5, A 86

F.1 Calculated and adjusted neutron spectrum, Key 2, position 9, D 94

F.2 Calculated and adjusted neutron spectrum, key 2, position 9, A 95

G.1 Calculated and adjusted neutron spectrum, key 4, position 2, D 104

G.2 Calculated and adjusted neutron spectrum, key 4, position 2, A 105

H.1 Calculated and adjusted neutron spectrum, key 4, position 10, D 114

H.2 Calculated and adjusted neutron spectrum, key 4, position 10, A 115

I.1 Schematic of dosimetry capsule with slot locations 119

LIST OF TABLES

		Page
1.	Comparison of measured and calculated reaction rates for fission and Be monitors	5
2.	Comparison of measured and corrected reaction rates of fission and Be monitors with calculations	11
3.	Comparison of different adjustment runs, key 7, position 5	17
4.	Comparison of simultaneous neutron and gamma adjustment to neutron adjustment run, key 7, position 5	19
5.	Irradiation parameters at the centers of capsules	21
6.	Adjusted neutron fluxes at the centers of the examined capsules	22
E.1	Calculated and adjusted irradiation parameters, key 7, position 5	80
E.2	Measured reaction rates, C/M, and A/M ratios, key 7, position 5	82
E.3	Calculated and adjusted neutron group fluxes, key 7, position 5, slot J	84
F.1	Calculated and adjusted irradiation parameters, key 2, position 9	89
F.2	Measured reaction rates, C/M, and A/M ratios, key 2, position 9	91
F.3	Calculated and adjusted neutron group fluxes, key 2, position 9	93
G.1	Calculated and adjusted irradiation parameters, key 4, position 2	99
G.2	Measured reaction rates, C/M, and A/M ratios, key 4, position 2	101
G.3	Calculated and adjusted neutron group fluxes, key 4, position 2, slot J	103
H.1	Calculated and adjusted irradiation parameters, key 4, position 10	109
H.2	Measured reaction rates, C/M, and A/M ratios, key 4, position 10	111
H.3	Calculated and adjusted neutron group fluxes, key 4, position 10, slot J	113

EXECUTIVE SUMMARY

This project addresses the potential problem of radiation embrittlement of reactor pressure vessel (RPV) supports. Surveillance specimens irradiated at the High Flux Isotope Reactor (HFIR) at relatively low neutron flux levels (about 1.5E+8 $cm^{-2}. s^{-1}$) and low temperature (about 50°C) showed embrittlement more rapidly than expected.[1] Commercial power reactors have similar flux levels and temperatures at the vessel support structures. The purposes of this work are to provide the neutron fluence spectra data that are needed to evaluate previously measured mechanical property changes in the HFIR, to explain the discrepancies in neutron flux levels between the nickel dosimeters and two other dosimeters, neptunium and beryllium, and to address any questions or peculiarities of the HFIR reactor environment.

The scope of this project consists of neutron and gamma transport calculations, dosimetry measurements, and least-squares logarithmic adjustment of the transport calculations and dosimetry measurements to obtain the best estimates for the neutron spectra. The neutron calculations were performed using the three-dimensional (3-D) transport code, TORT[2], and a one-dimensional (1-D) transport code, XSDRN[3], to obtain coupled neutron and gamma calculations. The neutron spectral adjustments were performed using the code LSL-M2[4]. The dosimetry measurements followed ASTM standards[5]. The measurements are traceable to fluence standards provided by NIST [Appendix A]. The gamma dosimeters, which were irradiated in the HFIR, were furnished and counted by NIST. The gamma measurements were performed to verify that the gamma field as obtained from 1-D neutron and gamma transport calculations, was adequate to determine the gamma contribution to the fast fission and the beryllium radiometric monitors.

This report will show the following major findings:

1. the discrepancies for the fast flux for energies above 1.0 MeV in key 7, position 5 of HFIR Dosimetry Experiment 1 (DOS1) are the results of photofission and photoneutron reactions in the neptunium and beryllium monitors respectively;

2. the photo-induced reactions dominate the value for the total reaction rates in the beryllium and fast threshold fission dosimeters in the HFIR capsule environment. This finding makes the use of these dosimeters good candidates as gamma dosimeters in certain radiation fields;

3. the fluxes at key 7, position 5 do not show any significant gradient in the surveillance capsule. However, key 4 and key 2 show large fast and thermal flux gradients in the capsule;

4. the stainless steel monitor located in the V-notch of the Charpy specimens of the surveillance capsule is adequate to determine the neutron flux above 1.0 MeV at the V-notch;

5. the total gamma dpa is about five times higher than the dpa from neutrons in key 7, position 5; and

6. the feasibility of the application of simultaneous adjustment of neutron and gamma fluxes performed in the analysis has been demonstrated. Even though this finding does not affect the current results, the methodology would be extremely useful in future work.

If gamma displacements can be shown to cause mechanical property changes, the HFIR specimens should be re-evaluated using the total dpa from neutron and gammas as the exposure parameter. Additional gamma measurements to verify the gamma contribution may be necessary at the surveillance keys. It is also recommended that a more sophisticated coupled neutron-gamma calculation should be performed (preferably 3-D) that takes into account neutrons arriving at the Charpy specimens from the photoneutron reaction in the beryllium reflector. These neutrons from the beryllium reflector may account for the approximately 30% scale factor in the adjustment runs.

ACKNOWLEDGMENTS

The authors wish to express their appreciation to the following consultants for their contribution to the planning, design, and review of the various tasks on this program: L. R. Greenwood of Battelle Pacific Northwest Laboratories, J. G. Williams of the University of Arizona, E. D. McGarry and Jim Grundl of the National Institute of Standards and Technology (NIST). L. R. Greenwood, Frank Ruddy of Westinghouse, and Brian Oliver of Rockwell International were very cooperative in providing dosimeters for the irradiations on relatively short notice. The solid state track recorders and helium accumulation fluence monitors were analyzed by Frank Ruddy and Brian Oliver respectively. E. D. McGarry provided the neutron fluence standards, and Bill McLaughlin provided the gamma dosimeters to provide a check of the gamma calculations. The comments of L. R. Greenwood, E. D. McGarry, and J. G. Williams are appreciated.

The valuable contributions from Ken Farrell, Greg Hirtz, Randy Hobbs, and Dennis Heatherly of the Oak Ridge National Laboratory (ORNL) have been responsible for keeping the fabrication, assembly, disassembly, and irradiations of the experiments on schedule. Thanks to Frank Dyer and David Glasgow of the Analytical Chemistry Division for counting all the radiometric dosimeters, and J. V. Pace of the Engineering Physics and Mathematics Division for performing all the transport calculations. The authors wish to give special thanks to Pat Hileman for the efficient preparation of this report and for making the numerous revisions that were requested. Thanks also to Cathy Shappert for providing the editorial review.

Finally, the authors gratefully acknowledge the programmatic support and encouragement of R. E. Johnson of the Nuclear Regulatory Commission (NRC). Comments and advice from Al Taboada, T. J. Walker, and Craig Hrabal, consultants from NRC, are appreciated.

ABBREVIATIONS

HAFM	Helium Accumulation Fluence Monitor
SSTR	Solid State Track Recorders
RM	Radiometric Monitors
ASTM	American Society for Testing and Materials
HFIR	High Flux Isotope Reactor
NIST	National Institute of Standards and Technology
BPNL	Battelle Pacific Northwest Laboratory
ORNL	Oak Ridge National Laboratory
DOS1-75	First HFIR dosimetry experiment in key 7, position 5
DOS2-75	Second HFIR dosimetry experiment in key 7, position 5
DOS2-29	Second HFIR dosimetry experiment in key 2, position 9
DOS2-42	Second HFIR dosimetry experiment in key 4, position 2
DOS2-410	Second HFIR dosimetry experiment in key 4, position 10
DOS3-75	Third HFIR dosimetry experiment in key 7, position 5
DOS3-29	Third HFIR dosimetry experiment in key 2, position 9
DOS3-42	Third HFIR dosimetry experiment in key 4, position 2
DOS3-410	Third HFIR dosimetry experiment in key 4, position 10
DOS4-75	Fourth HFIR dosimetry experiment in key 7, position 5
DOS4-G	Gamma measurements in the fourth HFIR dosimetry experiment in key 7, position 5
F>1.0 MeV	Neutron flux with energies greater than 1.0 MeV
F>0.1 MeV	Neutron flux with energies greater than 0.1 MeV
F<0.4 eV	Neutron flux with energies less than 0.4 eV
dpa	Displacements per atom for iron
dpa/s	Displacements per atom per second for iron
dpa (ASTM)	Displacements per atom, calculated with ASTM displacement cross section for iron
G-dpa	Displacements per atom induced by gamma rays, calculated using Baumann's[12] cross sections
G-flux	Total gamma rays flux
Be-9	Beryllium with atomic weight of 9
Be (n,x) He	The sum of the three reactions: Be-9 (n,a) He-6 --> Li-6; Be-9 (n,2n) Be-8 (2a); and Be-9 (n,d) Li-8 --> Be-8 (2a)
Slot ET*	Slot E, gradient wire at the top of the capsule
Slot EM*	Slot E, gradient wire at the middle of the capsule
Slot EB*	Slot E, gradient wire at the bottom of the capsule
M	Measured reaction rate in reactions per second per atom
C/M	Calculated-to-measured reaction rate ratios
A/M	The ratio of adjusted-to-measured reaction rates
M/C	Measured-to-calculated reaction rate ratios

*The location of all slots are shown in Fig. I.1 and T, M, B refers to top, middle, and bottom respectively.

1 INTRODUCTION

Surveillance specimens irradiated at the HFIR at relatively low neutron flux levels and low temperatures exhibited embrittlement more rapidly than expected. Commercial nuclear power reactors have similar neutron flux levels and temperatures at the vessel support structures. This study at the HFIR:

1. finds the cause(s) for the discrepancies which were found in DOS1* neutron flux levels inferred from the nickel dosimeter and from two other dosimeters, neptunium and beryllium; and

2. determines the neutron flux spectra data to evaluate the previously measured mechanical property changes in HFIR surveillance specimens.

The results of the proposed work are needed for the resolution of Generic Safety Issue 15 (GSI-15) which addresses the potential problem of radiation embrittlement of commercial reactor vessel supports.

This report discusses a three-step fluence spectrum determination analysis procedure[6] that addresses:

1. transport calculations to compute the flux spectra at Charpy specimens,

2. dosimetry measurements to determine reaction rates at the specimens, and

3. consolidation of measurements and calculations to reduce the uncertainties of the neutron exposure parameters using a spectrum adjustment technique.

---

*K. Farrell et al., "The DOS1 Neutron Dosimetry Experiment at the HB-4-A Key 7 Surveillance Site on the HFIR Pressure Vessel," ORNL/TM-12511, (to be published).

2 EXPERIMENTAL PROGRAM

2.1 Experimental Locations

The surveillance locations chosen for the DOS2, DOS3, and DOS4 experiments were key 7, position 5, key 2, position 9, and key 4, positions 2 and 10 (Fig. 1). All locations were chosen so that the ongoing HFIR surveillance program would not be compromised.

2.2 Dosimetry Capsules

The dosimetry capsules are intended to reproduce the physical conditions of the standard surveillance capsules. Hence, the flux dosimeters were placed in standard cans furnished from the inventory of the surveillance program. Further details of this container are available in its quality assurance documents recorded in File JOB 5-1-143 in the Research Reactors Division (RRD) Document Control Center. These dosimetry cans were notched and engraved with characters to distinguish them from the surveillance packages. All fabrication, assembly and disassembly procedures are maintained in the RRD Document Control Center.

The three ferritic steel Charpy specimens in each surveillance capsules are simulated by carbon steel blocks to hold the dosimeters. A complete description of DOS2, DOS3, and DOS4 experiments and measured results were sent to the NRC project manager and to all consultants in the program.

2.3 Radiometric Measurements

Except for the HAFMs and the SSTRs, the neutron radiometric dosimeters were analyzed at ORNL. Prior to the counting, neutron fluence standards for the iron and nickel sensors were used so that the results would be traceable back to NIST. Two neptunium monitors were also verified with NIST. Several spectrometers were utilized for the counting. Periodic quality control checks are made (daily, when making measurements) to verify that the efficiencies of the particular counting geometry are correct and that all components of the spectrometry system are functioning properly. Calibrations are performed with weighted portions of a solution of mixed radionuclides, designated QCY.48, which is produced and sold every six months by Amersham International, plc. The daily control checks are made with a Co-60 source that was purchased from Amersham and is traceable to NIST. The measured activity of this source is allowed to differ from the specified value by no more than 5%. If the observed difference exceeds this value, measurements must cease until the error is corrected. Calibrations of the energy scale of the spectrometer systems are made with a sample of U-232 that emits gamma rays with energies in the range 238 and 2614 keV. A presentation and passouts of the counting methods were presented to NRC staff and independent consultants on the project at the March 4, 1993 meeting.

The HAFMs were analyzed by B. Oliver of Rockwell International [Appendix B] and the SSTRs by F. Ruddy of Westinghouse Electric Company [Appendix C]. The results from the SSTR fission monitors were in agreement with the radiometric fission monitors except for the U-235 SSTR at key 7, position 5. Several adjustment runs were performed to investigate the influence of the radiometric U-235 monitor and the SSTR U-235 monitor. The runs indicated that the radiometric dosimeter gave results that agreed with the middle segment of the gradient cobalt dosimeters.

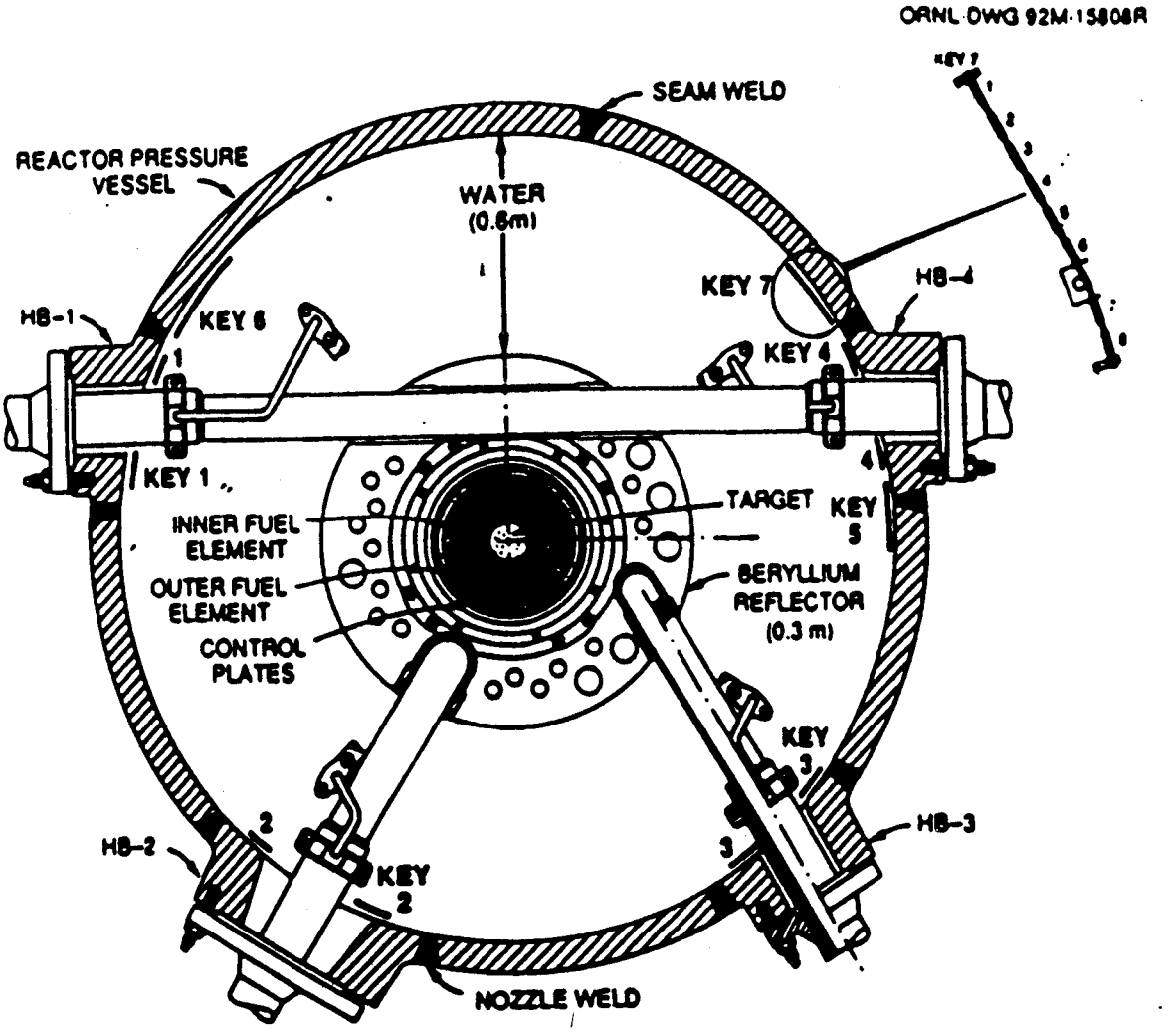

Fig. 1 Horizontal cross section through the HFIR at the core midplane, showing locations of the surveillance keys

3 METHODOLOGY

3.1 Background

To determine the neutron spectra at the HFIR surveillance positions, the three-step analysis procedure that combines transport calculations of the neutron and gamma field and measurements using radiometric monitors is used to obtain the best estimates for the neutron spectra and the related irradiation parameter rates. The experimental program is described in Section 2, and the transport calculations are presented in Appendix D.

This methodology is typically applied whenever accurate and reliable neutron irradiation parameters are needed (e.g., in the experiments that study changes in material properties caused by the neutron irradiation or in power reactor surveillance capsule analysis).

Applying this procedure to the HFIR surveillance capsules created a temporarily unexplained outcome: the DOS1 experiment showed that the fast-neutron flux (E >1 MeV) values as derived from the measured activity of Np and Be monitors were respectively approximately 17 times and 15 times higher than the flux value derived from the Ni monitors. Careful checking of the measurements ruled out experimental error. In order to help find the solution to this situation additional dosimetry experiments were initiated.

The DOS2 and DOS3 experiments provided comprehensive dosimetry results for key 7 position 5, key 2 position 9, and key 4 positions 2 and 10. In addition to the Ni, threshold activation monitors Al, Ti, Cu, and Fe and thermal monitors Sc, Co and Au were used. In the DOS2 experiment the dosimeters were used "bare," while in the DOS3 experiment, a 4-mil gadolinium cover was used in order to attenuate the thermal neutron flux and to prevent interference with the monitors responses. In the DOS3 experiment the fission monitors U-235, U-238 and Np-237 were used as radiometric monitors and independently verified with solid-state track recorders of the same fission isotopes. Also, the beryllium HAFMs were used in the DOS2 experiment, and in one location of DOS3.

The analysis of the DOS2 and DOS3 measurements showed again that the measured reaction rates for the Np-237 and Be monitors, as well as for the U-238 monitors were inconsistent with the reaction rates observed for other fast neutron monitors. The ratios of measured-to-calculated neutron reaction rates for these monitors were much larger than for the other monitors used as shown in Table 1. The measurements at key 7 position 5 were particularly suitable for analyzing these discrepancies because measured activities showed no significant gradients inside the capsule. For this reason it was decided to analyze data from that position first.

It is well known that fission monitors are sensitive not only to the neutrons but also to photofission reactions. Measured specific activities contain the contributions from both gamma- and neutron-induced fissions. A similar outcome appears for the Be monitor. The helium generated in Be occurs from both neutron-induced reactions and photon-induced reactions.

Since the measured responses for U-238, Np-237 and Be-9 monitors were much larger than the reaction rates obtained by folding the calculated neutron spectrum with neutron cross sections, the attention was focused on the possible contributions from the photon-induced reactions for these detectors.

Table 1 Comparison of measured and calculated reaction rates for fission and Be monitors

	Measured*	Calculated**	M/C***	M/C for Ni monitor
KEY 7.5				
Be (n,x) He				
DOS1	1.46E-15	7.60E-17	19.2	1.35 TOP
DOS2	1.44E-15	7.60E-17	18.9	1.42 BOT.
DOS2	1.42E-15	7.60E-17	18.7	
DOS3	1.46E-15	7.60E-17	19.3	
U-238 (n,f)	1.60E-15	6.24E-17	25.6	
Np-237 (n,f)	4.59E-15	2.25E-16	20.4	
U-238 (n,f) SSTR	1.36E-15	6.24E-17	21.8	
Np-237 (n,f) SSTR	4.75E-15	2.25E-16	21.1	
U-235 (n,f)	7.75E-15	8.13E-15	1.0	
U-235 (n,f) SSTR	1.50E-14	8.13E-15	1.8	
KEY 2.9				
Be (n,x) He	1.82E-15	2.84E-16	6.4	1.47 TOP
Be (n,x) He	2.19E-15	2.84E-16	7.7	2.90 BOT.
U-238 (n,f)	2.74E-15	2.69E-16	10.2	
Np-237 (n,f)	9.57E-15	1.15E-15	8.4	
U-238 (n,f) SSTR	2.01E-15	2.69E-16	7.5	
Np-237 (n,f) SSTR	8.62E-15	1.15E-15	7.5	
U-235 (n,f)	2.85E-13	2.05E-13	1.4	
KEY 4.2				
Be (n,x) He	1.38E-15	1.12E-16	12.3	0.91 TOP
U-238 (n,f)	1.48E-15	1.11E-16	13.3	1.60 BOT.
N-237 (n,f)	6.84E-15	5.41E-16	12.6	
U-238 (n,f) SSTR	1.65E-15	1.11E-16	14.9	
Np-237 (n,f) SSTR	6.08E-15	5.41E-16	11.2	
U-235 (n,f)	5.46E-13	3.48E-13	1.6	
U-235 (n,f) STR	5.97E-13	3.48E-13	1.7	
KEY 4.10				
Be (n,x) He	7.96E-16	2.08E-16	3.8	0.69 TOP
U-238 (n,f)	1.62E-15	1.90E-16	8.5	1.37 BOT.
Np-237 (n,f)	6.52E-15	8.51E-16	7.7	
U-238 (n,f) SSTR	1.29E-15	1.90E-16	6.8	
Np-237 (n,f) SSTR	5.66E-15	8.51E-16	6.7	
U-235 (n,f)	5.45E-13	3.89E-13	1.4	
U-235 (n,f) SSTR	6.98E-13	3.89E-13	1.8	

*Reaction rate per atom per second, including neutron and gamma reactions
**Reaction rate per atom per second, for neutron reactions only
***Measured-to-calculated reaction rate ratio

3.2 Gamma-Induced Reactions

An estimation of the gamma field was obtained from a 1-D coupled neutron-gamma calculation using the computer code XSDRN.

In the 1-D cylindrical, axially symmetric geometry many simplifications were made to model the actual geometry of the HFIR reactor. In particular the experimental beam tubes and other structures between cylindrical beryllium reflector and the reactor vessel were omitted. Therefore, one does not expect that the absolute values for neutron and gamma fluxes obtained from 1-D calculation will agree well with 3-D calculations or the measurements.

Variation of neutron-and gamma-induced reaction rates as a function of the distance from the core vertical axis, as obtained from the 1-D calculation, is illustrated on Fig. 2 for the Np monitor. The neutron-induced fissions dominate strongly inside the core and beryllium reflector. However, in the water, neutron flux attenuates much faster than gamma flux, so that at about 20 cm from the beryllium reflector the gamma-induced and neutron-induced fission rates are equal. After 20 cm, the fissions from gammas become increasingly dominant over fissions from neutrons. Similar behavior was found for the U-238 and Be monitors also.

At the position of the capsule, the gamma-induced reaction rates for Np-237, U-238 and Be from the 1-D calculations were larger by factors of 51, 52 and 61 than the corresponding neutron-induced reaction rates. However, at the location of the capsule, the fast-neutron flux from 1-D calculation was almost an order of magnitude lower than the fast flux from 3-D calculation, for key 7, position 5. A possible explanation, accounting for part of this discrepancy, is that in the 1-D calculation there was just water between the beryllium reflector and the capsule location, while in the HFIR, there is a tangential experimental beam tube between the reflector and key 7, position 5. This beam tube was modeled in the 3-D calculations, and is filled with air so that the resulting neutron flux attenuation is significantly lower than in the 1-D water geometry. This necessitated evaluating the 1-D results at a location closer to the core. A new location (radius) was selected so that the fast neutron flux from 1-D calculation at this radius is equal to the fast flux from 3-D calculation at the capsule location. The fast flux from the 3-D calculations at the capsule location was, for key 7 position 5, 1.17E+8 neutrons $cm^{-2}. s^{-1}$, while in 1-D calculation the fast flux of 1.16E+8 neutrons $cm^{-2}. s^{-1}$ was found at 100.06 cm from the core vertical axis (Fig. 3).

This selection was supported at a later date by the DOS4-G experiment, which provided the measurement of the absorbed gamma dose rate in silicon. The measured value was 36.4 Gy/s. The dose rate, obtained from calculated gamma fluxes at the above described location gave the value of 36.6 Gy/s (Fig. 4).

Also, the comparison of 1-D calculated neutron spectra showed only minor differences between the capsule location and the new location. The same result holds for the gamma spectrum. Therefore, it seems reasonable to calculate the gamma-to-neutron reaction rate ratios at the above mentioned location and use the corrections for the Np-237, U-238, U-235 and Be monitors in the capsule.

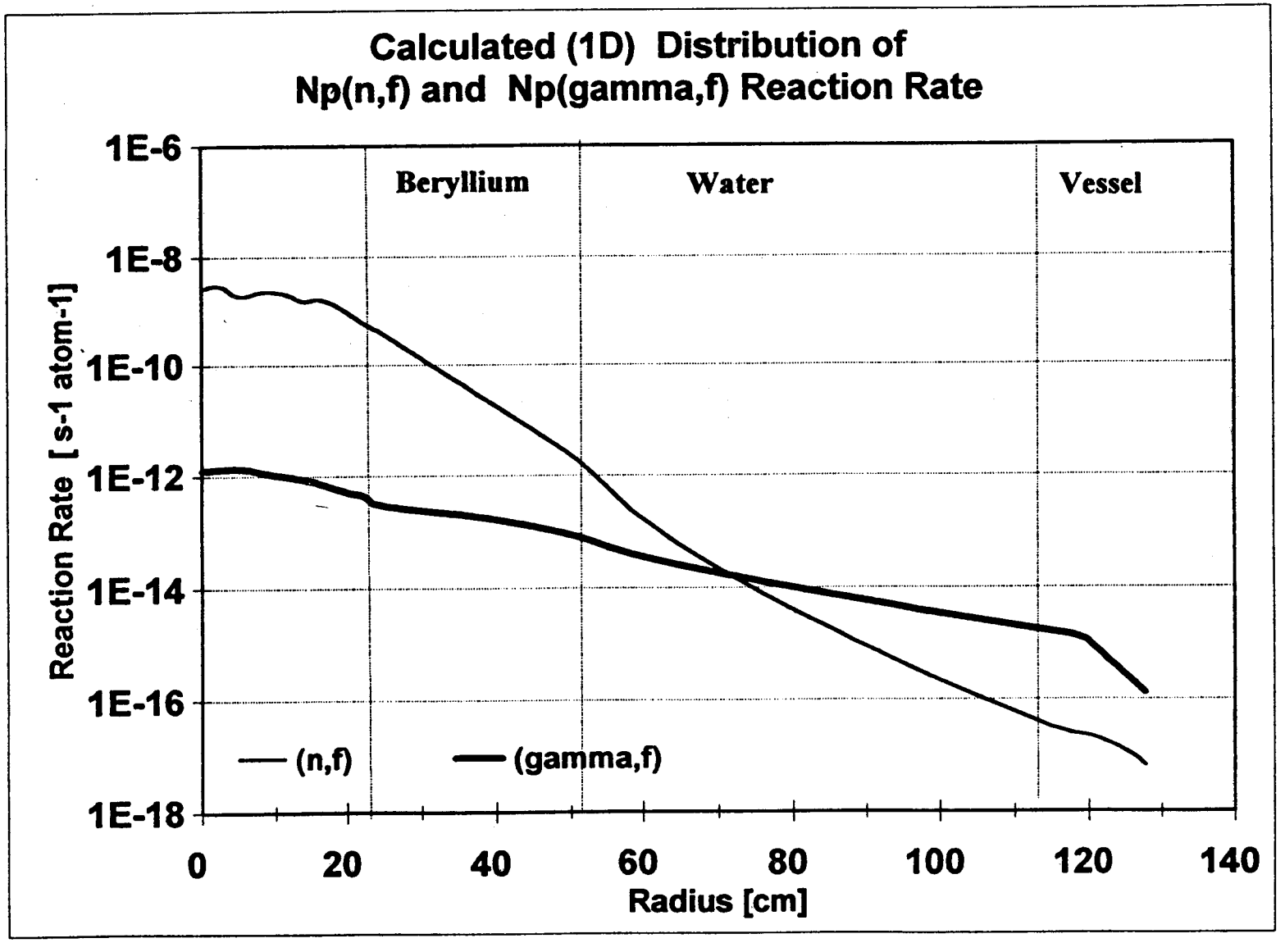

Fig. 2 Calculated (1-D) distribution of Np(n,f) and Np(gamma,f) reaction rate

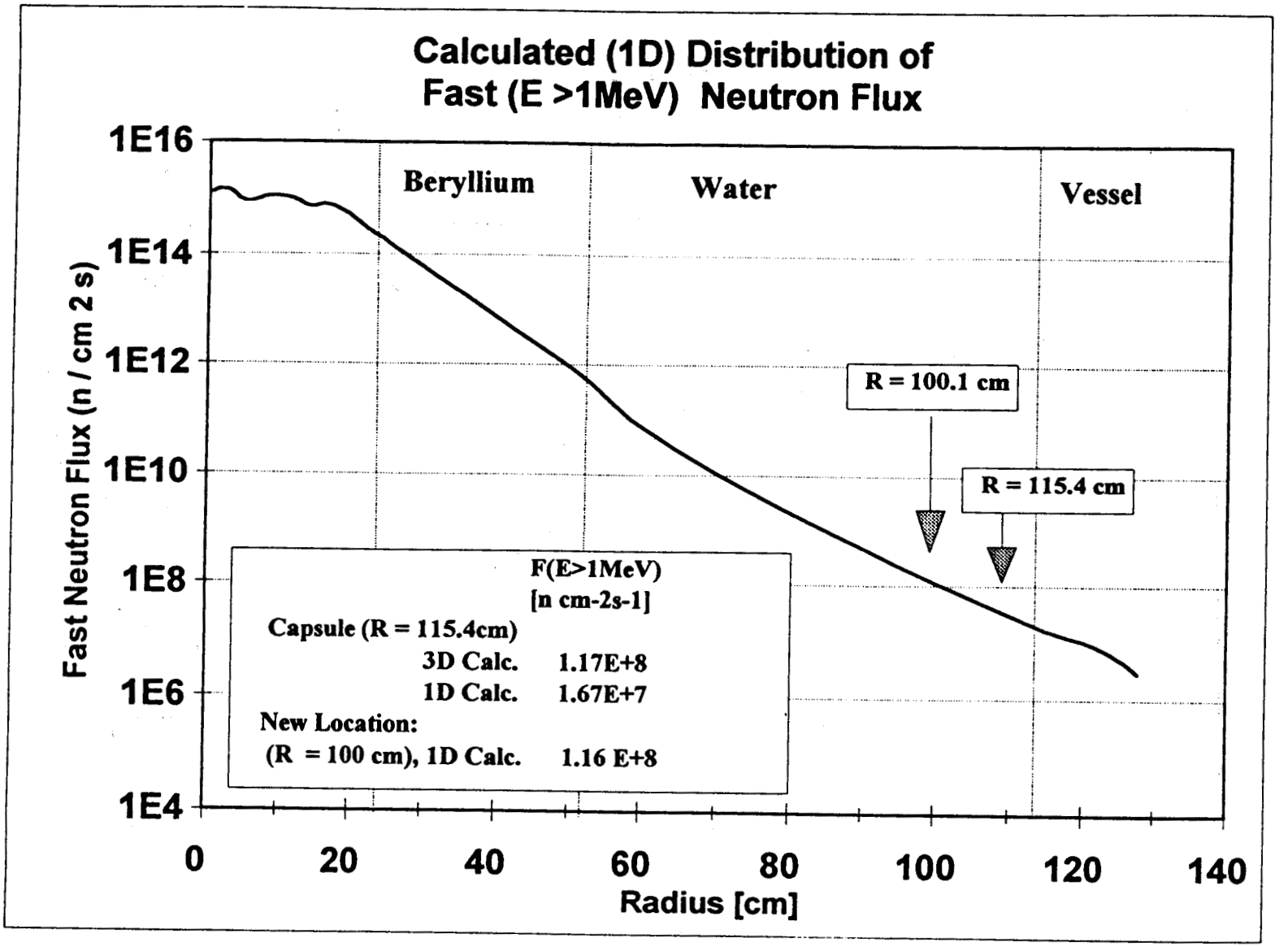

Fig. 3 Calculated (1-D) distribution of fast (E > 1 MeV) neutron flux

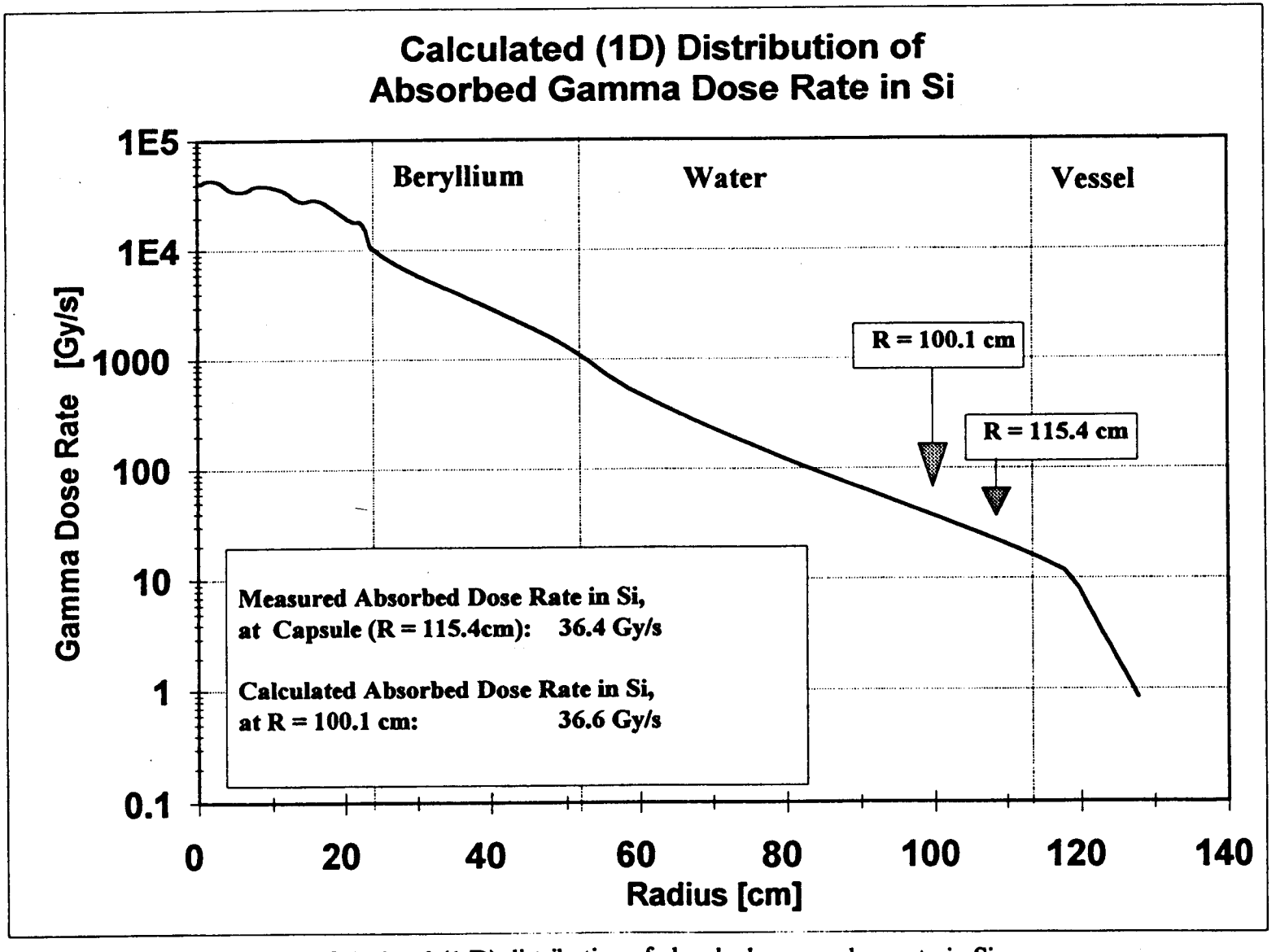

Fig. 4 Calculated (1-D) distribution of absorbed gamma dose rate in Si

3.3 Photon-Induced Reaction Rate Correction Factor

The correction factor CF, is defined as follows:

$$CF = \frac{R^n}{R^n + R^\gamma}$$

where

R^γ = calculated reaction rate induced by gamma flux:

$$R^\gamma = \sum_{g=1}^{NOGG} \sigma_g^\gamma \phi_g^\gamma$$

R^n = calculated reaction rate induced by neutron flux:

$$R^n = \sum_{g=1}^{NONG} \sigma_g^n \phi_g^n$$

ϕ_g^n = calculated (1-D) neutron flux in group g,

ϕ_g^γ = calculated (1-D) gamma flux in group g,

σ_g^n = neutron cross section in group g,

σ_g^γ = gamma cross sections in group g,

NONG = number of neutron groups in 1-D calculation,

NOGG = number of gamma groups in 1-D calculation.

These correction factors for Np-237, U-238, Be-9, and U-235 are listed in Table 2. The neutron-induced reaction rates represent only 4.5%, 5.5%, 6.1% of the total reaction rate for the Be-9, U-238, and Np-237 monitors respectively. For these three monitors, one concludes that the gamma-induced reactions account for most of their responses. The "corrected" measurements bring the values for the U-238 and the Np-237 in agreement with the other dosimeters, while the Be-9 monitor appears to be over corrected. The U-235 monitor is much less affected because the neutron fission cross section is much larger than the photo fission cross section.

Table 2 Comparison of measured and corrected reaction rates of fission and Be monitors with calculations

(Corrections are for the contribution of gammas induced reactions.)

	Measured*	Calculated*	M/C**	Correction Factor	Corrected M/C**	M/C for Ni monitor
KEY 7.5						
Be (n,x) He						
DOS1	1.46E-15	7.60E-17	19.2	4.535E-02	0.9	1.35 TOP
DOS2	1.44E-15	7.60E-17	18.9	4.535E-02	0.9	1.42 BOT.
DOS2	1.42E-15	7.60E-17	18.7	4.535E-02	0.8	
DOS3	1.46E-15	7.60E-17	19.3	4.535E-02	0.9	
U-238 (n,f)	1.60E-15	6.24E-17	25.6	5.512E-02	1.4	
Np-237 (n,f)	4.59E-15	2.25E-16	20.4	6.141E-02	1.3	
U-238 (n,f) SSTR	1.36E-15	6.24E-17	21.8	5.512E-02	1.2	
Np-237 (n,f) SSTR	4.75E-15	2.25E-16	21.1	6.141E-02	1.3	
U-235 (n,f)	7.75E-15	8.13E-15	1.0	8.222E-01	0.8	
U-235 (n,f) SSTR	1.50E-14	8.13E-15	1.8	8.222E-01	1.5	

*Reactions per second per atom
**Measured-to-calculated reaction rate ratio

3.4 Adjustment Options

With the knowledge that the U-238, Np-237, and Be-9 monitors detect mostly gammas in the HFIR surveillance locations investigated, the three possible paths for the adjustment of the calculated neutron spectrum are

A. to perform the adjustment with all dosimeters including those that require corrections;
B. to perform the adjustment with all dosimeters except the dosimeters that require gamma corrections; and
C. to perform the simultaneous adjustment of the neutron and gamma spectra using all detectors.

Approach A has the disadvantage that large corrections are applied to the Np-237, U-238, and the Be-9 monitors. Such large corrections to a few monitors may distort the results, but the consistency of the corrected reaction rates with the other dosimeters can be shown through the adjustment procedure.

Approach B applies the adjustment procedure to all the measurements and rejects any measurement that is inconsistent. In this study, the adjustment procedure rejected the uncorrected Np-237, U-238, and the Be-9 measurements. The disadvantage of this approach is that the cause for the rejection is not explained.

Approach C represents major modification and improvement to the current adjustment methodology. The equation used to calculate the neutron-induced reaction rates is exactly the same as the equation to calculate the photo-induced reaction rates. By adding the gamma spectrum and cross sections to the neutron set, the two can be adjusted simultaneously. This approach has several advantages; no corrections for gamma contribution to the measured reaction rates are necessary, gamma measurements can be added to the other neutron measurements, and gamma and neutron irradiation parameters are determined (e.g., neutron and gamma dpa/s). The disadvantages are more input data, namely calculated gamma spectrum and cross sections for gamma reactions. Also, some assumptions need to be made regarding the gamma spectrum covariance matrix.

3.5 Adjustment Procedure

The adjustment code LSL-M2 was used for all of the adjustment runs. In runs where only the neutron spectra were adjusted, ten different locations inside a capsule were considered. Four of these locations correspond to the slot D, slot J, slot B, and slot A. The Ni and Co gradient wires on the same side of the capsule (i.e., E and G on one side, and F and H on the other side) were grouped together. A schematic of the dosimetry capsule with slot locations is shown in Appendix I, Fig. I.1. On each side three locations were considered: the top, middle and bottom portions of the wires. This makes additional six locations, treated in the adjustment procedure.

Three-dimensional transport calculations provided multigroup neutron fluxes at 1 point per capsule; thus the same calculated spectrum was input in the adjustment code for all ten locations in each capsule. Measurements in all the capsules except the key 7, position 5 showed big variations in reaction rates from top to bottom of the capsules, indicating severe neutron

gradients. For this reason and to avoid large adjustments of the neutron spectra at certain locations, the adjustment runs employed the scaling option which splits the total spectrum adjustment in two parts: one is scaling of the magnitude of the calculated spectrum and the other is the "true" adjustment, or in other words actual modification of the calculated spectrum through the adjustment procedure. Accordingly, in the tables of the calculated and adjusted values given in Appendices E-H, the scale factors and adjustment factors are listed. Their products give the total adjustment factors, which equal the ratios of adjusted to calculated values of the exposure parameters.

The spectrum correlation coefficient matrix, as calculated for the simulated surveillance capsule position for the ORR PSF Metallurgical Experiment, was used.[7,8] The original calculation of the fluence variance-covariances covers only the range from 18 MeV to 0.1 MeV. Therefore two energy groups from 1 E-4 eV to 0.1 eV and from 0.1 eV to 0.1 MeV were added with large variances of 150% and 75%, respectively and small correlations of 0.2 and 0.1. Also, the variances of energy groups above 0.1 MeV were increased from the original values to 40% and the high-energy boundary was extended to 20 MeV. The spectrum covariance matrix was converted in the group structure used in the adjustment with the computer code FLXPRO from the LSL-M2 code package. Obviously the assumed spectrum variance-covariance information is only approximate; however, it does not appear to be critical for the analysis since comprehensive dosimetry measurements are available, and in such cases the adjustment results are in general not very sensitive to the details in the spectrum covariance matrix. The cross correlation factors for the spectra at different locations were assumed to be 0.8.

The activation cross-section library in 640-energy groups was created from the IRDF 90 and ENDF V dosimetry files. To account for the 4 mils gadolinium cover in the DOS3 experiment the set of cross sections was generated, where the 640-group cross sections were multiplied by the attenuation factors, defined as:

$$AF = \exp(-(D*AV/AT) * TH * CS),$$

where

AF = attenuation factor,
D = density of cover material (7.9004 g/cm^3 for Gd),
AV = Avogadros number,
AT = atomic weight (157.25 for Gd),
TH = thickness of the cover (4 mils),
CS = total absorption cross section of Gd (taken from the IRDF90 file).

The above formula is, of course, only a crude approximation and does not consider the geometry of the covers and the dosimeters. However, it appears to be reasonably accurate for the current application with the possible exception of gold dosimeters.

Resulting cross sections were then converted in 40 energy groups in the same way as the bare cross sections. Computer code FLXPRO from the LSL-M2 code package was used for this purpose.

Data for the photofission cross sections were taken from Verbinski.[9] The photoneutron cross section for beryllium, which leads to the formation of helium through the reaction $Be^9 + \gamma \rightarrow n + \alpha + \alpha$, was generated first from the plot in the "Reactor Handbook"[10] and later from the Warshaw[11] evaluation. No significant differences in the calculated reaction rates were observed. The gamma displacement cross section in iron was taken from Baumann.[12]

Measured activities were converted to reaction rates, taking into account the reactor power history for the cycle of the irradiation. Computer code ACT from the LSL-M2 code package was used for this purpose. Reaction rates so obtained were mostly used without any further correction, except in the following cases:

1. For the key 7, position 5, U-238, Np-237, and Be reaction rates were corrected for the gamma contribution as discussed in details above,

2. The Au and Co dosimeters were corrected for the self-shielding, since pure metal wires of 20 mils (Co) and 8 mils (Au) outer diameter were used in both DOS2 and DOS3 experiments. The correction factors were obtained from the ratios of measured activities of diluted and pure Au and Co wires, which were used in DOS4 experiment. The correction factors were 1.13 and 1.96 for bare and Gd shielded Co, respectively, and 1.68 and 5.10 for the bare and Gd-shielded Au, respectively.

3. The activities for Co gradient wires for DOS2 and DOS3 and Ni gradient wires for DOS3 for the top, middle, and bottom segments (Fig. I.1) were determined as follows:

   a. the bent section of the gradient wire was cut off at the top of the capsule (Fig. I.1);

   b. 1-cm sections, starting at the top, were cut off from the remainder of the wire;

   c. the bottom segment was slightly longer than 1 cm and was left that way; and

   d. the activities of the top, middle, and bottom segments were plotted against the wire length starting from the bottom (X=0). The coordinates along the X-axis of the latter segments were plotted at their respective midpoints.

   The activities of the Ni gradient wires for DOS2 were determined using the following procedure:

   a. the bend in the wires were straightened and 1-cm segments, starting at the top, were cut off the full length of the wire;

   b. the bottom segment was slightly longer than 1 cm and was left that way;

   c. the activities of all the 1-cm segments were counted and plotted on a curve starting from the bottom segment;

   d. the activities were plotted at the coordinates corresponding to the midpoints of each segment;

   e. the activities corresponding to the coordinates for the top, middle, and bottom segments were then obtained by interpolation.

The variances of the measured reaction rates were estimated from the observed spread of experimental data and were treated as uncorrelated.

For the adjustment the neutron spectrum was collapsed from the 64 groups in which the transport (3-D) calculation was done to the 40 energy groups.

4 RESULTS AND DISCUSSION

All three approaches described in Section 3.4 were used for key 7, position 5. This key is the only location where gamma measurements were made so that approaches A and C are supported by experimental data.

Four different adjustment runs are presented in Table 3. Run R4 is taken as the standard (best run). This run uses a total of 69 measured reaction rates from DOS1, DOS2, DOS3 and DOS4 experiments. Gamma corrections were made to the U-235, U-238, Np-237, and the Be-9 dosimeters. Six dosimeters were not used since their reaction rates required large adjustments and were, therefore, rejected as not consistent with the others. The adjusted values of the exposure parameters are listed together with their standard deviation in percent. The ratios of adjusted values for each of the other runs (R1, R2, and R3) to the values from run R4 are listed along with the fractional standard deviation.

The effect of rejecting the six dosimeters in run R4 is seen from the column labeled R1/R4. The six dosimeters not used in run R4 were added to run R1. The adjusted exposure parameters from the two runs agree within 1% and their standard deviations are also in agreement. However, the chi square per degree of freedom is 1.2 in run R1 and 0.81 in run R4, which clearly indicates that the rejected dosimeters were inconsistent with the others. Nevertheless, including some of the slightly inconsistent measurements in run R1 has practically no effect on the adjusted irradiation parameters since the adjustment is directed by the large body of 69 consistent measurements.

In the run R3 all the dosimeters that needed gamma corrections were not used so that adjustment is performed according to Approach B. The results are in good agreement with the run R4. The largest difference in the adjusted values from the two runs is observed for the thermal flux in the slot J and is 12%, which is still smaller that the quoted standard deviation of 19%. One can conclude therefore that Approach B is acceptable in determining the adjusted neutron exposure parameters.

The monitors in run R2 were not corrected for gamma-induced reactions, but were corrected in run R4. As expected, this change has a dramatic effect on the results as shown in Table 3. The chi square per degree of freedom rose to the value of 23, clearly indicating that major inconsistencies exist in the input data. The conclusion is drawn that one must not use the Np-237, U-238 and Be monitors in the neutron adjustment procedure without correcting the measured reaction rates for the gamma contributions.

Finally, Table 4 gives the comparison of the adjusted irradiation parameters from run R4 (neutron column) and the simultaneous neutron and gamma (N + gamma column) spectrum adjustment run. In the coupled neutron-gamma adjustment run, spectra at only the four locations were adjusted simultaneously because of the current limitations in the adjustment computer code LSL-M2. At these locations the same dosimetry measurements as in run 4 were used, and the measured absorbed gamma dose rate in silicon was added in the position of slot B. In the simultaneous neutron and gamma adjustment the reaction rates, as measured, of the fission and Be monitors are used as input.

Table 3 Comparison of different adjustment runs, key 7, position 5

	R1/R4		R2/R4		R3/R4		R4	
Slot D							VALUE	STD.
F > 1MeV*	1.01 ±	0.06	6.41 ±	0.06	0.99 ±	0.08	1.547E+08 ±	6
F > 0.1MeV*	1.01 ±	0.09	7.44 ±	0.09	0.99 ±	0.11	2.289E+08 ±	9
F < 0.4 eV*	0.99 ±	0.05	1.00 ±	0.05	1.00 ±	0.05	2.835E+08 ±	5
dpa/s**	1.01 ±	0.05	4.93 ±	0.05	1.00 ±	0.06	2.421E-13 ±	5
Slot A								
F > 1MeV	1.01 ±	0.07	5.34 ±	0.07	1.00 ±	0.08	1.580E+08 ±	7
F > 0.1MeV	1.01 ±	0.10	6.08 ±	0.10	1.00 ±	0.11	2.361E+08 ±	10
F < 0.4 eV	1.00 ±	0.04	1.00 ±	0.04	1.00 ±	0.04	2.879E+08 ±	4
dpa/s	1.01 ±	0.06	4.14 ±	0.06	1.00 ±	0.06	2.474E-13 ±	6
Slot B								
F > 1MeV	1.01 ±	0.05	25.04 ±	0.06	1.01 ±	0.68	1.504E+08 ±	6
F > 0.1MeV	1.00 ±	0.08	27.53 ±	0.08	1.00 ±	0.68	2.249E+08 ±	8
F < 0.4 eV	0.99 ±	0.07	1.01 ±	0.07	1.00 ±	0.08	2.742E+08 ±	7
dpa/s	1.01 ±	0.05	19.31 ±	0.05	1.01 ±	0.66	2.346E-13 ±	5
Slot J								
F > 1MeV	1.01 ±	0.06	13.47 ±	0.06	1.06 ±	0.08	1.491E+08 ±	6
F > 0.1MeV	1.01 ±	0.09	15.15 ±	0.09	1.04 ±	0.11	2.241E+08 ±	9
F < 0.4 eV	1.01 ±	0.18	1.03 ±	0.19	0.88 ±	0.19	3.086E+08 ±	19
dpa/s	1.01 ±	0.05	10.07 ±	0.05	1.05 ±	0.07	2.360E-13 ±	5
Slot ET								
F > 1MeV	1.01 ±	0.07	5.35 ±	0.07	1.00 ±	0.08	1.538E+08 ±	7
F > 0.1MeV	1.00 ±	0.10	6.10 ±	0.10	1.00 ±	0.11	2.295E+08 ±	10
F < 0.4 eV	1.00 ±	0.06	1.00 ±	0.06	1.00 ±	0.06	2.987E+08 ±	6
dpa/s	1.00 ±	0.06	4.15 ±	0.06	1.00 ±	0.07	2.408E-13 ±	6
Slot EM								
F > 1MeV	1.01 ±	0.07	5.35 ±	0.07	1.00 ±	0.08	1.562E+08 ±	7
F > 0.1MeV	1.00 ±	0.10	6.10 ±	0.10	1.00 ±	0.11	2.332E+08 ±	10
F < 0.4 eV	1.00 ±	0.06	1.00 ±	0.06	1.00 ±	0.06	2.731E+08 ±	6
dpa/s	1.00 ±	0.06	4.15 ±	0.06	1.00 ±	0.07	2.444E-13 ±	6
Slot EB								
F > 1MeV	1.01 ±	0.07	5.36 ±	0.07	1.00 ±	0.08	1.569E+08 ±	7
F > 0.1MeV	1.00 ±	0.10	6.10 ±	0.10	1.00 ±	0.11	2.345E+08 ±	10
F < 0.4 eV	1.00 ±	0.06	1.00 ±	0.06	1.00 ±	0.06	2.707E+08 ±	6
dpa/s	1.00 ±	0.06	4.16 ±	0.06	1.00 ±	0.07	2.456E-13 ±	6
Slot FT								
F > 1MeV	1.01 ±	0.07	5.35 ±	0.07	1.00 ±	0.08	1.507E+08 ±	7
F > 0.1MeV	1.00 ±	0.10	6.10 ±	0.10	1.00 ±	0.11	2.249E+08 ±	10
F < 0.4 eV	1.00 ±	0.06	1.00 ±	0.06	1.00 ±	0.06	2.859E+08 ±	6
dpa/s	1.00 ±	0.06	4.15 ±	0.06	1.00 ±	0.07	2.359E-13 ±	6

Table 3 (continued)

	R1/R4		R2/R4		R3/R4		R4	
Slot FM							VALUE	STD.
F > 1MeV	1.01 ±	0.07	5.35 ±	0.07	1.00 ±	0.08	1.583E+08 ±	7
F > 0.1MeV	1.00 ±	0.10	6.09 ±	0.10	1.00 ±	0.11	2.360E+08 ±	10
F < 0.4 eV	1.00 ±	0.06	1.00 ±	0.06	1.00 ±	0.06	2.630E+08 ±	6
dpa/s	1.00 ±	0.06	4.16 ±	0.06	1.00 ±	0.07	2.473E-13 ±	6
Slot FB								
F > 1MeV	1.01 ±	0.07	5.35 ±	0.07	1.00 ±	0.08	1.608E+08 ±	7
F > 0.1MeV	1.00 ±	0.10	6.10 ±	0.10	1.00 ±	0.11	2.400E+08 ±	10
F < 0.4 eV	1.00 ±	0.06	1.00 ±	0.06	1.00 ±	0.06	2.836E+08 ±	6
dpa/s	1.00 ±	0.06	4.16 ±	0.06	1.00 ±	0.07	2.515E-13 ±	6
	Chi^2 = 1.21 #R = 65 DOSIMETERS FROM DOS1,2,3,4 SLOT J: ADDED NI (EM+FM)/2		Chi^2= 22.92 #R = 59 Same as R4, but: NO GAMMA CORRECTIONS		Chi^2 = 0.52 #R = 45 Same as R4, but: all dosimeters that need gamma correction NOT USED		Chi^2 = 0.81 #R = 59 Not used: D: Au (DOS 4) A: Au (DOS3) B: U-235--Ru U-238--Zr Np-237--Ru J: Co (in Gd)	

* Units are $cm^{-2} . s^{-1}$
** Units are s^{-1}

NOTE: Chi^2 is chi square per degree of freedom. #R is number of residuals. Scaling option is used, therefore, the number of residuals is equal to the number of measured reaction rates used minus the number of locations at which the spectrum is adjusted (10 in these runs).

Table 4 Comparison of simultaneous neutron and gamma adjustment to neutron adjustment run, key 7, position 5

	Neutron		N + Gamma		
	Value	Std. %	Value	Std. %	
	A1		A2		A2/A1
Slot D					
F > 1 MeV*	1.55E+08	± 6	1.54E+08	± 8	0.99
F > 0.1 MeV*	2.29E+08	± 9	2.26E+08	± 11	0.99
F < 0.4 eV*	2.84E+08	± 5	2.84E+08	± 5	1.00
dpa (ASTM)**	2.42E-13	± 5	2.41E-13	± 6	0.99
G-dpa**			1.34E-12	± 15	
G-flux***			1.39E+13	± 27	
Dose rate in Si****			3.66E+01	± 22	
Slot J					
F > 1 MeV*	1.49E+08	± 6	1.58E+08	± 8	1.06
F > 0.1 MeV*	2.24E+08	± 9	2.37E+08	± 11	1.06
F < 0.4 eV*	3.09E+08	± 19	3.11E+08	± 19	1.01
dpa (ASTM)**	2.36E-13	± 5	2.50E-13	± 7	1.06
G-dpa**			1.22E-12	± 7	
G-flux***			1.27E+13	± 20	
Dose rate in Si****			3.31E+01	± 13	
Slot B					
F > 1 MeV*	1.50E+08	± 6	1.41E+08	± 27	0.94
F > 0.1 MeV*	2.25E+08	± 8	2.09E+08	± 27	0.93
F < 0.4 eV*	2.74E+08	± 7	2.72E+08	± 7	0.99
dpa (ASTM)**	2.35E-13	± 5	2.21E-13	± 26	0.94
G-dpa**			1.31E-12	± 8	
G-flux***			1.39E+13	± 9	
Dose rate in Si****			3.62E+01	± 5	
Slot A					
F > 1 MeV*	1.58E+08	± 7	1.59E+08	± 8	1.00
F > 0.1 MeV*	2.36E+08	± 10	2.36E+08	± 11	1.00
F < 0.4 eV*	2.88E+08	± 4	2.88E+08	± 4	1.00
dpa (ASTM)**	2.47E-13	± 6	2.49E-13	± 6	1.00
G-dpa**			1.38E-12	± 32	
G-flux***			1.45E+13	± 35	
Dose rate in Si****			3.81E+01	± 33	

*Units are neutrons $cm^{-2}.\ s^{-1}$
**Units are s^{-1}
***Units are gammas $cm^{-2}.\ s^{-1}$
****Units are $Gy.s^{-1}$

As seen from Table 4, the adjusted neutron exposure parameters from the two runs agree very well. The largest difference observed is 7% for F > 0.1 MeV at slot B. The adjusted absorbed dose rate in Silicon is 36.2 Gy/s, which compares well to the measured value of 36.4 Gy/s. The measured responses of fission dosimeters and Be monitors are consistent with the responses of other monitors not affected by the gamma field, and with the measured absorbed gamma dose rate in the Silicon. These agreements support the conclusion that the measured reaction rates of Np-237, U-238 and Be monitors are larger than the reaction rates of other threshold monitors due to the significant contributions from the gamma-induced reactions. The chi-square per degree of freedom for the neutron-gamma run was 0.77 and the number of residuals was 42.

Table 4 also shows that at key 7, position 5, the displacements per atom rate induced by gamma rays is about 5 times higher than the neutron-induced dpa rate. Therefore, it may be of interest to re-evaluate the mechanical property changes of the HFIR specimens based on the total dpa from the neutrons and the gamma rays.

The analysis of key 7 position 5 showed that the neutron adjustment parameters, obtained by rejecting all the dosimeters that needed substantial corrections for gamma contributions, gave results that are in excellent agreement with the adjustments where the affected dosimeters were corrected for gamma contributions and taken into account in the adjustment procedure. Also, results from both of these adjustment runs are in good agreement with the results obtained from the simultaneous adjustment of the neutron and gamma field. This latter approach appears to be the most consistent technique to analyze dosimetry measurements when considerable contribution from the gamma field is suspected. The comparisons of different adjustment runs, described above, show also that reliable fast-flux irradiation parameters can be derived from the calculated spectra and measured activities of the stainless steel wires, located in the V-notch of the Charpy specimens.

Based on the results for key 7, position 5 and because no independent gamma field measurements were available at the other locations, the neutron spectrum adjustment runs were done without the Np-237, U-238, and Be dosimeters. Detailed results of the adjustment runs are listed in Appendices E, F, G, and H.

Adjusted irradiation parameters for the four surveillance locations considered are summarized in Table 5. For each of the capsules, slot J is located at the center of the capsule. Irradiation parameters for that location, therefore, correspond to the position of the V-notch of the Charpy specimens irradiated in the HFIR surveillance capsules. The calculated (3-D transport calculation) and adjusted neutron spectra for the Slot J, are illustrated in the Figs. 5-8. Adjusted group fluxes for these locations are also tabulated in Table 6.

From Table 5 it can be seen that the neutron field is considerably different at the surveillance positions analyzed. Differences are in the magnitude as well as in the neutron spectrum. Even though details can be seen from Table 5, let us mention here for example that the fast (E > 1 MeV) neutron flux is 8 times greater at key 2, position 9 than at key 7, position 5. Thermal flux at key 4, position 10 is even 90 times higher than at the key 7, position 5. The thermal-to-fast-flux ratio is approximately 2, 13, 75, and 67 for the key 7, position 5, key 2, position 9, key 4, position 2, and key 4, position 10 respectively. Therefore, while neutron flux with energies below 0.1 MeV do not contribute significantly to the dpa rate at the key 7, position 5, it is much more important for the other locations where neutron spectrum is considerably

Table 5 Irradiation parameters at the centers of capsules

	Key 7 Position 5		Key 2 Position 9		Key 4 Position 2		Key 4 Position 10	
	Value	Std. %	Value	Std. %	Value	Std. %	Value	Std. %
F > 1 MeV*	1.49E+08	± 6	1.21E+09	± 9	3.10E+08	± 10	4.09E+08	± 10
F > 0.1MeV*	2.24E+08	± 9	2.11E+09	± 12	6.43E+08	± 13	8.05E+08	± 13
F < 0.4 eV*	3.09E+08	± 19	1.61E+10	± 6	2.33E+10	± 6	2.75E+10	± 6
dpa/s**	2.36E-13	± 5	1.89E-12	± 7	6.66E-13	± 6	8.62E-13	± 6

*Units are neutrons . cm^{-2}. s^{-1}
**Units are s^{-1}

Table 6 Adjusted neutron fluxes at the centers of the examined capsules

Group Upper Energy Boundary [eV]	Key 7 Position 5 [$cm^{-2}. s^{-1}$]	Key 2 Position 9 [$cm^{-2}. s^{-1}$]	Key 4 Position 2 [$cm^{-2}. s^{-1}$]	Key 4 Position 10 [$cm^{-2}. s^{-1}$]
2.000E+07	1.087E+06	2.356E+06	8.033E+05	8.997E+05
1.271E+07	3.399E+06	9.059E+06	2.659E+06	3.575E+06
1.013E+07	8.408E+06	2.698E+07	7.235E+06	1.102E+07
8.072E+06	1.398E+07	5.743E+07	1.310E+07	2.316E+07
6.434E+06	1.150E+07	5.791E+07	1.212E+07	2.105E+07
5.523E+06	1.301E+07	7.595E+07	1.549E+07	2.533E+07
4.742E+06	1.193E+07	8.075E+07	1.665E+07	2.518E+07
4.071E+06	8.687E+06	7.089E+07	1.547E+07	2.164E+07
3.495E+06	9.697E+06	8.778E+07	1.897E+07	2.473E+07
3.000E+06	7.005E+06	6.626E+07	1.523E+07	1.904E+07
2.724E+06	2.126E+07	2.229E+08	5.409E+07	6.589E+07
2.038E+06	5.608E+06	6.294E+07	1.700E+07	2.083E+07
1.850E+06	6.937E+06	8.044E+07	2.260E+07	2.763E+07
1.655E+06	6.343E+06	7.464E+07	2.198E+07	2.656E+07
1.480E+06	7.801E+06	9.213E+07	2.867E+07	3.438E+07
1.282E+06	1.248E+07	1.457E+08	4.778E+07	5.790E+07
1.000E+06	1.302E+07	1.520E+08	5.179E+07	6.111E+07
7.653E+05	2.169E+07	2.543E+08	9.141E+07	1.106E+08
4.704E+05	2.162E+07	2.591E+08	9.586E+07	1.149E+08
2.297E+05	1.866E+07	2.269E+08	9.390E+07	1.097E+08
1.000E+05	4.016E+07	3.658E+08	3.275E+08	3.942E+08
1.202E+04	1.092E+07	1.050E+08	9.783E+07	1.149E+08
6.004E+03	1.076E+07	1.041E+08	9.995E+07	1.193E+08
3.000E+03	3.086E+07	3.105E+08	3.173E+08	3.768E+08
3.911E+02	1.025E+07	1.070E+08	1.168E+08	1.389E+08
1.978E+02	1.027E+07	1.089E+08	1.235E+08	1.478E+08
1.000E+02	1.452E+07	1.573E+08	1.863E+08	2.232E+08
3.817E+01	2.019E+07	2.259E+08	2.853E+08	3.419E+08
1.000E+01	7.279E+06	8.386E+07	1.113E+08	1.332E+08
6.178E+00	1.084E+07	1.276E+08	1.750E+08	2.090E+08
3.000E+00	8.293E+06	1.002E+08	1.420E+08	1.684E+08
1.770E+00	2.546E+07	3.351E+08	5.000E+08	5.591E+08
3.970E-01	3.824E+06	5.546E+07	9.632E+07	1.142E+08
3.300E-01	4.939E+06	9.798E+07	2.028E+08	2.212E+08
2.700E-01	8.708E+06	2.627E+08	6.280E+08	6.451E+08
2.150E-01	2.178E+07	8.834E+08	2.238E+09	2.195E+09
1.620E-01	4.626E+07	2.309E+09	4.003E+09	4.492E+09
1.040E-01	9.470E+07	5.228E+09	6.757E+09	8.447E+09
5.000E-02	1.170E+08	6.594E+09	8.503E+09	1.034E+10
1.000E-02	1.145E+07	6.501E+08	8.364E+08	9.958E+08
1.000E-05*				

*Lower energy boundary of the 40th group.

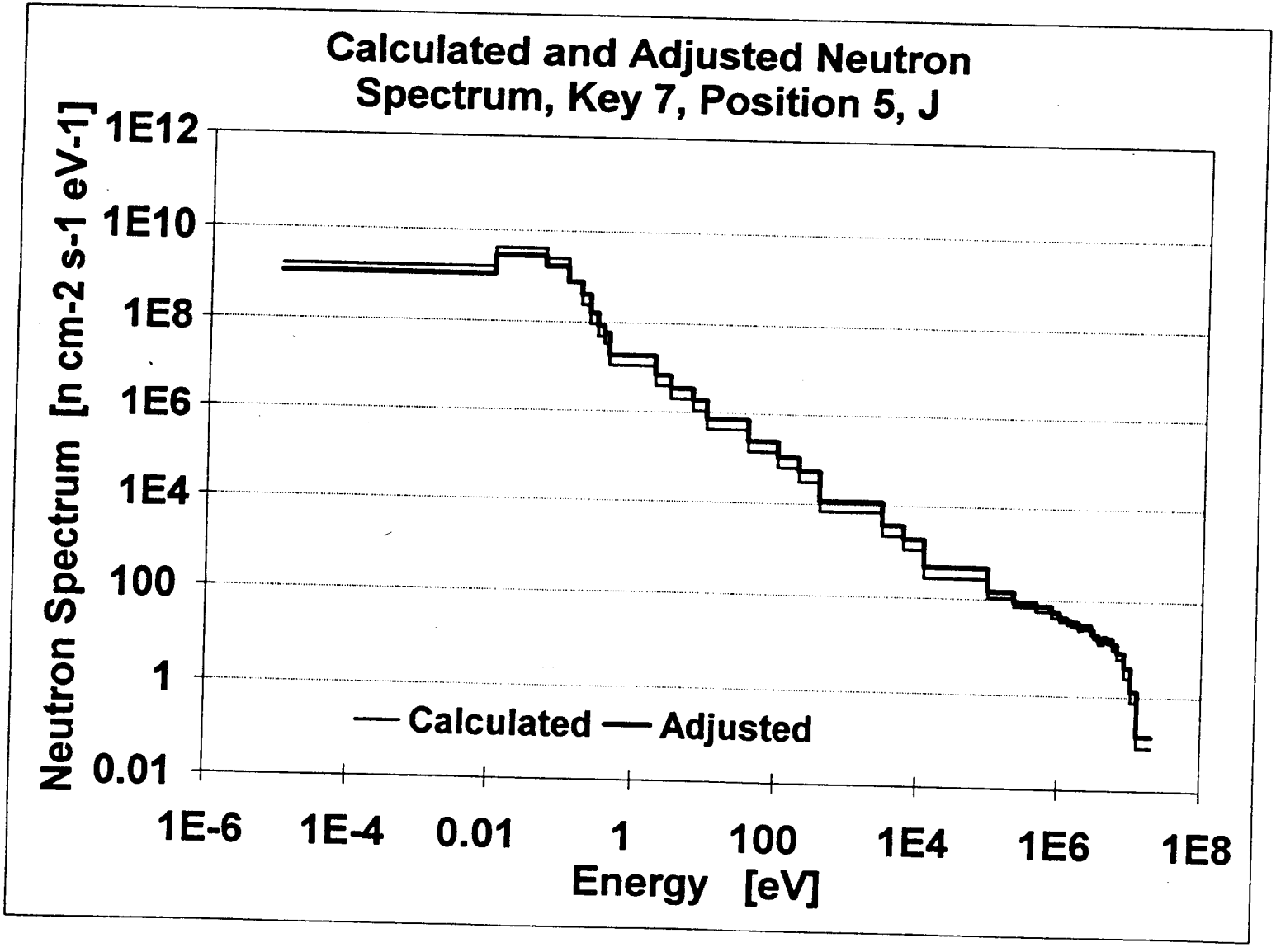

Fig. 5 Calculated and adjusted neutron spectrum, key 7, position 5, J

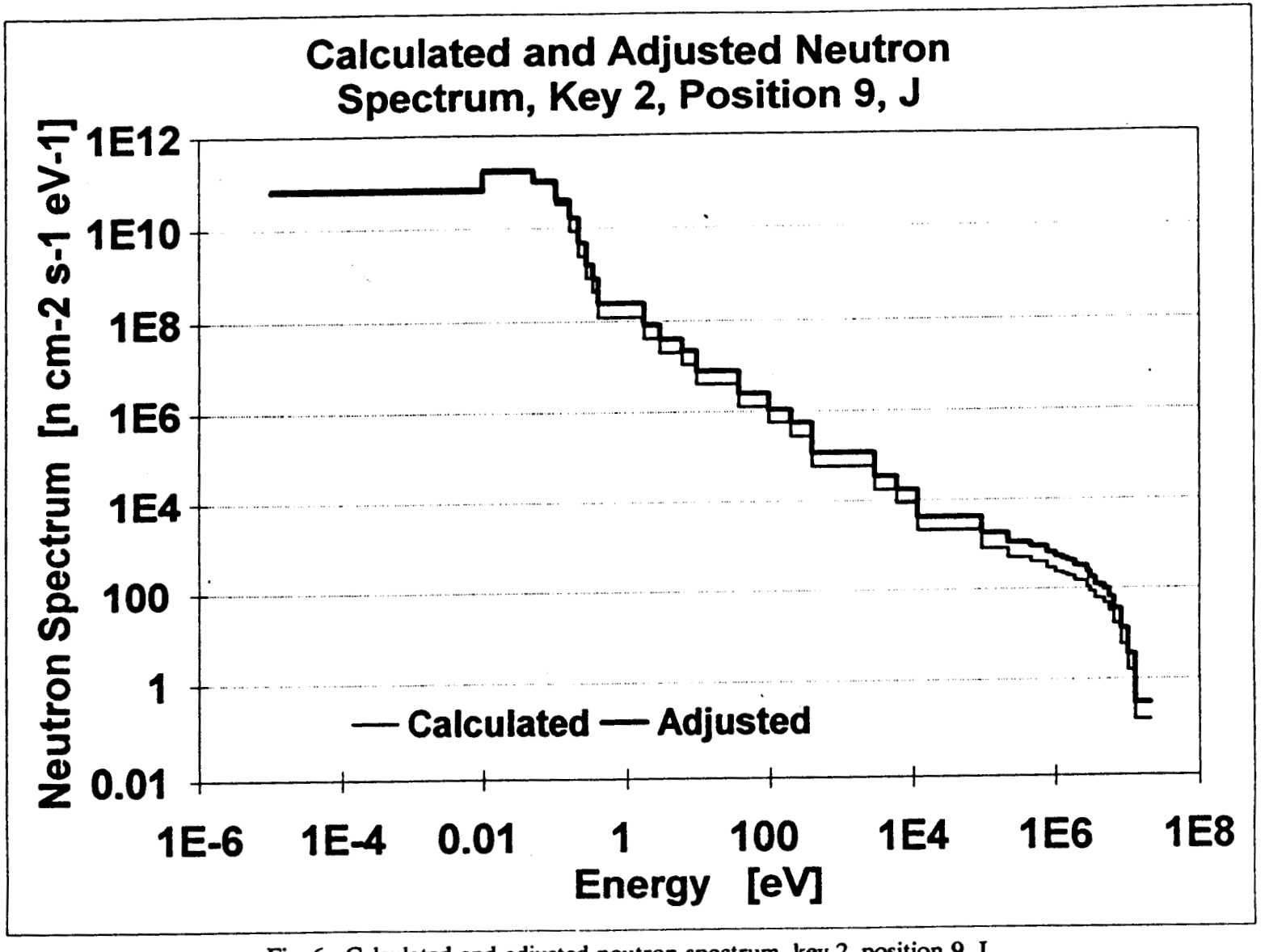

Fig. 6 Calculated and adjusted neutron spectrum, key 2, position 9, J

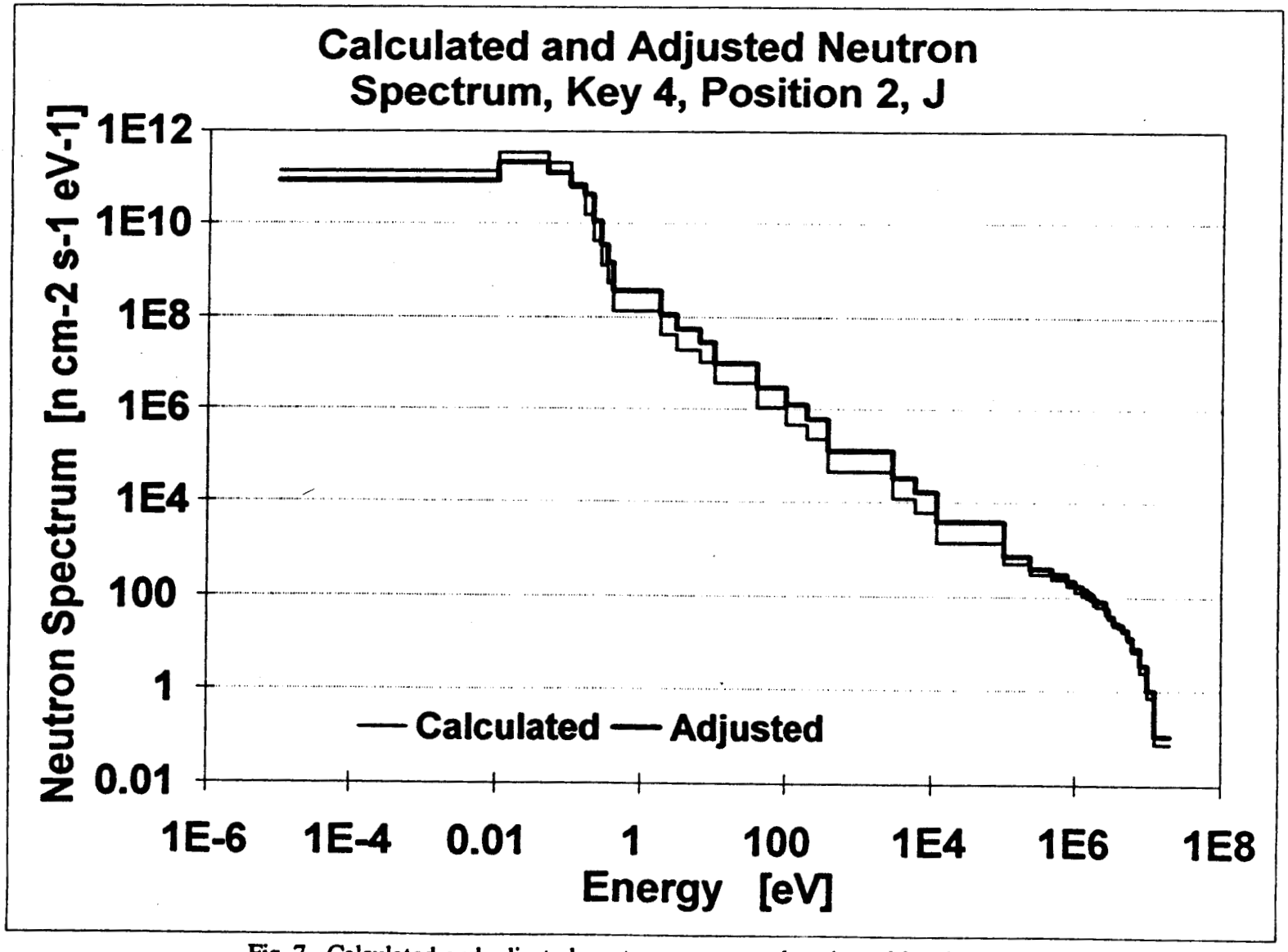

Fig. 7 Calculated and adjusted neutron spectrum, key 4, position 2, J

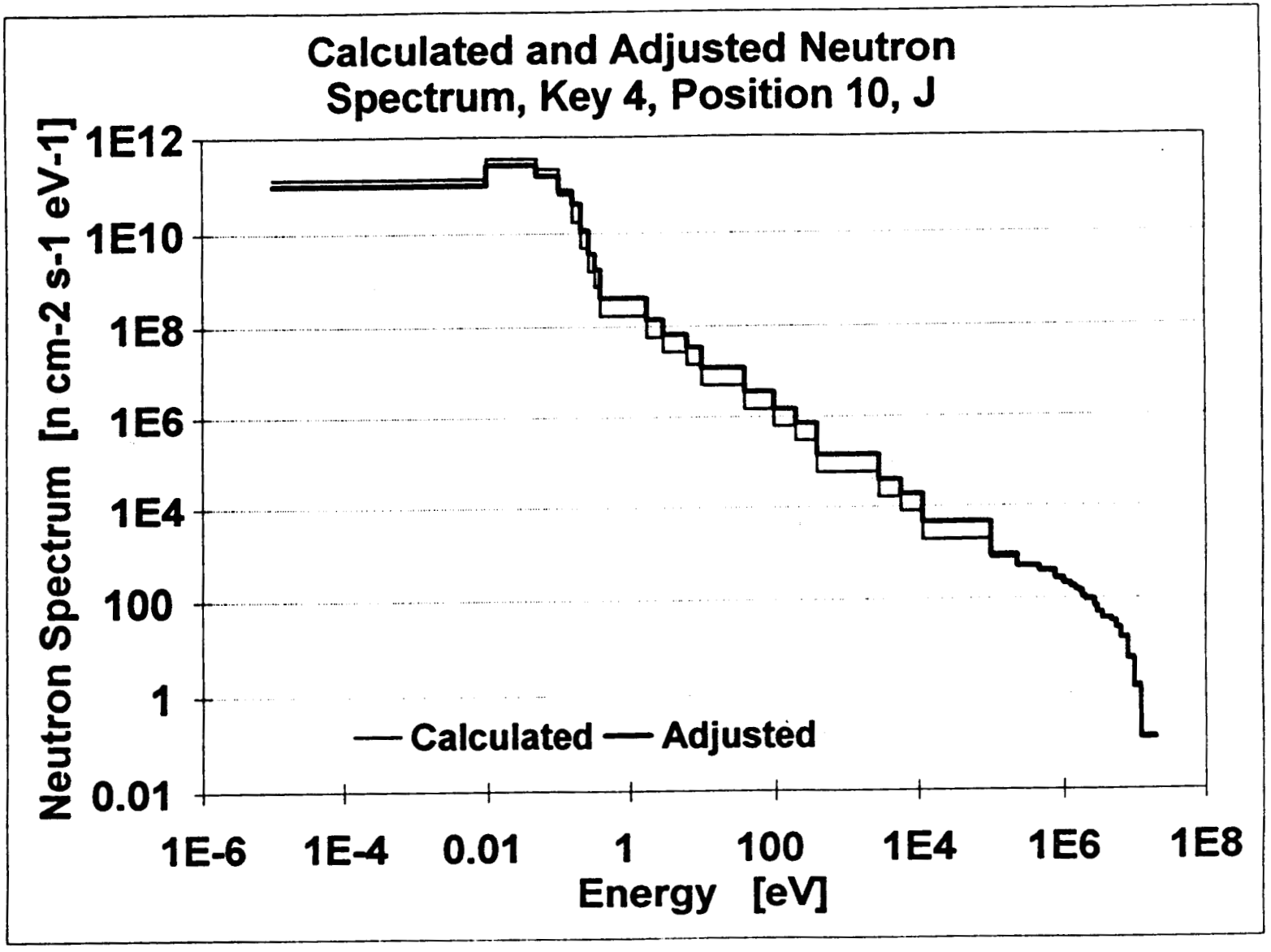

Fig. 8 Calculated and adjusted neutron spectrum, key 4, position 10, J

softer. Neutrons with energies below 0.1 MeV contribute 3%, 9%, 33%, and 30% to the dpa rate for key 7, position 5; key 2, postiion 9; key 4, position 2; and key 4, position 10, respectively. The dpa rate-to-fast-flux ratio is 1.58E-21 cm^2, 1.56E-21 cm^2, 2.15E-21 cm^2, and 2.11E-21 cm^2 for the key 7, position 5, key 2, position 9, key 4, position 2, and key 4, position 10 respectively. Variations in these ratios from one position to the other, which are of about 35%, reflect the considerable differences in the neutron spectrum at different surveillance locations and indicate that besides fast neutrons, lower energy neutrons also contribute significantly to the dpa rate. Therefore, they are included in the calculation of the neutron-induced dpa rate. Besides the above-mentioned differences between surveillance positions analyzed within this work, it needs to be mentioned that for all the locations except at the key 7, position 5, significant variations in the neutron field inside the surveillance capsules were found. In all of the capsules located around the experimental beam tubes, the neutron flux was considerably higher at the capsule end which was closer to the beam tube. This end of the capsule is called bottom, and the opposite end is called top. This notation is used in all of the tables given in the Appendices E, F, G, and H, where the measured activities as well as adjusted irradiation parameters for the locations of gradient wires are given. As mentioned before the gradients inside the key 7, position 5 are insignificant. For the other locations, however, the bottom-to-top ratios are 2.0, 1.8, and 2.0 for the fast flux (E > 1 MeV) and flux over 0.1 MeV, and 3.1, 5.8, and 5.7 for the thermal flux for the key 2, position 9, key 4, position 2, and key 4, position 10 respectively. These variations in the neutron field are very probably caused by the neutrons that leak or are scattered out of the experimental beam tubes. There is no significant gradient in the transverse direction in any of the capsuled analyzed.

These gradients complicate the analysis of the dosimetry experiments, since the calculated spectrum was provided in just one point for each capsule. However, they are not important for the determination of the irradiation parameters based on the activities from the steel monitor wires located in the V-notches of the Charpy specimens in the HFIR surveillance capsules.

5 CONCLUSIONS AND RECOMMENDATIONS

A comprehensive dosimetry experiment was performed at the following HFIR surveillance sites; key 7, position 5, key 4, positions 2 and 10, and key 2, position 9. The results are

1. The best estimates for the fast-neutron flux (E > 1.0 MeV), fast-neutron flux (E > 0.1 MeV), thermal neutron flux (E < 0.4 eV), and displacement rates per atom at the Charpy V-notch in the four capsules analyzed are shown in Table 5.

2. Photo-induced reactions accounted for the discrepancies between the nickel dosimeters and the beryllium and fast-fission threshold dosimeters in the DOS1 experiment. The wide water region between the beryllium reflector and the pressure vessel of the HFIR resulted in the extremely high gamma-to-neutron flux ratios at the surveillance capsules.

3. Insignificant flux gradients were present in key 7, position 5, but the keys adjacent to the beam tubes, key 2 and 4, show substantial fast and thermal neutron flux gradients. The thermal-to-fast ratios at the keys 2 and 4 are significant.*

4. In key 7, position 5, where gamma measurements were made, the dpa rate from gammas is approximately five times higher than the dpa rate from neutrons.

5. Based on the current study, the adjustment procedure using the stainless steel dosimeter in the Charpy V-notch and neutron transport calculations should give reliable fast neutron exposure parameters.**

6. The feasibility of adjusting gamma and neutron fluxes simultaneously was also demonstrated, probably for the first time. This simultaneous adjustment of gamma and neutron spectra adds very important gamma information to the three-step procedure for fluence determination of reactor pressure vessels.

Although it has not been shown that the rapid embrittlement of the HFIR specimens can be attributed to gammas or to neutrons, re-evaluation of mechanical property changes of the specimens in key 7, using the total dpa from gammas and neutrons, may show some interesting results. We believe that the HFIR's special environment, involving extremely high gamma-to-neutron ratios, is probably significantly different from the environment at the support structures of a pressurized water reactor so that any application of the embrittlement data from HFIR should be treated very carefully.

---

*L. K. Mansur and K. Farrell, "On Mechanisms by which a Soft Neutron Spectrum May Induce Accelerated Embrittlement," Journal of Nuclear Materials 170 (1990) 236-245.

**The current experiment showed that reaction rates of Ni-58 and Fe-54 are in agreement with the other dosimeters. In ORNL/TM-10444, page 193, Table E-1 it was shown that the reaction rates from iron and nickel in the 304 stainless steel dosimeter used in the HFIR surveillance capsules were in agreement with the pure iron and nickel dosimeters.

6 REFERENCES

1. R. D. Cheverton, J. G. Merkle, and R. K. Nanstad, eds., "Evaluation of HFIR Pressure-Vessel Integrity Considering Radiation Embrittlement," ORNL/TM-10444, April 1988.

2. W. A. Rhoades and R. L. Childs, "The TORT Three-dimensional Discrete Ordinates Neutron/Photon Transport Code," ORNL-6268, November 1987.

3. N. M. Greene and C. W. Craven, Jr., "XSDRN: A Discrete Ordinate Spectral Averaging Code," ORNL/TM-2500, July 1969.

4. F. W. Stallmann, "LSL-M2: A Computer Program for Least Squares Logarithmic Adjustment of Neutron Spectra," NUREG/CR-4349, ORNL/TM-9933, March 1986.

5. 1992 Annual Book of ASTM Standards, Vol. 12.02, Nuclear, Solar, and Geothermal Energy.

6. F. B. K. Kam et al., "Pressure Vessel Fluence Analysis and Neutron Dosimetry," NUREG/CR-5049, December 1987.

7. R. E. Maerker, M. L. Williams, B. L. Broadhead , J. J. Wagschall, and C. V. Fu, "Revision and Extension of the Data Base in the LEPRICON Dosimetry Methodology," EPRI NP-3841, Electric Power Research Institute, Palo Alto, Calif., January 1985.

8. F. W. Stallmann, "Determination of the Damage Exposure Parameter Values in the PSF Metallurgical Irradiation Experiment," NUREG/CR-3841, ORNL/TM-9166, U.S. Nuclear Regulatory Commission, Washington, D.C., October 1984.

9. V. V. Verbinski et al., "Photointerference Corrections in Neutron Dosimetry for Reactor Pressure Vessel Lifetime Studies," *Nucl. Sci. and Eng.*: 75, pp. 159-166 (1980).

10. E. P. Blizard et al., "Reactor Handbook," Volume III, Part B, Shielding, p. 23.

11. S. I. Warshaw, "4 π Photoneutron Cross-Section for ^{9}Be from Threshold to 16 MeV: Initial Evaluations," Physical Data Note, 14 August 1989.

12. N. P. Baumann, "Gamma-Ray Induced Displacement in D20 Reactors," Proc. Seventh ASTM-Euratom Symposium on Reactor Dosimetry, pp. 689-697, 1992.

APPENDIX A

LETTER REPORT ON NIST SUPPORT

NIST
UNITED STATES DEPARTMENT OF COMMERCE
National Institute of Standards and Technology
Gaithersburg, Maryland 20899

LETTER REPORT ON NIST SUPPORT FOR MEASUREMENT OF NEUTRON AND GAMMA FIELDS AT HIFR SURVEILLANCE CAPSULE LOCATIONS.

E.D. McGarry & J.A. GRUNDL
Neutron Interactions and Dosimetry Group
National Institute for Standards and Technology

Neutron Dosimetry Fluence Standards

NIST has developed and maintains both U-235 and Cf-252 neutron-fission-spectrum fields for irradiations calibration work. The most direct output from these fields is a certified fluence to which a dosimeter was exposed. A natural validation of a dosimeter-response measuring system is to derive a fluence from its evaluation of dosimeter response and compare with the certified value.

Iron and Nickel Neutron Fluence Standards for HFIR

A central issue related to measurement of the radiation fields at the HFIR pressure vessel surveillance capsule locations was that 1992-dosimetry results from fission foils or Helium Accumulation Fluence Monitors did not agree with fluences predicted by threshold (n,p) reactions.

In January 1993 NIST supplied ORNL radioactive disks from U-235 fission spectrum irradiations of the Ni58(n,p)Co58 and Fe54(n,p)Mn54 threshold reactions. In February NIST supplied test reports for these irradiations (see attached reports). Table I compares ORNL and NIST results, which agree within the NIST stated uncertainties.

Np237 Fluence Standard for HFIR

Prior to the DOS-2,-3, and -4 HFIR dosimetry measurements, NIST had received and gamma counted the DOS-1 Np-273 dosimeter. The fission product results agreed within 5 to 7% with those found by ORNL. Along with DOS-1, NIST also received a second Np-237 foil that was unirradiated. It was identified as NIST-1, given a certified U-235 fluence exposure, and supplied to ORNL for additional dosimeter measurement verification, if necessary.

Gamma Dosimetry for HFIR

Gamma dosimetry was accomplished to confirm the unusually large gamma dose predicted by transport calculations at the locations of the Np237 dosimeters, which in turn explains the larger-than-expected response of the Np237(n,f) reaction in HIFR because of photofission in neptunium.

The dosimetry method, suggested and implemented by Dr. William McLaughlin at NIST, was to measure the change in optical absorption in polychlorostyrene film after its exposure to gamma radiation. This gamma dosimeter, developed by Far West Technology Inc., is 25 w/o chlorine, 69 w/o carbon, and 5.8 w/o hydrogen, with a sensitivity range of 2 to 50 kiloGrays. the hydrogen concentration is low to minimize sensitivity to neutrons, which produce knock on protons. Several sets of aluminum wrapped dosimeters, each 1 cm X 1 cm X 0.05 mm, were supplied to ORNL for HIFR irradiation and then returned to NIST. The optical densities were recorded by a spectrophotometer, before and after exposure, and large exposures of 26.0 and 26.4 kiloGray (silicon dose) were reported. See the attached NIST Report of Special Measurements.

Neutron Response of the Gamma Dosimeters

The gamma dosimeters are supposed to have a small neutron sensitivity, However, the data to substantiate this is not readily available; perhaps because of previous security classification (?). Therefore, an additional test of this sensitivity was accomplished at NIST by irradiating the dosimeters in the neutron plus gamma radiation fields near a Cf-252 source.

The neutron-to-gamma fluence-in-air ratio for the source is 4 (in units of neutrons > 1 MeV / gamma > 2 MeV). A pair of dosimeters were mounted on opposite side of the source with a separation distance of 3.8 ±0.15 cm, which represents an average source-to-dosimeter distance of 1.9 cm with an uncertainty of about 15% for the pair response. The dosimeters were exposed to a certified neutron fluence of 3.3E+013 n/cm^2 (E > 1 MeV). This corresponds to a total neutron fluence of 4.8E+013 n/cm^2 ± 20%. The length of the irradiation was 311.2 hours. This total neutron dose corresponds to a total gamma dose of 1.6 kGy in silicon, (which divided by 0.9 is approximately the dose in tissue). The total dose is for no absorber around the gamma dosimeters which were, however, in aluminum. It is known from previous dose measurements with the NIST Cf252 sources that about 0.6 of the total neutron dose is received when the source is enclosed in two millimeters of iron. Assuming that the thicker aluminum around the gamma dosimeters is equivalent, the shielded total gamma dose would be (1.6 x 0.6) = 0.96 kGy Si. The dose measured with the polychlorostyrene gamma dosimeters was 0.90 kGy Si.

Conclusions: The estimated gamma dose from the Californium irradiation conservatively accounts for all of the measured response. For the HFIR exposure, the estimated dose (if it were assumed that all the response were from the Cf252 neutrons) would be 0.003 kGy Si, as compared to the reported 26 kGy Si HFIR dose. However, because of a temperature dependence of polychlorostyrene, shown in Fig. 1, the reported NIST results appear to require an adjustment of about 20% to account for temperature response at a HFIR irradiation temperature of nominally 50 degrees centigrade.

TEST REPORT OF FLUENCE STANDARD MADE IN U235 FISSION SPECTRUM

Fluence Standard # Ni-AK for Ni58(n,p)Co58 Reaction

The subject fluence standard was made in a U235 fission spectrum irradiation that ended 5/24/1991. The irradiation was continuous at steady reactor power. The fluence was monitored by activation of a separate nickel foil that was subsequently counted on a GeLi gamma detector previously calibrated against a known fluence exposure in a Cf252 neutron field.

Irradiation Details:

SOI: 16:15 EST 21 May 1991
EOI: 15:25 EST 24 May 1991
LOI: 2.5620E+05 seconds

	QUANTITY	VALUE	+%
1.	Cf252 Cal of Co-58 [cps/g(Sat)/Cf neut]	1.893E+05	2.8%
2.	1/2" Diam. Nickel Monitor [cps/g @ EOI]	3924.0	0.32%
3.	This Irradiation's Saturation Factor	0.0286	0.15%
4.	Free Field Fluence Rate @ Center of U235 Field [1.893E+05 * (3924/.0286)]	2.597E+10	2.9%
5.	Free Field Fluence @ Dosimeter Nickel AK [2.597E+10 * 1.15 * 2.562E+05]	7.65E+15	3.1%
6.	Mass Nickel AK (grams)	0.2814	0.2%
7.	U235 Cross section of N58(n,p)Co58 (mb)	105.0	2.6%
8.	Ni58(n,p)Co58 Reaction Rate (@ Satuaration) [2.59E+10 * 1.15 * 0.105E-24]	3.14E-15	4.2%*

Note the significant part of the uncertainty in the cross section, which does not come into play until the final conversion to reaction rate.

TEST REPORT OF FLUENCE STANDARD MADE IN U235 FISSION SPECTRUM

Fluence Standard # Fe-B1 for Fe54(n,p)Mn54 Reaction

The subject fluence standard was made in a U235 fission spectrum irradiation that ended 1/13/1991. Except for 23 minutes near the middle of the irradiation when there was a big decrease in power, the irradiation was continuous at steady reactor power. The fluence was monitored by activation of a separate nickel foil that was subsequently counted on a GeLi gamma detector previously calibrated against a known fluence exposure in a Cf252 neutron field.

Irradiation Details:

SOI: 15:38 EST 10 January 1991
EOI: 14:03 EST 13 January 1991
Time at Power: 2.521E+05 seconds

	QUANTITY	VALUE	+%
1.	Cf252 Cal of Co-58 [cps/g(Sat)/Cf neut]	1.893E+05	2.8%
2.	1/2" Diam. Nickel Monitor [cps/g @ EOI]	5275	1.8%
3.	This Irradiation's Saturation Factor	0.02857	0.3%
4.	Free Field Fluence Rate @ Center of U235 Field [1.893E+05 * (5275/1.015)/.02857]	3.43E+10	3.3%
5.	Free Field Fluence @ Dosimeter Iron Fe-B1 [3.43E+10 * 1.056 * 2.521+05]	9.13E+15	3.6%
6.	Mass Iron Fe-B1 (grams)	0.5088	0.15%
7.	U235 Cross section of Fe54(n,p)Mn54 (mb)	81.0	3.0%
8.	Fe54(n,p)Mn54 Reaction Rate (@ Satuaration) [3.43E+10 * 1.056 * 0.081E-24]	2.93E-15	4.7%*

Note the significant part of the uncertainty in the cross section, which does not come into play until the final conversion to reaction rate.

NIST IRON AND NICKEL NEUTRON FLUENCE STANDARDS

MONITOR NUMBER	COUNTING DATE	COUNTING TIME	DET. NUMBER	COUNTING GEOMETRY (mm)	SAMPLE WEIGHT (g)	EOI DATE	EOI TIME	SPECIFIC ACTIVITY at EOI (Bq/g)	1-SIGMA COUNTING ERROR (%)	REACTION RATE	
										ORNL	NIST
NICKEL AK	25-Jan-93	16:27	1	80	0.2814	24-May-91	16:25	6.50E+05	0.4	3.24E-15	3.14E-15
IRON FE-B1	27-Jul-93	18:43	3	102	0.5104	13-Jan-91	14:03	1.17E+04	0.3	2.90E-15	2.93E-15

United States Department of Commerce
National Institute of Standards and Technology
Gaithersburg, MD 20899 USA

REPORT OF SPECIAL MEASUREMENT

OF: HFIR Pressure Vessel
by use of NIST
FWT-67-20 Chlorostyrene Dosimeters

FOR: Oak Ridge National Lab (ORNL)
through
Jim Grundl, Neutron Interactions and Dosimetry Group Leader

ATTN: F. B. Kam
Reference:

DESCRIPTION: Chlorostyrene film packets were sent to ORNL for irradiation in their irradiator. Each packet consisted of three calibrated FWT-67-20 film dosimeters, held inside a 0.015mm layer of aluminum foil. Upon their return to NIST, the dosimeters were analyzed using a Cary 3 spectrophotometer(S/N 1101115, 4.0 nm S.B.W.). Absorbed dose interpretations were made from a calibration of the radiochromic dosimeters performed in June 1993. The results are summarized in the following table.

Dosimeter ID	NIST Interpolated Dose, kGy(D_{si})
31-33	26.0
40-42	26.4

Fig. 1

Temperature Dependence of Solid Phase Chemical Dosimeters.
Curve #5 Refers to Polychlorostyrene with 25 w/o Chlorine.

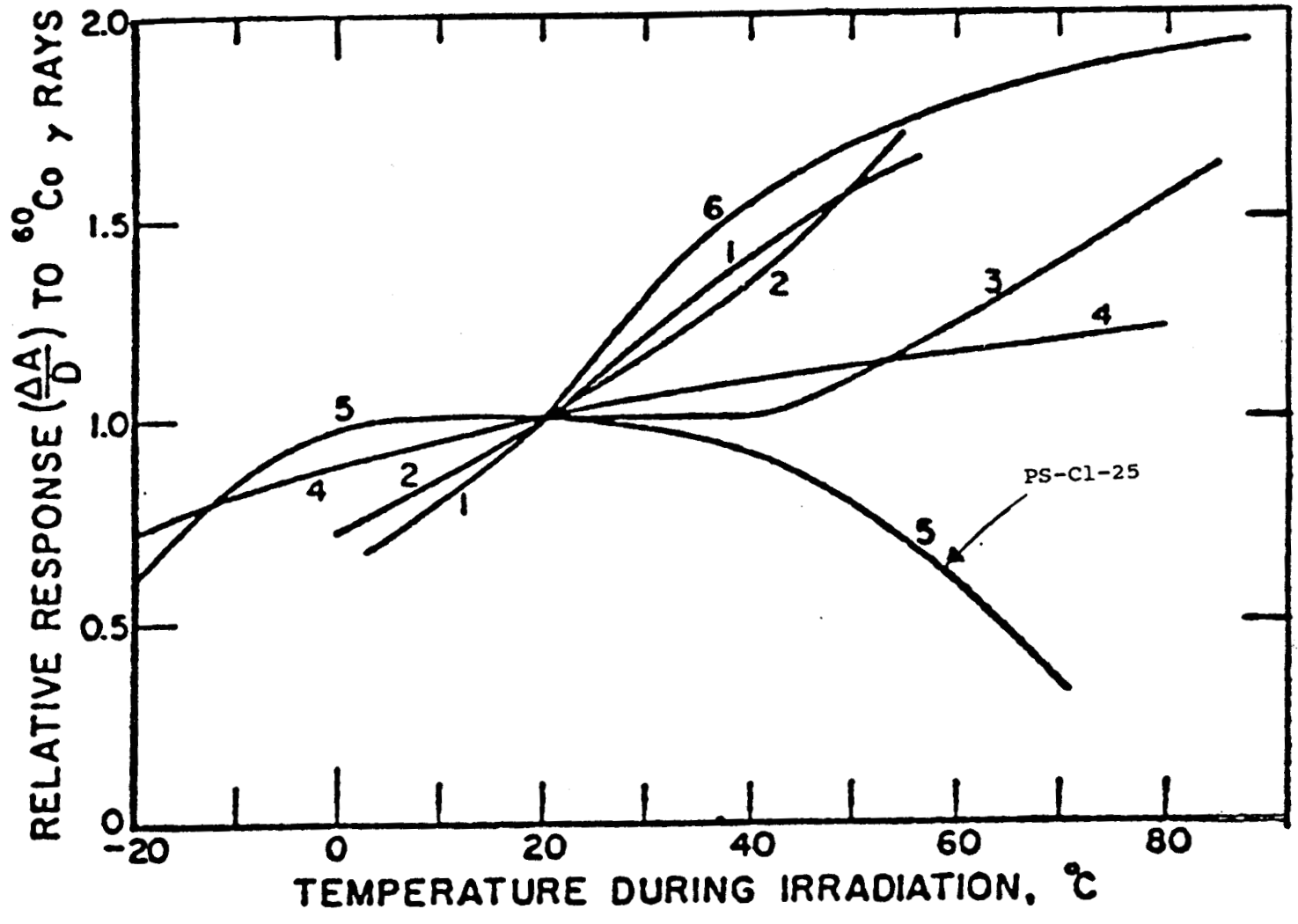

APPENDIX B

HELIUM ANALYSES OF BERYLLIUM HAFMs FROM HFIR: DOS-2/3

Enclosure
92RC00784
April 29, 1993

HELIUM ANALYSES OF BERYLLIUM HAFMs FROM HFIR: DOS-2/3

B. M. Oliver

April 29, 1993

Rockwell International
Rocketdyne Division
6633 Canoga Avenue
Canoga Park, California 91309

Work performed under ORNL Contract 36B-99979V

HELIUM ANALYSES OF BERYLLIUM HAFMs FROM HFIR: DOS-2/3

B. M. Oliver

Rockwell International
Canoga Park, California 91309

A. SUMMARY

Helium concentrations measured in six beryllium metal helium accumulation fluence monitors (HAFMs) irradiated in the High Flux Isotope Reactor (HFIR) at Oak Ridge National Laboratory (ORNL) are reported. The samples were irradiated as part of tests DOS-2 and -3 in the HFIR. The purpose of the tests were to check earlier measured helium generation and activation measurements conducted as part of the DOS-1 dosimetry experiment.

Mean helium concentration values measured in the beryllium HAFMs ranged from 1.51 appb at the Key 4,10 location, to 4.16 appb at the Key 2,9 location. The average measured helium concentration for the three beryllium HAFM sets at the DOS-2/3, Key 7,5 location is 2.73±0.04 appb, which is in excellent agreement with a value of 2.78±0.03 appb measured earlier at the Key 7,5 location in the DOS-1 experiment. Reproducibility between the duplicate analyses averaged 0.8%, very close to the inherent reproducibility of the analysis system.

No difference is observed in the measured helium concentrations for the bare and shielded beryllium HAFMs at the Key 7,5 location, indicating that the correction for small residual boron impurities in the beryllium is small at this location. Additionally, no difference is observed in the measured helium concentrations for the Lot 6 and Lot 7 beryllium material at the Key 7,5 location.

B. HELIUM ANALYSIS SAMPLES

Six sets of helium accumulation fluence monitors irradiated in the HFIR DOS-2 and -3 experiments were received from ORNL for helium analysis. The samples were received in two separate plastic bottles, one containing a single aluminum capsule labeled H56 and the other containing five aluminum capsules labeled H52, H53, H54, H55, and H57. The H56 capsule had been irradiated in a gadolinium cover. The remaining five capsules were irradiated bare.

Each capsule contained two sets of beryllium pieces from Rockwell Lot No. 6 and No. 7. The Lot 7 material had been used in the earlier DOS-1 experiment. Each set had been prepared previously at Rockwell and contained three individual pieces of beryllium metal weighing from 3 to 4 mg each wrapped in aluminum foil. The Lot 7 material was obtained from Electronics Space Products International (ESPI). The material has a stated purity of 99.99%. Previous measurements at Rockwell have indicated a residual helium content in the beryllium material of 0.050±0.030 appb (10^{-9} atom fraction), and a residual boron impurity of 8.9±2.0 wt. ppm (7.4±1.7 appm). The Lot 6 beryllium was obtained from Kawecki Berylco Industries, Inc. The stated beryllium purity is 99.78%. Residual boron content in the material, determined by Rockwell, is 5.6±0.7 wt ppm (4.7± 0.6 appm). No residual helium has been detected in the Lot 6 beryllium.

Five of the six capsules also contained separate lengths of Al-Li and Al-B dosimetry wire. The Al-Li alloy came from Rockwell Lot 5(I) material, originally fabricated by the Central Bureau for Nuclear Measurements (CBNM) at Geel, Belgium.[1] The composition of the Al-Li is Al-0.73±0.01 wt.% Li, with a ^{6}Li content of 95.7±0.1 at.%. The Al-B alloy [Rockwell Lot 6(I)] was also fabricated by CBNM, and has a composition of Al-0.484±0.01 wt.% B, with a ^{10}B content of 19.8 atom %. Capsule H57 did not contain any Al-Li or Al-B material.

Table 1 summarizes the HAFM samples included in each irradiation capsule. The mass values in Table 1 are those measured at ORNL during capsule assembly.

TABLE 1

HELIUM ACCUMULATION FLUENCE MONITORS IN HFIR: DOS-2/3

Capsule	Al-Li Alloy	Al-B Alloy	Be-Lot 6	Be-Lot 7
H52	7.78	8.73	14.85	17.89
H53	7.65	8.69	13.46	15.51
H54	7.38	8.90	17.70	16.90
H55	7.64	8.80	19.81	17.76
H56	7.64	8.76	19.08	18.28
H57	none	none	17.20	19.91

C. SAMPLE PREPARATION

Following identification by package number, each irradiation capsule was opened by cutting off the welded end using a small wire blade saw. The contents of each capsule were removed, and the individual samples identified and placed in separate coin envelopes. The present analysis effort was limited to the Be-Lot 7 samples located in each capsule, and the Be-Lot 6 sample located in Capsule H55.

Each of the analyzed beryllium samples were prepared in the same way. First, the package was carefully unwrapped and the individual beryllium pieces removed. Each piece was then examined under a low-power optical microscope to verify sample integrity, and weighed. The two highest mass pieces were then taken for duplicate helium analysis. Duplicate helium analyses are performed routinely to give an indication of the analysis reproducibility and also to give an indication of the gross helium homogeneity within each sample.

After selection, each beryllium piece was etched to remove ~0.05 mm off the surface. The purpose of the etching step was to remove surface material which could have been affected by α-recoil either into or out of the sample during irradiation. Etching was done in dilute hydrochloric acid (HCl), followed by rinsing in deionized water and then acetone. At intervals during the etching process, the sample was approximately weighted to verify the amount of material removed. Prior to helium analysis, the mass of each beryllium piece was accurately determined using a substitution weighing scheme and mass standards traceable to the National Institute for Standards and Technology (NIST).

D. HELIUM ANALYSIS PROCEDURE

The helium content of each specimen was determined by gas mass spectrometry following vaporization in a resistance-heated tungsten-wire crucible in one of the mass spectrometer system's high-temperature vacuum furnaces.(2) The absolute amount of ^{4}He released was measured relative to a known quantity of added ^{3}He "spike." The ^{3}He spikes were obtained by expanding and partitioning a known quantity of gas through a succession of calibrated volumes.(3) The mass spectrometer was calibrated for mass sensitivity during each series of runs by analyzing known mixtures of ^{3}He and ^{4}He.

E. HELIUM ANALYSIS RESULTS

The results of the helium measurements are given in Table 2, where they are listed as total atoms of helium released and as helium concentrations in atomic parts per billion (10^{-9} atom fraction). Conversion from total helium to helium concentration was based on a calculated value of 6.682 x 10^{22} atoms of beryllium per gram of material.

Two corrections have been applied to the helium data in Table 2. The first correction is to account for the small residual helium content of 0.05±0.03 appb in the Lot 7 material. This value had been determined at Rockwell through previous analysis of numerous unirradiated specimens of the Lot 7 material. During the present analysis series, an additional unirradiated piece of the beryllium was also analyzed and gave a value of 0.053, which is consistent with the previously determined 0.050± 0.030 appb value. Analysis of a single piece of unirradiated Lot 6 beryllium, showed no detectable residual helium (<0.006 appb). For the Lot 7 beryllium, the residual helium correction ranged from ~1.2 to 2.9% of the total helium generation.

The second correction was to account for helium generation from the known small boron impurities in the two beryllium lots (5.6 and 8.9 wt. ppm for Lots 6 and 7 respectively). The correction was calculated using a helium generation value for ^{10}B of 1628 appb, as measured earlier in the Key 7,5 location of the DOS-1 experiment, normalized for the thermal neutron flux at the present HFIR locations. Flux values used in the normalizations were from Pace et al.[4]. The boron impurity corrections ranged from 0.002 appb (~0.1 %) at Key 7,5, to 0.191 appb (~11%) at Key 4,10. No boron correction was applied to Sample H56-Be7, since the H56 irradiation capsule was shielded with gadolinium.

Absolute uncertainty (1σ) in the individual helium analysis results in Table 2, based on the cumulative uncertainties in the sample mass, isotope ratio measurement, and spike size, is estimated to be ~1%. Additional uncertainty from the two corrections applied to the data were discussed above.

F. DISCUSSION OF RESULTS

Mean helium concentration values measured in the DOS-2/3 beryllium HAFMs ranged from 1.51 appb at the Key 4,10 location in HFIR, to 4.16 appb at the Key 2,9 location. Reproducibility between the duplicate analyses averaged 0.8%. This is very close to the inherent reproducibility of the mass spectrometer system (from ~0.4 to 0.5%), and therefore indicates excellent homogeneity and reproducibility in the helium contents.

In addition to the observations noted above, several important additional observations can also be made:

1) The average measured helium concentration for the three beryllium HAFM sets at the DOS-2/3, Key 7,5 location is 2.73±0.04 appb, which is in excellent agreement with a value of 2.78±0.03 appb measured earlier at the Key 7,5 location in the DOS-1 experiment.

2) No significant difference is observed in the measured helium concentrations for the bare and shielded beryllium HAFMs at the Key 7,5 location. This verifies that the correction for small residual boron impurities in the beryllium is small at this location, and further, is introducing negligible additional uncertainty. Boron impurity corrections are somewhat larger at the other irradiation locations due to significantly higher thermal neutron flux levels.

3) No significant difference is observed in the measured helium concentrations for the Lot 6 and Lot 7 beryllium material at the Key 7,5 location. This verifies that there is no systematic effect on the helium generation from any differences which may exist between the two

TABLE 1

HELIUM CONCENTRATIONS IN DOS-2/3 BERYLLIUM SAMPLES

Specimen	HFIR Location	Specimen Mass[a] (mg)	Measured ^4He (10^{11} atoms)	Helium Concentration (appm) Measured[b]	Corrected[c]	Average[d]
H52-Be7-A	Key 2,9	2.560	6.154	3.598	3.450	3.45
-B	bare	2.718	6.541	3.602	3.454	±0.00
H53-Be7-A	Key 4,2	2.109	4.054	2.877	2.644	2.61
-B	bare	2.586	4.864	2.815	2.582	±0.04
H54-Be7-A	Key 4,10	2.396	2.833	1.770	1.529	1.51
-B	bare	2.643	3.050	1.727	1.486	±0.03
H55-Be7-A	Key 7,5	2.588	4.773	2.760	2.708	2.69
-B	bare	2.658	4.856	2.734	2.682	±0.02
H55-Be6-A	Key 7,5	2.903	5.289	2.727	2.725	2.73
-B	bare	2.430	4.455	2.744	2.742	±0.01
H56-Be7-A	Key 7,5	2.014	3.789	2.816	2.766	2.77
-B	shielded	2.396	4.522	2.824	2.774	±0.01
H57-Be7-A	Key 2,9	3.985	11.56	4.341	4.193	4.16
-B	bare	3.747	10.72	4.282	4.134	±0.04

[a]Mass uncertainty is ±1 μg.
[b]Helium concentration in atomic parts per million (10^{-6} atom fraction) with respect to the total number of beryllium atoms in the specimen.
[c]Measured helium concentrations corrected for residual helium in the material and for helium generation from small amounts of boron impurity (see text).
[d]Mean and standard deviation (1σ) of Column 6 data.

material lots. This strongly suggests that no unknown impurities are contributing to the observed helium generation.

REFERENCES

1. J. Van Audenhove, Central Bureau for Nuclear Measurements, Geel, Belgium, CBNM Lots SP 3335(I) and SP 3336(I), July, 1979.

2. Harry Farrar IV and B. M. Oliver, "A Mass Spectrometer System to Determine Very Low Levels of Helium in Small Solid and Liquid Samples," J. Vac. Sci. Technol. A4, 1740 (1986).

3. B. M. Oliver, J. G. Bradley, and Harry Farrar IV, "Helium Concentration in the Earth's Lower Atmosphere," Geochim. Cosmochim. Acta 48, 1759 (1984).

4. J. V. Pace III, C. O. Slater, and M. S. Smith, "Letter Report on Beginning-Of-Cycle HFIR Flux/Response Calculations at Keys 2, 4, 5, and 7", July 30, 1992.

APPENDIX C

RESULTS FOR SOLID STATE TRACK RECORDERS

STC REPORT 93-9TD1-ORNLA-R1

NEUTRON DOSIMETRY RESULTS FOR SOLID STATE TRACK RECORDERS IRRADIATED IN THE HIGH FLUX ISOTOPE REACTOR AT OAK RIDGE NATIONAL LABORATORY

F. H. Ruddy, J. G. Seidel, and J. L. Gonzalez
Track Recorder Laboratory

May 24, 1993

Westinghouse STC
1310 Beulah Road
Pittsburgh, Pennsylvania 15235-5098

Westinghouse

NEUTRON DOSIMETRY RESULTS FOR SOLID STATE TRACK RECORDERS IRRADIATED IN THE HIGH FLUX ISOTOPE REACTOR AT OAK RIDGE NATIONAL LABORATORY

F. H. Ruddy, J. G. Seidel, and J. L. Gonzalez
Track Recorder Laboratory

ABSTRACT

Solid State Track Recorder (SSTR) neutron dosimetry sets exposed in the High Flux Isotope Reactor at Oak Ridge National Laboratory have been analyzed.

Absolute fission rates have been obtained for each of the 12 SSTR neutron dosimeters that were exposed, with 11 out of 12 having uncertainties less than 5%.

Results of physical examination, uniformity analyses, and calibration data review of the ultra low-mass fissionable deposits indicate that all 12 of the deposits are reusable in subsequent dosimetry measurements.

93-9TD1-ORNLA-R1

Westinghouse

1. INTRODUCTION

Solid State Track Recorder (SSTR) neutron dosimeters were prepared at Westinghouse Science & Technology Center (W STC) under contract to Martin Marietta Energy Systems for exposures at Oak Ridge National Laboratory in the High Flux Isotope Reactor (HFIR). A total of twenty-one ultra low-mass fissionable deposits of ^{235}U, ^{237}Np, and ^{238}U with mica SSTRs were assembled into ten dosimetry packets during November, 1992. The as-built information for these dosimeters is contained in Table 1. Following irradiation of four of these dosimetry packets in the reactor, the dosimeters were retrieved and shipped to W STC for analysis. The SSTR neutron dosimeters were received and disassembled for analyses in March, 1993. Analyses of these SSTR neutron dosimeters have been completed, and the calculated fission reaction rates and associated experimental uncertainties are contained in this report.

Westinghouse

Table 1 SSTR Neutron Dosimetry As-Built Information for HFIR

Location*	Packet Label**	Cover	Deposit Label/SSTR Label ^{235}U	^{237}Np	^{238}U
Key 7, P5	HFIR-1B	Al	W-459/W32-1	---	---
Key 7, P5	HFIR-1C	Gd	W-482/W32-2	W-534/W32-3	W-211/W32-4
Key 4, P2	HFIR-2B	Al	W-433/W32-5	---	---
Key 4, P2	HFIR-2C	Gd	W-462/W32-6	W-535/W32-7	W-201/W32-8
Key 2, P9	HFIR-3B	Al	W-451/W32-9	---	---
Key 2, P9	HFIR-3C	Gd	W-456/W32-10	W-565/W32-11	W-198/W32-12
Key4, P8	HFIR-4B	Al	W-83/W32-13	---	---
Key4, P8	HFIR-4C	Gd	W-75/W32-14	W-564/W32-15	W-200/W32-16
spare	HFIR-5B	Al	W-449/W32-17 W-454/W32-20	---	---
spare	HFIR-5C	Gd	W-500/W32-21	W-554/W32-22	W-217/W32-23

*The SSTR neutron dosimetry packets were designed for irradiations in these locations. However, the actual deployment was different (see text and Table 6).

**Packets labeled B are for bare or Al covered irradiation positions. Packets labeled C are for Gd or Cd covered irradiation positions.

Westinghouse

2. DOSIMETRY SET DESIGN

Isotopic reaction rates for the dosimetry locations were estimated by L. Greenwood[1] using his SCOPER computer code and F. Kam's calculated neutron spectra and ENDF/B-V cross sections (see Appendix A).

These neutron fluences were used to calculate the fissionable deposit masses that would give optimum track densities as a result of exposure to fluences equal to those calculated. Deposit masses were sized to give approximately 20,000 tracks for each location. In addition, a fifth dosimetry set was assembled containing two ^{235}U deposits and ^{238}U and ^{237}Np deposits sized to give useful results if exposed in any of the four locations.

All SSTR dosimetry sets were fabricated and assembled in a dust-free laboratory. Each set was double-wrapped in 0.5 mil Al foil to protect the dosimeters from dust while outside of the laboratory. Even small amounts of dust can lead to fissionable background due to the ubiquitous presence of natural uranium as an impurity at the ppm level. The SSTR dosimetry sets were not designed to be sealed against the incursion of water or other solvents.

Westinghouse

3. DOSIMETRY SET RECOVERY AND DISASSEMBLY

Four of the SSTR neutron dosimetry packets described in Table 1 were loaded in dosimetry capsules and the capsules were deployed in HFIR. At the end of the irradiation, the dosimeters were removed and the SSTR dosimetry packets were separated and sent to W STC for analysis.

During disassembly of the SSTR neutron dosimetry sets, the initial as-built locations of the mica SSTRs and fissionable deposits listed in Table 1 were verified. No exceptions to the as-built data were noted. However, it was noted during disassembly that the packets had apparently been washed with a solvent, rewrapped, and relabelled. It was determined[2] that, because of HFIR operating rules, the ink from the marker pen used to label the packets had to be removed prior to irradiation. During the course of the washing and relabling, some solvent penetrated into the interior of the packets. Although the packets were dry when received, some smearing of the ink markings on the backs of deposits was noted, particularly in the case of capsule HFIR-1C. Therefore, particular attention was directed to the appearance of the tracks in the SSTRs. The presence of solvent within the SSTR packet during the irradiation would attenuate the ranges of the fission tracks in the SSTRs leading to smaller tracks. Also, damage to the deposits in the form of partial dissolution or contamination by the solvent could result. In all cases, the track sizes appeared normal and the track densities dropped abruptly at the edges of the deposits, indicating that no observable deposit damage or contamination had occurred.

No other evidence of physical damage to any of the SSTR packets was observed, and the overall as-received condition of the sets was good. After disassembly each mica SSTR and fissionable deposit was closely inspected under a microscope for physical damage which may have occurred during exposure or shipment. All deposits and all SSTRs appeared free from detectable physical damage.

Westinghouse

4. SSTR PROCESSING AND ANALYSIS

All 12 SSTRs were etched in 49% HF at 22.0°C for a minimum of one hour. Deposit uniformities were consistent with previous experience in most cases and presented no difficulties for track scanning.

All SSTRs but one were scanned with the W STC Automated Track Scanner[3]; SSTR W32-2 could not be scanned with the automated scanner because of its large track density (greater than 10^6 tracks per cm^2.). This SSTR was subjected to a manual estimating procedure.[4] Although replicate agreement of the two manual scans was within 25%, because of the very high track density the number counted is probably low. Therefore, the fission rate derived from SSTR W32-2 should be regarded as a lower limit. The number of fissions obtained for each SSTR is contained in Table 2. In all cases, at least two independent scans were performed and replicate agreement between the two scans was required. The minimum and maximum track counts obtained were 22,957 and 1,458,815 respectively.

All of the automated track scanning data and scanner operating parameters have been stored on computer disks on a microscope field-of-view by field-of-view basis. A listing of the computer file names corresponding to each SSTR scan is contained in Table 3.

In addition to the data files, in all cases the SSTR itself is being stored as a permanent record of the SSTR neutron dosimetry exposure.

Westinghouse

Table 2. High Flux Isotope Reactor SSTR Scanning Data

SSTR Label	Manual JGS	Manual JLG	Automated Scan 1	Automated Scan 2	Avg*
W32-2	894,006	1,458,815			1.18×10^6 (±24%)
W32-3			329,134	324,793	326,963 (±0.66%)
W32-4			279,720	261,401	270,561 (±3.39%)
W32-6			103,001	99,548	101,274 (±1.70%)
W32-7			96,639	97,404	97,021 (±0.39%)
W32-8			208,906	208,810	208,857 (±0.02%)
W32-10			84,028	83,174	83,601 (±0.51%)
W32-11			75,728	77,114	76,421 (±0.91%)
W32-12			92,338	90,802	91,569 (±0.84%)
W32-14			23,482	22,958	23,220 (±1.13%)
W32-15			67,127	66,782	66,954 (±0.26%)
W32-16			164,865	166,909	165,887 (±0.62%)

* The number in parentheses represents the standard deviation of the average of the results of independent scans of each SSTR.

Westinghouse

Table 3. Permanent Computer Files for the High Flux Isotope Reactor SSTR Scans

SSTR Label	File Name Scan 1	File Name Scan 2
W32-3	HF32-3A	HF32-3D
W32-4	HF32-4A	HF32-4B
W32-6	HF32-6A	HF32-6B
W32-7	HF32-7A	HF32-7B
W32-8	HF32-8A	HF32-8B
W32-10	HF32-10C	HF32-10D
W32-11	HF32-11A	HF32-11B
W32-12	HF32-12A	HF32-12B
W32-14	HF32-14B	HF32-14C
W32-15	HF32-15A	HF32-15B
W32-16	HF32-16A	HF32-16B

Westinghouse

5. SSTR NEUTRON-INDUCED FISSION RATES

The SSTR track counts and the fissionable deposit mass calibration data were used to calculate fission rates in fissions per atom for each of the SSTRs scanned. In all cases, the fissionable deposit mass scales have been renormalized to the results of benchmark irradiations of representative deposits at the National Institute for Standards and Technology (NIST).[7-12]

The measured fission rates are listed in Table 4.

The overall uncertainties were calculated from a quadrature summation of the individual sources of uncertainty listed in Table 5.

After the irradiation it was reported[2] that the intended locations for the SSTR packets that are listed in Table 1 were not used. The SSTR fission reaction rates are listed with the locations actually used in Table 6. The relocation of the SSTR packet HFIR-1C is primarily responsible for the generally high track densities for this packet and the track density exceeding the scannable limit in SSTR W32-2.

In general, the reaction rates measured are higher than calculational estimates[1] prior to the exposures. The track densities obtained were therefore generally higher than anticipated, but still well within the scannable range.

Table 4 High Flux Isotope Reactor SSTR Fission Rates

Packet Label	Isotope	Deposit Label	Mass(ng)	SSTR Label	Number of Fissions*	Fissions/Atom
HFIR-1C	^{235}U	W-482	0.8981(±0.73%)	W32-2	1.18×10^{6}(±24%)**	$>5.1\times10^{-7}$**
	^{237}Np	W-534	7.897(±1.95%)	W32-3	326,963(±0.66%)	1.63×10^{-8}(±2.4%)
	^{238}U	W-211	28.04(±0.64%)	W32-4	270,561(±3.39%)	3.81×10^{-9}(±4.1%)
HFIR-2C	^{235}U	W-462	3.490×10^{-2}(±2.40%)	W32-6	101,274(±1.70%)	1.13×10^{-6}(±3.2%)
	^{237}Np	W-535	3.316(±1.98%)	W32-7	97,021(±0.39%)	1.15×10^{-8}(±2.4%)
	^{238}U	W-201	26.36(±1.77%)	W32-8	208,857(±0.02%)	3.13×10^{-9}(±2.4%)
HFIR-3C	^{235}U	W-456	2.475×10^{-2}(±1.80%)	W32-10	83,601(±0.51%)	1.32×10^{-6}(±2.4%)
	^{237}Np	W-565	2.809(±1.71%)	W32-11	76,421(±0.91%)	1.07×10^{-8}(±2.5%)
	^{238}U	W-198	14.86(±0.40%)	W32-12	91,569(±0.84%)	2.44×10^{-9}(±2.5%)
HFIR-4C	^{235}U	W-75	0.319(±1.00%)	W32-14	23,220(±1.13%)	2.84×10^{-8}(±2.7%)
	^{237}Np	W-564	2.937(±2.08%)	W32-15	66,954(±0.26%)	8.98×10^{-9}(±2.5%)
	^{238}U	W-200	25.43(±0.91%)	W32-16	165,887(±0.62%)	2.58×10^{-9}(±2.4%)

*The number in parentheses is the standard deviation of the average of at least two replicate scans of the same SSTR.

**The track density for this SSTR exceeds the upper limit for accurate track counting. Although a relative standard deviation of 24% was obtained, the track count may be low by as much as a factor of two. Therefore, the derived fission rate should be regarded as a lower limit.

Westinghouse

Westinghouse

Table 5. Sources Of Uncertainty In SSTR Neutron-Induced Fission Rate Measurements

Source of Uncertainty	Magnitude (1σ)
1. Track Identification	
Manual Estimate - agreement between independent scanners	25%[4]
Automated	1.0-1.8%[3]
2. Optical Efficiency*	
Manual	0.86%[5]
Automated	1.19%[6]
3. Statistics on number of tracks observed.	$10^2(1/N)^{1/2}$ where N is the number of tracks observed.
4. Deposit Mass Uncertainty (includes uncertainties due to radiometric counting statistics, decay constants, spike ratios, and counter efficiencies).	$\leq$ 4%

* The optical efficiency is the ratio of tracks/cm^2 in an SSTR to fissions/cm^2 in a neighboring thin deposit held in firm contact with the SSTR.

Table 6. SSTR NEUTRON DOSIMETRY RESULTS FOR HFIR

SSTR ID	LOCATION	ISOTOPE	FISSIONS/ATOM
W32-2	K2,P9	^{235}U	$>5.1\times10^{-7}$
W32-3	K2,P9	^{237}Np	1.63×10^{-8} (±2.4%)
W32-4	K2,P9	^{238}U	3.81×10^{-9} (±4.11)
W32-6	K4,P2	^{235}U	1.13×10^{-6} (±3.2%)
W32-7	K4,P2	^{237}Np	1.15×10^{-8} (±2.4%)
W32-8	K4,P2	^{238}U	3.13×10^{-9} (±2.4%)
W32-10	K4,P10	^{235}U	1.32×10^{-6} (±2.4%)
W32-11	K4,P10	^{237}Np	1.07×10^{-8} (±2.5%)
W32-12	K4,P10	^{238}U	2.44×10^{-9} (±2.5%)
W32-14	K7,P5	^{235}U	2.84×10^{-8} (±2.7%)
W32-15	K7,P5	^{237}Np	8.98×10^{-9} (±2.5%)
W32-16	K7,P5	^{238}U	2.58×10^{-9} (±2.4%)

6. SUMMARY

12 SSTR neutron dosimeters were exposed in the High Flux Isotope Reactor and fission rates have been obtained from each SSTR.

Absolute uncertainties on the fission rates are less than 4% in ten out of twelve cases. All 12 deposits were found to be in excellent condition and can be used for subsequent cavity dosimetry measurements.

The relevant analyses data for the High Flux Isotope Reactor SSTR neutron dosimeters will be kept in archival storage. The SSTRs themselves will be stored as permanent records of the dosimetry exposure.

7. REFERENCES

1. L. R. Greenwood, Private Communication (November, 1992).

2. F. B. K. Kam, Private Communication (May, 1993).

3. F. H. Ruddy, A. E. Manhardt, and J. G. Seidel, "Analysis of Solid State Track Recorders with the Westinghouse Research and Development Center Automated Track Counter", Sixth ASTM - Euratom Symposium on Reactor Dosimetry, Jackson, WY, June 1987 ASTM STP-1001, p. 676 1989).

4. F. H. Ruddy and J. H. Roberts, "Solid State Track Recorder Measurements at High Neutron Fluence and High Temperature", Nuclear Tracks and Radiation Measurements 11, 193 (1986).

5. J. H. Roberts, F. H. Ruddy and R. Gold, "Optical Efficiencies for Fission Fragment Track Counting in Muscovite Solid State Track Recorders", Nuclear Tracks and Radiation Measurements", 8, 365 (1984).

6. F. H. Ruddy, "Advances in High Fluence Solid State Track Recorder Neutron Dosimetry", Nuclear Tracks and Radiation Measurements 19, 521 (1991).

7. F. H. Ruddy, "Benchmark Referencing of Babcock & Wilcox Solid State Track Recorder Fissionable Deposits in Standard Neutron Fields", Westinghouse R&D Report 88-2S31-SSTRB-R2, August 5, 1988.

8. F. H. Ruddy and J. G. Seidel, "Solid State Track Recorder Pressure Vessel Surveillance Neutron Dosimetry at Commercial Light Water Reactors," Sixth ASTM-Euratom Symposium on Reactor Dosimetry, Jackson, WY, June 1987 ASTM STP-1001 p. 175 (1989).

9. F. H. Ruddy and E. D. McGarry, "Benchmark Referencing of Ultra Low-Mass Solid State Track Recorder Neutron Dosimetry in NBS Standard Neutron Fields" in Proceedings of IAEA Advisory Group Meeting on Status and Requirements of Nuclear Data for Radiation Damage and Related Safety Aspects, IAEA Press, Vienna (in press) Westinghouse Science & Technology Center Report 89-1S31-RAPRO-P4, August 31, 1989.

10. F. H. Ruddy and E. D. McGarry, "Benchmark Referencing of Solid State Track Recorder Neutron Dosimeters in Standard Neutron Fields" in Proceedings of the Seventh ASTM-Euratom Symposium on Reactor Dosimetry, Strasbourg, France, August 29, 1990, Kluwer Academic Publishers, London, 1992, p 825.

11. F. H. Ruddy and E. D. McGarry, "Solid State Track Recorder Neutron Dosimetry and Its Applications", OECD Nuclear Energy Agency Specialists Meeting on In-Core Instrumentation and Reactor Core Assessment, October 1, 1991 (Proceedings in press), Westinghouse Science & Technology Center Report 91-5TD1-SCANS-P1, September 16, 1991.

12. F. H. Ruddy, "Neutron Dosimetry in High Intensity Fields: A Review", Nuclear Tracks and Radiation Measurements 11, 197 (1986).

APPENDIX A

Reaction Rate Estimates Used for SSTR Neutron Dosimeter Design

Battelle
Pacific Northwest Laboratories
Battelle Boulevard
P.O. Box 999
Richland, WA 99352

FACSIMILE TRANSMITTAL

DATE: November 6, 1992

To: Frank Ruddy
Company: Westinghouse
City/State: Pittsburgh, PA
Facsimile #: 412-256-1007
Telephone #: 412-256-1064

From: Larry Greenwood
Analytical Chemistry Laboratory
Facsimile #: 509-376-1297
Telephone #: 509-376-6918

Transmittal Consists of [2] Page(s) including cover page.

Calculated Reaction Rates for HFIR Surveillance Positions

	Key 7, P5	Key 4, P2	Key 2, P1	Key 4, P8
U-235(n,f)	1.76E-13	1.34E-11	7.25E-12	3.97E-12
+Gd	2.40E-15	2.55E-14	2.49E-14	2.33E-14
U-238(n,f)	6.29E-17	1.13E-16	2.72E-16	1.64E-16
Np-237(n,f)	2.37E-16	9.27E-16	1.38E-15	9.43E-16

93-9TD1-ORNLA-R1

APPENDIX D

NEUTRON TRANSPORT CALCULATIONS FOR HFIR

Joseph V. Pace III,[1] Charles O. Slater,[1] Mark S. Smith[1]

THREE-DIMENSIONAL DISCRETE ORDINATES RADIATION TRANSPORT CALCULATIONS OF NEUTRON FLUXES FOR BEGINNING-OF-CYCLE AT SEVERAL PRESSURE VESSEL SURVEILLANCE POSITIONS IN THE HIGH FLUX ISOTOPE REACTOR

REFERENCE: Pace III, J. V., Slater, C. O., Smith, M. S., "Three-Dimensional Discrete Ordinates Radiation Transport Calculations of Neutron Fluxes for Beginning-of-Cycle At Several Pressure Vessel Surveillance Positions in the High Flux Isotope Reactor," Reactor Dosimetry ASTM STP 1228, Harry Farrar IV, E. Parvin Lippincott, and John G. Williams, Eds., American Society for Testing and Materials, Philadelphia, 1994.

ABSTRACT: The objective of this research was to determine improved thermal, epithermal, and fast fluxes and several responses at mechanical test surveillance location keys 2, 4, 5, and 7 of the pressure vessel of the Oak Ridge National Laboratory High Flux Isotope Reactor (HFIR) for the beginning of the fuel cycle. The purpose of the research was to provide essential flux data in support of radiation embrittlement studies of the pressure vessel shell and beam tubes at some of the important locations.

KEYWORDS: radiation damage, radiation transport, reactor pressure vessel, neutron fluxes, damage surveillance, dosimetry

---

The High Flux Isotope Reactor (HFIR) (Fig. 1) at the Oak Ridge National Laboratory began full-power operation in 1966 at 100 MW. As indicated by its name, it has a primary purpose of producing transuranium isotopes for research, industrial and medical applications. Because it has the highest steady-state neutron flux available in any of the world's reactors [1], it can provide for a myriad of other test and experiments in various irradiation facilities throughout the reflector.

The reflector core assembly is located in 2.44-m diameter pressure vessel (Fig. 2), which itself is located in a pool of water. It has a target in the center, inner and outer fuel regions, a reflector composed of removable and permanent beryllium, water, and finally the pressure vessel.

For the first 20 years of HFIR operation, radiation damage was monitored with a vessel-material surveillance program. In November 1986, these tests indicated that the reactor vessel was being embrittled by neutron irradiation faster than previously predicted. After the HFIR was shut down for approximately two years, it was allowed to restart, but with a power of 85 MW.

---

[1]Research staff, Oak Ridge National Laboratory, P.O. Box 2008, Oak Ridge, TN 37831-6363.

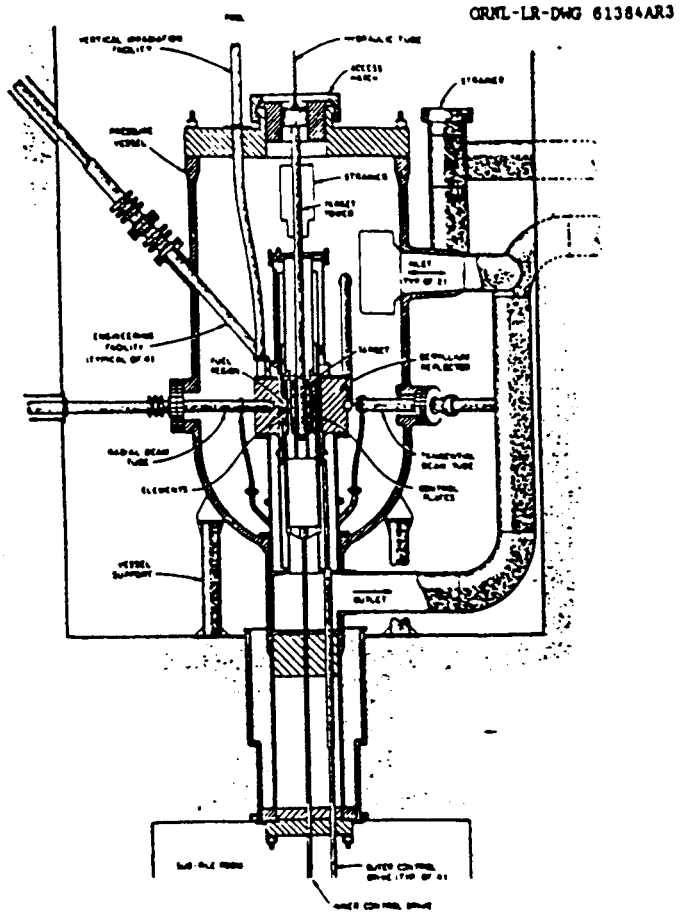

Fig. 1--Vertical section of the HFIR pressure vessel and core.

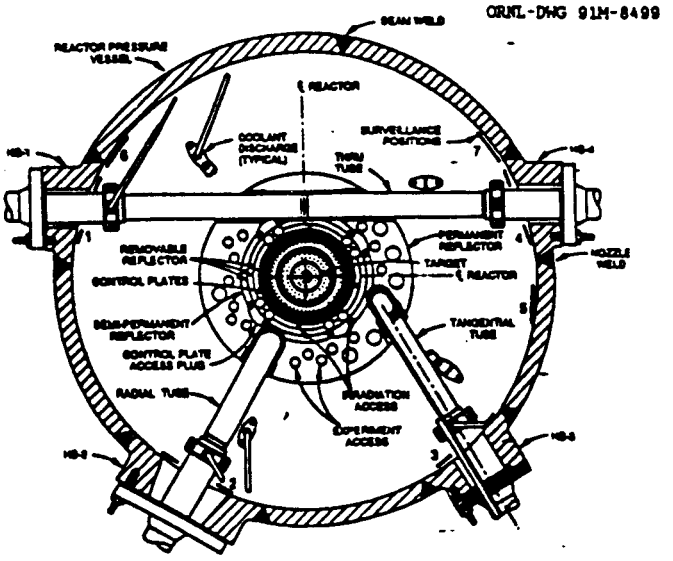

Fig. 2--Sectional plan view of the HFIR target, reactor core, beryllium reflector, coolant, and pressure vessel.

During the two-year shutdown period, extensive studies were undertaken to determine the radiation damage. As part of this effort, reactor fluxes were required to be determined independent of those derived from experiments. Therefore, this study was initiated to determine the thermal, epithermal, and fast beginning-of-cycle (BOC) neutron flux at keys (surveillance positions) 2, 4, 5, and 7 (shown as numbered line segments in Fig. 2) on the pressure vessel of the HFIR. The purpose of the calculations was to aid in determining the reduction in fracture toughness of the HFIR vessel.

CALCULATIONAL PROCEDURE

The procedure to calculate the flux at keys 2, 4, 5, and 7 was to produce a broad-group cross-section set, run a two-dimensional discrete-ordinates calculation to produce directional fluxes throughout the model, produce three-dimensional models which included the keys of interest, and make the three-dimensional calculations. The initial set of calculations was to be made for key 7.

Neutron cross sections required for the calculations were chosen from the 99 neutron group ANSL-V[2] library. One- [3] and two-dimensional [4] HFIR geometry models had been previously constructed for the updated HFIR safety analysis. The one-dimensional model for BOC and the cross-section library were used in the AMPX [5] modules BONAMI, NITAWL, and XSDRNPM to self-shield the cross sections and reduce them to a 64-neutron group structure, which was more economically manageable. This group structure contained 23 energy groups from 20 MeV to 1.07 MeV, 12 groups from 1.07 MeV to 0.1 MeV, 19 groups from 0.1 MeV to 0.397 eV, and 10 groups from 0.397 to 1.0×10^{-5} eV. There were a total of 12 upscatter groups, which covered the energy range 3 to 1.0×10^{-5} eV. The criteria for this broader group cross-section set was that the group fluxes in the water between the permanent beryllium and the pressure vessel could not deviate from the 99-group fluxes by more than five percent at each one-dimensional space mesh.

The 64-group cross sections and the two-dimensional model were input to the DORT code [6] to produce directional fluxes at locations near Key 7. Then the VISTA code [7] reformatted the DORT directional fluxes for input to the DOTTOR code [8]; this code transformed the VISTA flux into a surface boundary source for the three-dimensional discrete-ordinates transport code TORT [9].

A three-dimensional model of the HFIR which contained Beam Tube 4, and thus Keys 4 and 7, had been developed previously [10]. This configuration consisted of a 32x33x6 mesh with X values between 0.0 and 128.52 cm, Y values between -15.24 and 88.96 cm, and Z values between 0.0 and 15.24 cm. The transformed directional fluxes from the two-dimensional calculation were input to the three-dimensional radiation transport code. The boundary sources for TORT using these geometry models were calculated using an S_{10} angular quadrature and a P_3 Legendre expansion cross-section set of the 64 neutron-group library. Calculated three-dimensional flux results at Key 7 indicated that previous calculations in the late 1980's [10] had produced thermal fluxes that were an order of magnitude larger.

At this point, two additional efforts were made to help resolve this anomaly. First, several one-dimensional calculations were made to determine if the present transport or cross sections or both were in error. Second, a dosimetry specimen containing thermal activation material was inserted at Key 7 in the HFIR, since there were no experimental values to compare to the results of the transport calculations.

For the first effort, several one-dimensional calculations were made with the present set of cross sections, with those used previously in the late 1980's [11], and with another set which contained many thermal groups which contained upscatter [12]. The results indicated that the late 1980's set contained thermal cross sections which were not correct. Results from the second effort of the irradiation in the HFIR indicated that the thermal fluxes from the current set of calculations were in much better agreement.

The second model contained beam tube 2 with key 2, which consisted of a 53x16x16 mesh with X values between 27.66 and 127.0 cm, Y values between 0.0 and 20.24 cm, and Z values between 0 and 20.24. The TORT calculations were also performed with the same angular quadrature and cross-section expansion as those for key 7.

The three-dimensional XYZ geometry representation for Key 5 was modeled last. Previous calculations [10] indicated a concern that neutron streaming in beam tube 4 might influence the response at Key 5. Therefore, beam tube 4 was included in the calculational model.

Since the model had to include Key 5, Ionization Chamber 3, and beam tube 4, it was necessary to reduce the amount of data being handled to manageable sizes. Therefore, while the calculation was performed with the 64 neutron-group cross sections, the angular quadrature and the cross-section Legendre expansion were reduced to S_6 and P_1, respectively. The effects which lowering those parameters have on the fluxes at Keys 4 and 5 were studied for the top 52 groups using two-dimensional DORT calculations (thermal neutron fluxes were not calculated due to the additional computational time required for iterating over those groups). The DORT calculations were performed with an angular quadrature and a cross-section Legendre expansion of $S_{10}P_3$, $S_{10}P_1$, and S_6P_1, respectively. The results showed that the largest effect was due to the reduction of the scattering order (fluxes lowered by factors of 1.65 to 1.75 between the $S_{10}P_3$ and $S_{10}P_1$ cases). The overall effect of changing the calculation from $S_{10}P_3$ to S_6P_1 was a nearly uniform factor of 2.0 decrease in the flux at the specimen positions for all 52 groups. It is not certain whether this factor holds for Key 4 locations, where results are influenced greatly by neutron streaming in the beam tube. Nor is it certain that the factor is applicable to the thermal-neutron fluxes. Nevertheless, a factor of 2.0 was applied to the calculated fluxes and responses for the Key 5 positions.

RESULTS

As reported above, a dosimetry experiment was performed in 1992 at a HFIR surveillance location on the vessel wall at the mid-plane of the core. Position 5 (8 total positions) of key 7 (Fig. 2) was chosen as the exposure location for the experiment and corresponds to the fourth position nearest horizontal beam tube 4 which exits the reactor pressure vessel. The dosimetry capsule contained gold, silver, cobalt, nickel, and neptunium activation monitors; additionally, helium accumulation monitors of lithium/aluminum, boron/aluminum, and beryllium were included.

At this location, the measured thermal flux was 2.4×10^{12} neutrons.$m^{-2}.s^{-1}$ versus 3.7×10^{12} neutrons .$m^{-2}.s^{-1}$ from the calculations. The measured fast flux (> 1 MeV) from nickel monitors was 1.5×10^{12} neutrons .$m^{-2}.s^{-1}$ versus 1.2×10^{12} neutrons .$m^{-2}.s^{-1}$ for the calculations. Some of these discrepancies may be due to the calculation being made at the beginning of cycle; future work to reduce the variances will include calculations at the middle-of-cycle and end-of-cycle.

There were very large discrepancies in the measurements of the fast flux from the neptunium and beryllium monitors (2.6×10^{13} neutrons $.m^{-2}.s^{-1}$), a factor of 15 higher than from the nickel monitor. Initially, the problem was investigated by concentrating the effort on neutron contributions to the beryllium monitors from neutrons produced in the beryllium reflectors by gamma rays. Since gamma-ray cross sections were required, a coupled 39-neutron group (subset of the 99-neutron group) and 44-gamma group library was used. Several HFIR one-dimensional coupled neutron-gamma radiation transport calculations were made using the model developed for the cross-section production. This model contained the target area, inner and outer core, removable and permanent beryllium reflectors, water, and pressure vessel. No beam tubes were included since the model was one-dimensional. However, this time a beryllium gamma-neutron (g,n) cross section was included to account for the neutrons produced in the reflectors from gamma rays. The results of these calculations indicated that the neutron flux at the pressure vessel could increase only by about 30 percent, which was insufficient to cause the experimental discrepancy.

From the one-dimensional neutron-gamma calculations, it was noticed that the gamma-ray flux at the pressure vessel was three to four orders of magnitude larger than the neutron flux, with most of the gamma flux coming from the core[13] The HFIR was constructed such that once gamma-rays had left the core region, the only materials they encountered before the pressure vessel were the beryllium reflectors and the water, all of which were low-Z materials, and thus would not reduce the gamma flux very much. Therefore, the beryllium (g-n) and neptunium-237 gamma-fission (g,f) cross sections were folded with the gamma fluxes, and compared to the beryllium neutron and neptunium-237 neutron-fission (n,f) responses obtained from the neutron fluxes at the pressure vessel. The ratio of the helium production from the beryllium gamma-produced neutron flux to that from the core-produced neutron flux was 80; and the ratio of the neptunium-237 (g,f) response to the neptunium-237 (n,f) at the pressure vessel was 50. Thus, it appeared very possible that the increase in the helium production in beryllium and the increase in the neptunium-237 fission response in the monitors at the pressure vessel was due to the high gamma flux at that location, and thus the experimental flux values could not be compared with the calculated values. Additional experimental verification of this would be undertaken separately.

CONCLUSION

Neutron fluxes have been calculated using the three-dimensional discrete-ordinates code TORT for HFIR keys 2, 4, 5, and 7. For the only position where measurements were made, the three-dimensional neutron transport calculations have yielded results that are about 50 percent high in the thermal range and 20 percent low in the fast range. While some activation measurements yielded inconsistent flux values, the inconsistencies have partially been explained by gamma-ray interactions in the foil or neutron production by gamma-ray interactions near the vessel.

REFERENCES

[1] Pamphlet titled "High Flux Isotope Reactor", Oak Ridge National Laboratory, P.O. Box 2008, Oak Ridge, TN 37831-6387, July 1991.

[2] W.E. Ford, et al, "ANSL-V: ENDF/B-V Based Multigroup Cross-Section Libraries for Advanced Neutron Source (ANS) Reactor Studies,"Oak Ridge National Lab, ORNL-6618, 1990.

[3] R.T. Primm III, "Reactor Physics Input to the Safety Analysis Report for the High Flux Isotope Reactor", Oak Ridge National Lab, ORNL/TM-11956, October 1991.

[4] W.W. Engle, RZ Base Case, Shielding Input to the HFIR SAR, EPM.HFIR.91.001, Jun 1991.

[5] N.M. Greene, et al, "AMPX-77: A Modular Code System for Generating Coupled Multigroup Neutron-Gamma Cross-Section Libraries form ENDF/B-IV and/or ENDF/B-V", Oak Ridge National Lab, ORNL/CSD/TM-283, October 1992.

[6] W.A. Rhoades and R.L. Childs, "The DORT Two-Dimensional Discrete Ordinates Transport Code, "Nucl. Sci. & Engr. 99, 1, 88-89, May 1988.

[7] W.A. Rhoades, et al, "Vehicle Code System (VCS) User's Manual", Oak Ridge National Lab, ORNL-TM-4648, Aug 1974.

[8] J.L. Thompson, et al, "Development and Evaluation of DOTTOR, a Computer Code to Couple Two-Dimensional to Three-Dimensional Discrete Ordinates Calculations", Oak Ridge National Lab, ORNL/TM-9919, 1986.

[9] W.A. Rhoades and R.L. Childs, "The TORT Three-Dimensional Discrete Ordinates Neutron/Photon Transport Code", Oak Ridge National Lab, ORNL-6268, Nov 1987.

[10] R.L. Childs, W. A. Rhoades, and L.R. Williams, "Three-Dimensional Calculations of Neutron Streaming in the Beam Tubes of the ORNL HFIR Reactor", Proceedings, 7th International Conference on Radiation Shielding, VOL II, Sept. 1988.

[11] "The ELXSIR Cross-Section Library for LWR Pressure Vessel Irradiation Studies: Part of the LEPRICON Computer Code System", Oak Ridge National Lab, EPRI NP-3654, 1984.

[12] "SCALE: A Modular Code System for Performing Standardized Computer Analyses for Licensing Evaluation," NUREG/CR-0200 Rev. 4 (ORNL/NUREG/CSD-2/R4) Excerpts from Vols. I, II, and III, (Draft March 1992).

[13] I. Remec, F. Kam, "HFIR Neutron Spectra Determination," DRAFT NUREG/CR to be published.

APPENDIX E

RESULTS FOR KEY 7, POSITION 5

EXPLANATION OF THE TABLES AND FIGURES IN THE APPENDICES E-H

Table E.1 Lists the irradiation parameters for the 10 locations considered in the adjustment.

The tabulated quantities are:

Calculated	- quantities obtained from 3-D transport calculation
Value	- value of the parameter
STD	- standard deviation in percent
Adjusted	- quantities obtained after adjustment
Value	- value of the parameter
STD	- standard deviation in percent
Scale Fact.	- factor by which the calculated spectrum is scaled at the particular location
Adj. Fact.	- factor by which the parameter is changed due to "true" adjustment of the spectrum
Adj/Calc.	- ratio of adjusted to calculated value of the parameter. Also equal to the product of the scale and adjustment factor as defined above.

Table E.2 First column at the left gives the reaction identifier.

M measured reaction rate in reaction per second per atom, as were used in the adjustment runs. All necessary corrections are already included in the values listed. For key 7, position 5 listed values of fission and Be dosimeters contain correction for the contributions from gamma induced reactions. Self-shielding corrections for Co and Au monitors are also included.

C/M indicates calculated-to-measured reaction rate ratios. Calculated means as obtained by folding activation cross sections with the neutron fluxes form the 3-D calculation.

A/M is the ratio of adjusted-to-measured reaction rates. Adjusted reaction rates are obtained by folding the adjusted neutron fluxes with the activation cross sections.

Table E.3 Lists the group structure and neutron group fluxes as calculated, that is as obtained from 3-D transport calculation (column labeled "Calculated") and as obtained from adjustment (column labeled "Adjusted"). The spectrum is given for the position of slot J, which corresponds to the middle of the capsule, that is to the position of V-notch tips of the Charpy specimens in the surveillance capsules.

Fig. E.1 and E.2 give the neutron multigroup spectra as obtained from 3-D calculations "Calculated" and from the adjustment run "Adjusted," for the slot D and slot A in the dosimetry capsule.

NOTE: The equivalent set of Tables and Figures is presented in Appendices F, G, and H for the other three surveillance locations considered in the analysis.

Table E.1 Calculated and adjusted irradiation parameters, key 7, position 5

	Calculated Value*	Calculated Std.%	Adjusted Value	Adjusted Std. %	Scale Fact.	Adj. Fact.	Adj./ Calc.
Slot D							
F > 1MeV	1.17E+08	± 38	1.55E+08	± 6	1.290	1.03	1.33
F > 0.1MeV	1.75E+08	± 38	2.29E+08	± 9	1.290	1.01	1.31
F < 0.4 eV	3.97E+08	± 137	2.84E+08	± 5	1.290	0.55	0.71
dpa/s	1.82E-13	± 37	2.42E-13	± 5	1.290	1.03	1.33
Slot J							
F > 1MeV	1.17E+08	± 38	1.49E+08	± 6	1.421	0.90	1.28
F > 0.1MeV	1.75E+08	± 38	2.24E+08	± 9	1.421	0.90	1.28
F < 0.4 eV	3.97E+08	± 137	3.09E+08	± 19	1.421	0.55	0.78
dpa/s	1.82E-13	± 37	2.36E-13	± 5	1.421	0.91	1.30
Slot B							
F > 1MeV	1.17E+08	± 38	1.50E+08	± 6	1.305	0.99	1.29
F > 0.1MeV	1.75E+08	± 38	2.25E+08	± 8	1.305	0.98	1.28
F < 0.4 eV	3.97E+08	± 137	2.74E+08	± 7	1.305	0.53	0.69
dpa/s	1.82E-13	± 37	2.35E-13	± 5	1.305	0.99	1.29
Slot A							
F > 1MeV	1.17E+08	± 38	1.58E+08	± 7	1.395	0.97	1.36
F > 0.1MeV	1.75E+08	± 38	2.36E+08	± 10	1.395	0.97	1.35
F < 0.4 eV	3.97E+08	± 137	2.88E+08	± 4	1.395	0.52	0.73
dpa/s	1.82E-13	± 37	2.47E-13	± 6	1.395	0.97	1.36
Slot ET							
F > 1 MeV	1.17E+08	± 38	1.54E+08	± 7	1.351	0.98	1.32
F > 0.1 MeV	1.75E+08	± 38	2.30E+08	± 10	1.351	0.97	1.31
F < 0.4eV	3.97E+08	± 137	2.99E+08	± 6	1.351	0.56	0.75
dpa/s	1.82E-13	± 37	2.41E-13	± 6	1.351	0.98	1.32
Slot EM							
F > 1 MeV	1.17E+08	± 38	1.56E+08	± 7	1.370	0.98	1.34
F > 0.1 MeV	1.75E+08	± 38	2.33E+08	± 10	1.370	0.97	1.33
F < 0.4eV	3.97E+08	± 137	2.73E+08	± 6	1.370	0.50	0.69
dpa/s	1.82E-13	± 37	2.44E-13	± 6	1.370	0.98	1.34

Table E.1 (continued)

	Calculated Value*	Std.%	Adjusted Value	Std. %	Scale Fact.	Adj. Fact.	Adj./ Calc.
Slot EB							
F > 1 MeV	1.17E+08	± 38	1.57E+08	± 7	1.387	0.97	1.35
F > 0.1 MeV	1.75E+08	± 38	2.35E+08	± 10	1.387	0.96	1.34
F < 0.4eV	3.97E+08	± 137	2.71E+08	± 6	1.387	0.49	0.68
dpa/s	1.82E-13	± 37	2.46E-13	± 6	1.387	0.97	1.35
Slot FT							
F > 1 MeV	1.17E+08	± 38	1.51E+08	± 7	1.319	0.98	1.29
F > 0.1 MeV	1.75E+08	± 38	2.25E+08	± 10	1.319	0.97	1.28
F < 0.4eV	3.97E+08	± 137	2.86E+08	± 6	1.319	0.55	0.72
dpa/s	1.82E-13	± 37	2.36E-13	± 6	1.319	0.98	1.30
Slot FM							
F > 1 MeV	1.17E+08	± 38	1.58E+08	± 7	1.375	0.99	1.36
F > 0.1 MeV	1.75E+08	± 38	2.36E+08	± 10	1.375	0.98	1.35
F < 0.4eV	3.97E+08	± 137	2.63E+08	± 6	1.375	0.48	0.66
dpa/s	1.82E-13	± 37	2.47E-13	± 6	1.375	0.99	1.36
Slot FB							
F > 1 MeV	1.17E+08	± 38	1.61E+08	± 7	1.405	0.98	1.38
F > 0.1 MeV	1.75E+08	± 38	2.40E+08	± 10	1.405	0.97	1.37
F < 0.4eV	3.97E+08	± 137	2.84E+08	± 6	1.405	0.51	0.71
dpa/s	1.82E-13	± 37	2.52E-13	± 6	1.405	0.98	1.38

* Units are neutrons . cm^2. s^{-1} for F>1 MeV, F>0.1 MeV, F<0.4 eV, and s^{-1} for dpa rate (dpa/s).

Table E.2 Measured reaction rates, C/M, and A/M ratios, key 7, position 5

Reaction	M*	C/M	A/M
Slot D			
Al-27 (n,a) Na-24 [Bare]	1.304E-18	0.63	1.05
Al-27 (n,a) Na-24	1.305E-18	0.63	1.05
Ti-48 (n,p) Sc-48 [Bare]	5.854E-19	0.52	0.85
Ti-48 (n,p) Sc-48	4.948E-19	0.61	1.01
Cu-63 (n,a) Co-60 [Bare]	6.548E-19	0.66	1.04
Cu-63 (n,a) Co-60	6.255E-19	0.69	1.08
Ti-46 (n,p) Sc-46 [Bare]	9.759E-18	0.59	0.88
Ti-46 (n,p) Sc-46	8.817E-18	0.65	0.97
Fe-54 (n,p) Mn-54 [Bare]	3.290E-17	0.76	1.06
Fe-54 (n,p) Mn-54	3.406E-17	0.73	1.02
Ti-47 (n,p) Sc-47 [Bare]	7.638E-18	0.67	0.95
Ti-47 (n,p) Sc-47	6.890E-18	0.75	1.05
Fe-58 (n,g) Fe-59 [Bare]	2.904E-16	1.45	1.04
Fe-58 (n,g) Fe-59	1.734E-17	1.61	0.99
Sc-45 (n,g) Sc-46 [Bare]	6.328E-15	1.38	0.99
Sc-45 (n,g) Sc-46	2.367E-16	1.69	1.04
Ni-58 (n,p) Co-58	4.413E-17	0.72	1.00
Co-59 (n,g) Co-60	6.608E-16	1.62	0.97
Np-237 (n,f)	3.061E-16	0.74	0.98
Slot J			
U-235 (n,f)	1.233E-14	0.66	0.96
U-238 (n,f)	7.496E-17	0.83	1.09
Np-237 (n,f)	2.917E-16	0.77	1.00
Be (n,x) He	6.639E-17	1.14	1.50
Be (n,x) He	6.526E-17	1.16	1.53
Be (n,x) He	6.431E-17	1.18	1.55
Co-59 (n,g) Co-60 [Bare]	8.441E-15	1.48	1.16
Ni-58 (n,p) Co-58 [Bare]	4.485E-17	0.71	0.94
Ni-58 (n,p) Co-58	4.465E-17	0.71	0.95
Slot B			
U-235 (n,f) Ba-140	6.576E-15	1.24	1.03
U-235 (n,f) Zr-95	6.828E-15	1.19	0.99
U-238 (n,f) Ba-140	8.852E-17	0.71	0.93
U-238 (n,f) Ru-103	8.075E-17	0.77	1.02
Np-237 (n,f) Ba-140	2.919E-16	0.77	1.00
Np-237 (n,f) Zr-95	3.090E-16	0.73	0.94
Li-6 (n,a) H-3 [Bare]	2.035E-13	1.48	1.01
B-10 (n,a) Li-7 [Bare]	8.540E-13	1.44	0.99
Be (n,x) He	6.612E-17	1.15	1.50

Table E.2 (continued)

Reaction	M*	C/M	A/M
Slot A			
Ni-58 (n,p) Co-58 [Bare]	4.296E-17	0.74	1.04
Ni-58 (n,p) Co-58	4.632E-17	0.68	0.96
Co-59 (n,g) Co-60 [Bare]	8.946E-15	1.40	1.01
Co-59 (n,g) Co-60	1.045E-15	1.02	1.02
Au-197 (n,g) Au-198 [Bare]	3.998E-14	1.14	0.92
Au-197 (n,g) Au-198 [Bare]	3.886E-14	1.17	0.95
Co-59 (n,g) Co-60 [Bare]	8.880E-15	1.41	1.02
Ni-58 (n,p) Co-58 [Bare]	4.483E-17	0.71	0.99
Slot ET			
Ni-58 (n,p) Co-58 [Bare]	4.422E-17	0.72	0.98
Ni-58 (n,p) Co-58	4.332E-17	0.73	1.00
Co-59 (n,g) Co-60 [Bare]	9.376E-15	1.33	1.00
Co-59 (n,g) Co-60	9.980E-16	1.07	1.00
Slot EM			
Ni-58 (n,p) Co-58 [Bare]	4.444E-17	0.71	0.99
Ni-58 (n,p) Co-58	4.439E-17	0.71	0.99
Co-59 (n,g) Co-60 [Bare]	8.535E-15	1.46	1.01
Co-59 (n,g) Co-60	9.967E-16	1.07	1.00
Slot EB			
Ni-58 (n,p) Co-58 [Bare]	4.547E-17	0.70	0.97
Ni-58 (n,p) Co-58	4.393E-17	0.72	1.01
Co-59 (n,g) Co-60 [Bare]	8.422E-15	1.48	1.01
Co-59 (n,g) Co-60	1.065E-15	1.00	1.00
Slot FT			
Ni-58 (n,p) Co-58 [Bare]	4.355E-17	0.73	0.98
Ni-58 (n,p) Co-58	4.236E-17	0.75	1.00
Co-59 (n,g) Co-60 [Bare]	8.978E-15	1.39	1.00
Co-59 (n,g) Co-60	9.481E-16	1.13	1.01
Slot FM			
Ni-58 (n,p) Co-58 [Bare]	4.525E-17	0.70	0.99
Ni-58 (n,p) Co-58	4.491E-17	0.71	0.99
Co-59 (n,g) Co-60 [Bare]	8.228E-15	1.52	1.01
Co-59 (n,g) Co-60	9.420E-16	1.13	1.01
Slot FB			
Ni-58 (n,p) Co-58 [Bare]	4.591E-17	0.69	0.99
Ni-58 (n,p) Co-58	4.562E-17	0.69	0.99
Co-59 (n,g) Co-60 [Bare]	8.880E-15	1.41	1.01
Co-59 (n,g) Co-60	9.986E-16	1.07	1.01

*Reactions per second per atom

Table E.3 Calculated and adjusted neutron group fluxes, key 7, position 5, slot J

Group	Group Upper Energy Boundary* [eV]	Neutron Group Fluence Rate Calculated**	Adjusted**
1	2.000E+07	6.263E+05	1.087E+06
2	1.271E+07	2.016E+06	3.399E+06
3	1.013E+07	5.119E+06	8.408E+06
4	8.072E+06	1.016E+07	1.398E+07
5	6.434E+06	8.829E+06	1.150E+07
6	5.523E+06	1.037E+07	1.301E+07
7	4.742E+06	9.503E+06	1.193E+07
8	4.071E+06	7.303E+06	8.687E+06
9	3.495E+06	8.207E+06	9.697E+06
10	3.000E+06	5.729E+06	7.005E+06
11	2.724E+06	1.719E+07	2.126E+07
12	2.038E+06	4.511E+06	5.608E+06
13	1.850E+06	5.583E+06	6.937E+06
14	1.655E+06	5.104E+06	6.343E+06
15	1.480E+06	6.272E+06	7.801E+06
16	1.282E+06	9.993E+06	1.248E+07
17	1.000E+06	1.031E+07	1.302E+07
18	7.653E+05	1.709E+07	2.169E+07
19	4.704E+05	1.711E+07	2.162E+07
20	2.297E+05	1.425E+07	1.866E+07
21	1.000E+05	2.366E+07	4.016E+07
22	1.202E+04	6.436E+06	1.092E+07
23	6.004E+03	6.340E+06	1.076E+07
24	3.000E+03	1.818E+07	3.086E+07
25	3.911E+02	6.037E+06	1.025E+07
26	1.978E+02	6.053E+06	1.027E+07
27	1.000E+02	8.554E+06	1.452E+07
28	3.817E+01	1.189E+07	2.019E+07
29	1.000E+01	4.289E+06	7.279E+06
30	6.178E+00	6.385E+06	1.084E+07
31	3.000E+00	4.887E+06	8.293E+06
32	1.770E+00	1.500E+07	2.546E+07
33	3.970E-01	2.253E+06	3.824E+06
34	3.300E-01	2.910E+06	4.939E+06
35	2.700E-01	5.131E+06	8.708E+06
36	2.150E-01	1.283E+07	2.178E+07
37	1.620E-01	4.591E+07	4.626E+07
38	1.040E-01	1.392E+08	9.470E+07
39	5.000E-02	1.719E+08	1.170E+08
40	1.000E-02	1.682E+07	1.145E+07
	1.000E-05***		

*Energy in eV
**Group fluxes in neutrons $cm^{-2}. s^{-1}$
***Lower energy boundary of 40th group

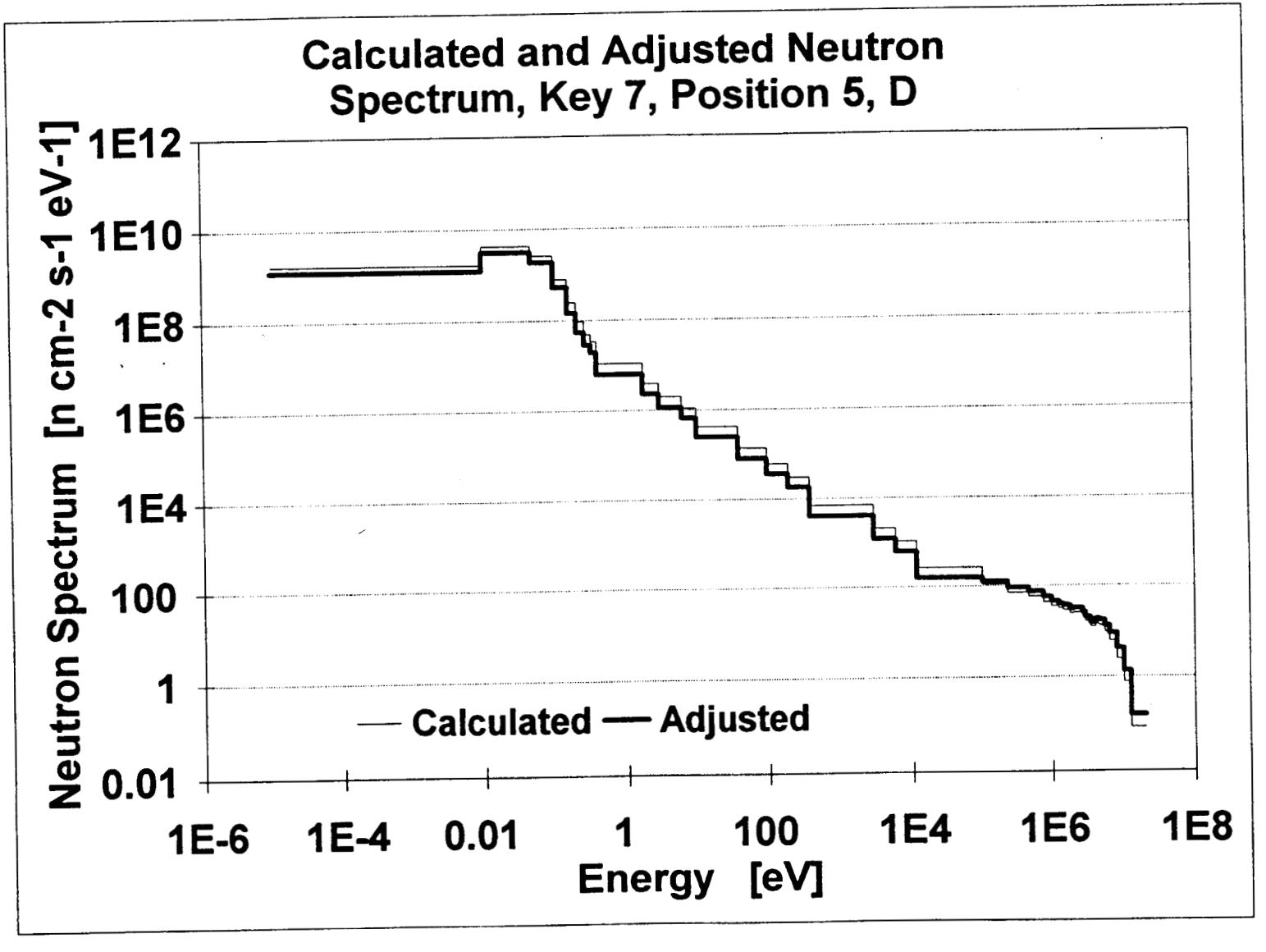

Fig. E.1 Calculated and adjusted neutron spectrum, key 7, position 5, D

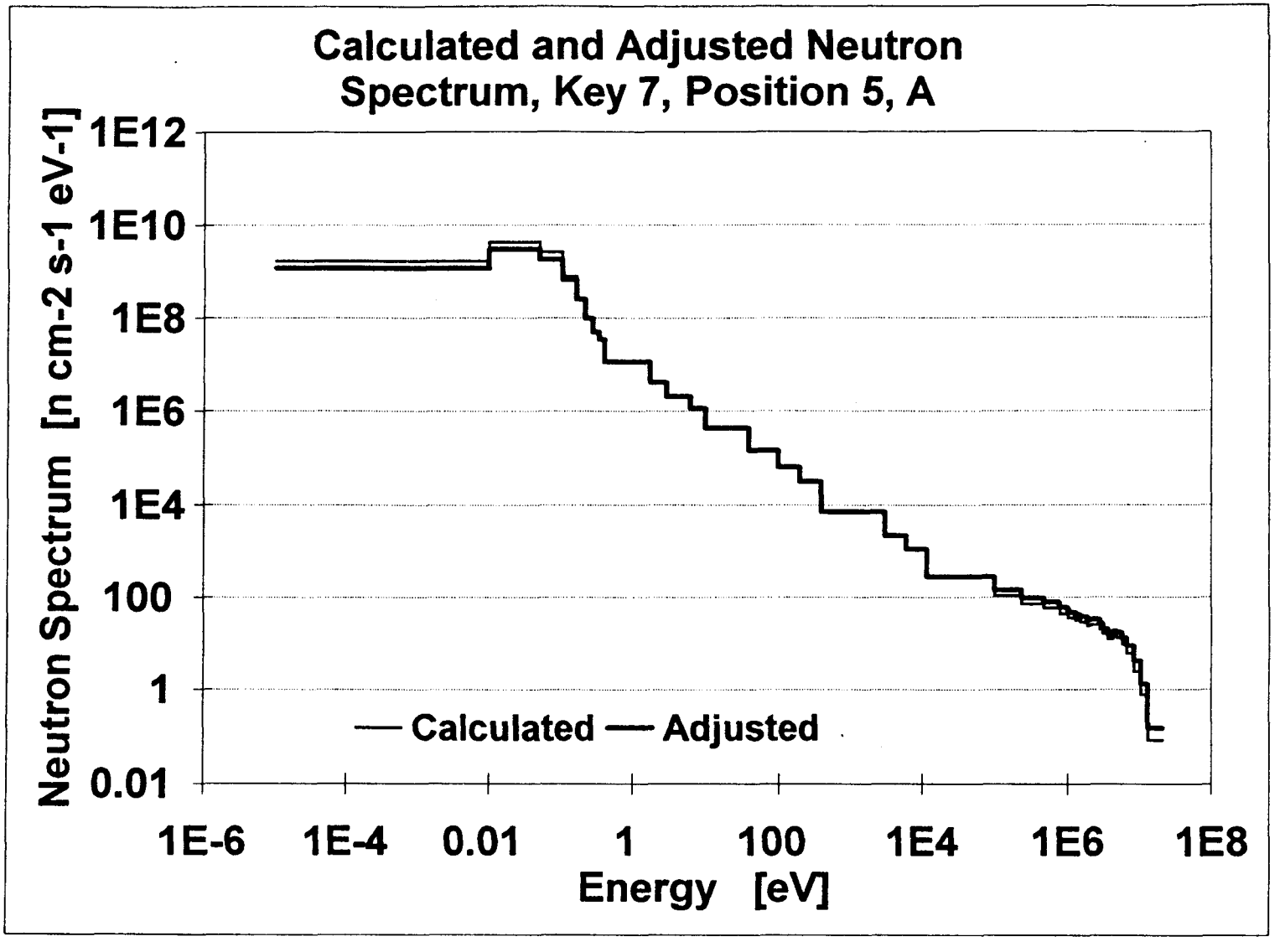

Fig. E.2 Calculated and adjusted neutron spectrum, key 7, position 5, A

APPENDIX F

RESULTS FOR KEY 2, POSITION 9

Table F.1 Calculated and adjusted irradiation parameters, key 2, position 9

	Calculated Value*	Calculated Std.%	Adjusted Value	Adjusted Std. %	Scale Fact.	Adj. Fact.	Adj./ Calc.
Slot D							
F > 1MeV	5.67E+08	± 38	8.81E+08	± 8	1.357	1.15	1.55
F > 0.1MeV	9.79E+08	± 38	1.51E+09	± 12	1.357	1.13	1.54
F < 0.4 eV	1.67E+10	± 139	9.38E+09	± 5	1.357	0.41	0.56
dpa/s	9.72E-13	± 41	1.34E-12	± 6	1.357	1.01	1.38
Slot J							
F > 1MeV	5.67E+08	± 38	1.21E+09	± 9	2.123	1.01	2.14
F > 0.1MeV	9.79E+08	± 38	2.11E+09	± 12	2.123	1.01	2.15
F < 0.4 eV	1.67E+10	± 139	1.61E+10	± 6	2.123	0.45	0.96
dpa/s	9.72E-13	± 41	1.89E-12	± 7	2.123	0.92	1.95
Slot B							
F > 1MeV	5.67E+08	± 38	1.12E+09	± 39	1.950	1.01	1.98
F > 0.1MeV	9.79E+08	± 38	1.94E+09	± 40	1.950	1.02	1.98
F < 0.4 eV	1.67E+10	± 139	1.55E+10	± 41	1.950	0.47	0.92
dpa/s	9.72E-13	± 41	1.75E-12	± 31	1.950	0.92	1.80
Slot A							
F > 1MeV	5.67E+08	± 38	1.74E+09	± 9	3.223	0.95	3.07
F > 0.1MeV	9.79E+08	± 38	3.05E+09	± 12	3.223	0.97	3.11
F < 0.4 eV	1.67E+10	± 139	3.24E+10	± 6	3.223	0.60	1.94
dpa/s	9.72E-13	± 41	2.82E-12	± 7	3.223	0.90	2.90
Slot ET							
F > 1 MeV	5.67E+08	± 38	8.70E+08	± 9	1.492	1.03	1.53
F > 0.1 MeV	9.79E+08	± 38	1.51E+09	± 12	1.492	1.03	1.54
F < 0.4eV	1.67E+10	± 139	9.57E+09	± 6	1.492	0.38	0.57
dpa/s	9.72E-13	± 41	1.34E-12	± 7	1.492	0.92	1.37
Slot EM							
F > 1 MeV	5.67E+08	± 38	1.22E+09	± 9	2.119	1.02	2.16
F > 0.1 MeV	9.79E+08	± 38	2.12E+09	± 12	2.119	1.02	2.16
F < 0.4eV	1.67E+10	± 139	1.61E+10	± 6	2.119	0.45	0.96
dpa/s	9.72E-13	± 41	1.90E-12	± 7	2.119	0.92	1.96

Table F.1 (continued)

	Calculated Value*	Std.%	Adjusted Value	Std. %	Scale Fact.	Adj. Fact.	Adj./ Calc.
Slot EB							
F > 1 MeV	5.67E+08	± 38	1.70E+09	± 9	3.042	0.98	2.99
F > 0.1 MeV	9.79E+08	± 38	2.95E+09	± 12	3.042	0.99	3.02
F < 0.4eV	1.67E+10	± 139	2.83E+10	± 6	3.042	0.56	1.69
dpa/s	9.72E-13	± 41	2.70E-12	± 7	3.042	0.91	2.78
Slot FT							
F > 1 MeV	5.67E+08	± 38	8.65E+08	± 9	1.493	1.02	1.53
F > 0.1 MeV	9.79E+08	± 38	1.50E+09	± 12	1.493	1.03	1.53
F < 0.4eV	1.67E+10	± 139	9.27E+09	± 6	1.493	0.37	0.55
dpa/s	9.72E-13	± 41	1.33E-12	± 7	1.493	0.91	1.36
Slot FM							
F > 1 MeV	5.67E+08	± 38	1.21E+09	± 9	2.132	1.00	2.14
F > 0.1 MeV	9.79E+08	± 38	2.10E+09	± 12	2.132	1.01	2.15
F < 0.4eV	1.67E+10	± 139	1.61E+10	± 6	2.132	0.45	0.96
dpa/s	9.72E-13	± 41	1.89E-12	± 7	2.132	0.91	1.94
Slot FB							
F > 1 MeV	5.67E+08	± 38	1.77E+09	± 9	3.206	0.97	3.11
F > 0.1 MeV	9.79E+08	± 38	3.08E+09	± 12	3.206	0.98	3.15
F < 0.4eV	1.67E+10	± 139	3.01E+10	± 6	3.206	0.56	1.80
dpa/s	9.72E-13	± 41	2.82E-12	± 7	3.206	0.91	2.91

* Units are neutrons . cm^{-2}. s^{-1} for F>1 MeV, F>0.1 MeV, F<0.4 eV, and s^{-1} for dpa rate (dpa/s).

Table F.2 Measured reaction rates, C/M, and A/M ratios, key 2, position 9

Reaction	M*	C/M	A/M
Slot D			
Al-27 (n,a) Na-24 [Bare]	3.177E-18	0.60	0.95
Ti-48 (n,p) Sc-48 [Bare]	1.154E-18	0.61	0.96
Ti-48 (n,p) Sc-48	1.055E-18	0.67	1.04
Cu-63 (n,a) Co-60 [Bare]	1.569E-18	0.70	1.08
Cu-63 (n,a) Co-60	1.618E-18	0.68	1.05
Ti-46 (n,p) Sc-46 [Bare]	2.845E-17	0.58	0.90
Ti-46 (n,p) Sc-46	2.599E-17	0.64	0.98
Fe-54 (n,p) Mn-54 [Bare]	1.268E-16	0.70	1.07
Fe-54 (n,p) Mn-54	1.305E-16	0.68	1.03
Ti-47 (n,p) Sc-47 [Bare]	3.270E-17	0.58	0.89
Ti-47 (n,p) Sc-47	2.924E-17	0.65	0.99
Fe-58 (n,g) Fe-59 [Bare]	9.140E-15	1.92	1.08
Sc-45 (n,g) Sc-46 [Bare]	2.114E-13	1.75	0.98
Sc-45 (n,g) Sc-46	5.599E-15	1.91	1.04
Slot J			
Ni-58 (n,p) Co-58 [Bare]	2.473E-16	0.46	0.97
Ni-58 (n,p) Co-58	2.348E-16	0.49	1.02
Co-59 (n,g) Co-60 [Bare]	4.706E-13	1.09	1.02
Co-59 (n,g) Co-60	3.144E-14	0.62	1.03
Slot B			
U-235 (n,f) Ba-140	2.922E-13	0.70	1.00
U-235 (n,f) Zr-95	2.769E-13	0.74	1.06
U-235 (n,f) Ru-103	2.847E-13	0.72	1.03
Slot A			
Ni-58 (n,p) Co-58 [Bare]	3.455E-16	0.33	1.00
Ni-58 (n,p) Co-58	3.364E-16	0.34	1.02
Co-59 (n,g) Co-60 [Bare]	9.410E-13	0.55	1.02
Co-59 (n,g) Co-60	6.766E-14	0.29	1.01

Table F.2 (continued)

Reaction	M*	C/M	A/M
Slot ET			
Ni-58 (n,p) Co-58 [Bare]	1.763E-16	0.65	0.98
Ni-58 (n,p) Co-58	1.686E-16	0.68	1.02
Co-59 (n,g) Co-60 [Bare]	2.785E-13	1.84	1.02
Co-59 (n,g) Co-60	1.935E-14	1.01	1.04
Slot EM			
Ni-58 (n,p) Co-58 [Bare]	2.481E-16	0.46	0.98
Ni-58 (n,p) Co-58	2.358E-16	0.49	1.03
Co-59 (n,g) Co-60 [Bare]	4.744E-13	1.08	1.01
Co-59 (n,g) Co-60	3.007E-14	0.65	1.03
Slot EB			
Ni-58 (n,p) Co-58 [Bare]	3.495E-16	0.33	0.96
Ni-58 (n,p) Co-58	3.209E-16	0.36	1.04
Co-59 (n,g) Co-60 [Bare]	8.338E-13	0.62	1.01
Co-59 (n,g) Co-60	5.366E-14	0.36	1.01
Slot FT			
Ni-58 (n,p) Co-58 [Bare]	1.736E-16	0.66	0.99
Ni-58 (n,p) Co-58	1.686E-16	0.68	1.02
Co-59 (n,g) Co-60 [Bare]	2.667E-13	1.92	1.03
Co-59 (n,g) Co-60	1.989E-14	0.98	1.05
Slot FM			
Ni-58 (n,p) Co-58 [Bare]	2.465E-16	0.47	0.97
Ni-58 (n,p) Co-58	2.338E-16	0.49	1.02
Co-59 (n,g) Co-60 [Bare]	4.668E-13	1.10	1.02
Co-59 (n,g) Co-60	3.281E-14	0.59	1.03
Slot FB			
Ni-58 (n,p) Co-58 [Bare]	3.491E-16	0.33	1.00
Ni-58 (n,p) Co-58	3.425E-16	0.33	1.02
Co-59 (n,g) Co-60 [Bare]	8.776E-13	0.58	1.02
Co-59 (n,g) Co-60	6.025E-14	0.32	1.01

*Reactions per second per atom

Table F.3 Calculated and adjusted neutron group fluxes, key 2, position 9, slot J

Group	Group Upper Energy Boundary* [eV]	Neutron Group Fluence Rate Calculated**	Adjusted**
1	2.000E+07	1.057E+06	2.356E+06
2	1.271E+07	4.058E+06	9.059E+06
3	1.013E+07	1.209E+07	2.698E+07
4	8.072E+06	2.755E+07	5.743E+07
5	6.434E+06	2.803E+07	5.791E+07
6	5.523E+06	3.698E+07	7.595E+07
7	4.742E+06	3.932E+07	8.075E+07
8	4.071E+06	3.444E+07	7.089E+07
9	3.495E+06	4.265E+07	8.778E+07
10	3.000E+06	3.055E+07	6.626E+07
11	2.724E+06	1.019E+08	2.229E+08
12	2.038E+06	2.874E+07	6.294E+07
13	1.850E+06	3.674E+07	8.044E+07
14	1.655E+06	3.410E+07	7.464E+07
15	1.480E+06	4.212E+07	9.213E+07
16	1.282E+06	6.662E+07	1.457E+08
17	1.000E+06	6.962E+07	1.520E+08
18	7.653E+05	1.169E+08	2.543E+08
19	4.704E+05	1.194E+08	2.591E+08
20	2.297E+05	1.057E+08	2.269E+08
21	1.000E+05	1.857E+08	3.658E+08
22	1.202E+04	5.333E+07	1.050E+08
23	6.004E+03	5.285E+07	1.041E+08
24	3.000E+03	1.577E+08	3.105E+08
25	3.911E+02	5.434E+07	1.070E+08
26	1.978E+02	5.531E+07	1.089E+08
27	1.000E+02	7.985E+07	1.573E+08
28	3.817E+01	1.147E+08	2.259E+08
29	1.000E+01	4.258E+07	8.386E+07
30	6.178E+00	6.478E+07	1.276E+08
31	3.000E+00	5.089E+07	1.002E+08
32	1.770E+00	1.702E+08	3.351E+08
33	3.970E-01	2.816E+07	5.546E+07
34	3.300E-01	4.975E+07	9.798E+07
35	2.700E-01	1.334E+08	2.627E+08
36	2.150E-01	4.486E+08	8.834E+08
37	1.620E-01	1.859E+09	2.309E+09
38	1.040E-01	5.953E+09	5.228E+09
39	5.000E-02	7.509E+09	6.594E+09
40	1.000E-02	7.402E+08	6.501E+08
	1.000E-05		

*Energy in eV
**Group fluxes in neutrons $cm^{-2}. s^{-1}$
***Lower energy boundary of 40th group

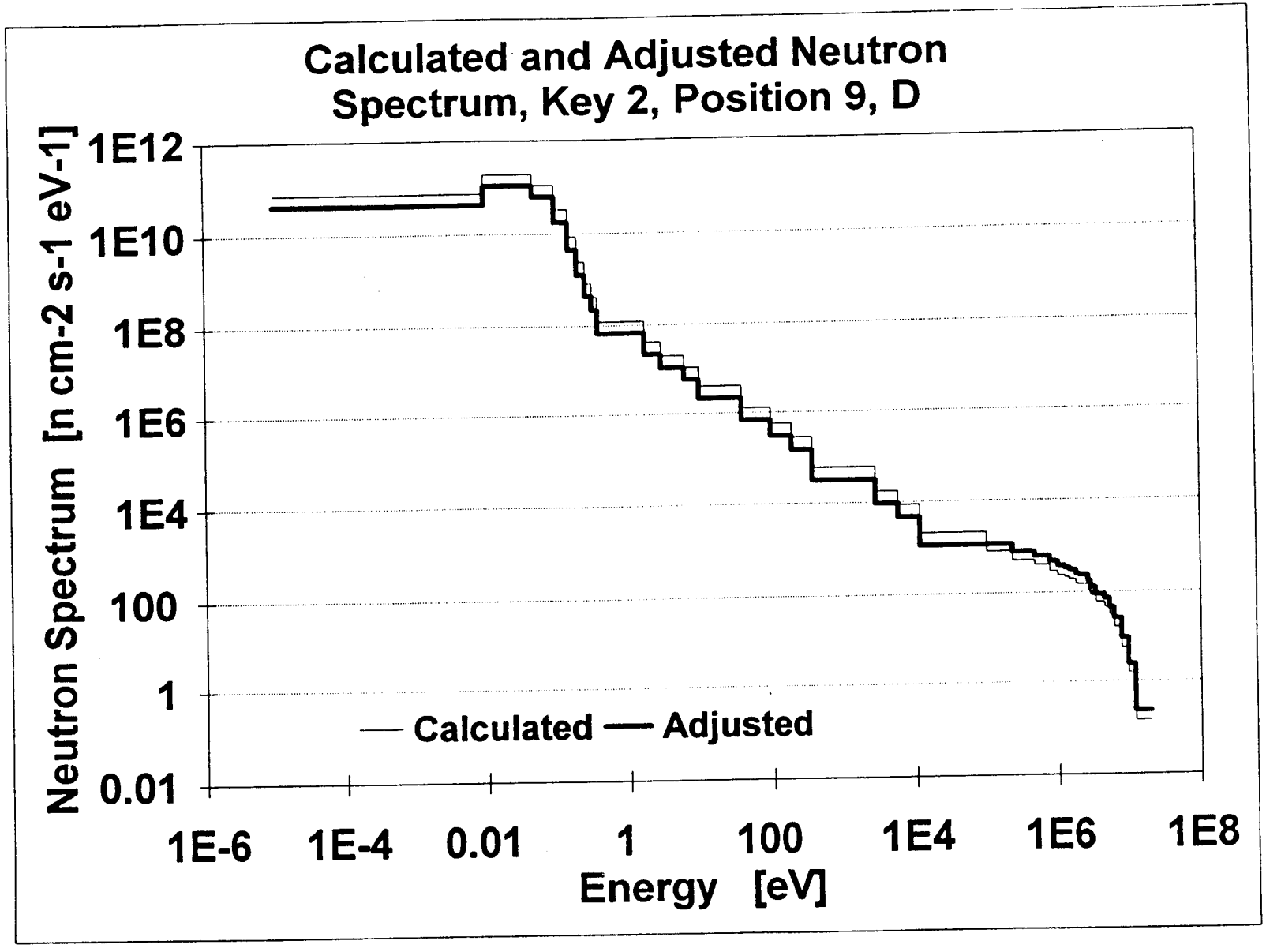

Fig. F.1 Calculated and adjusted neutron spectrum, key 2, position 9, D

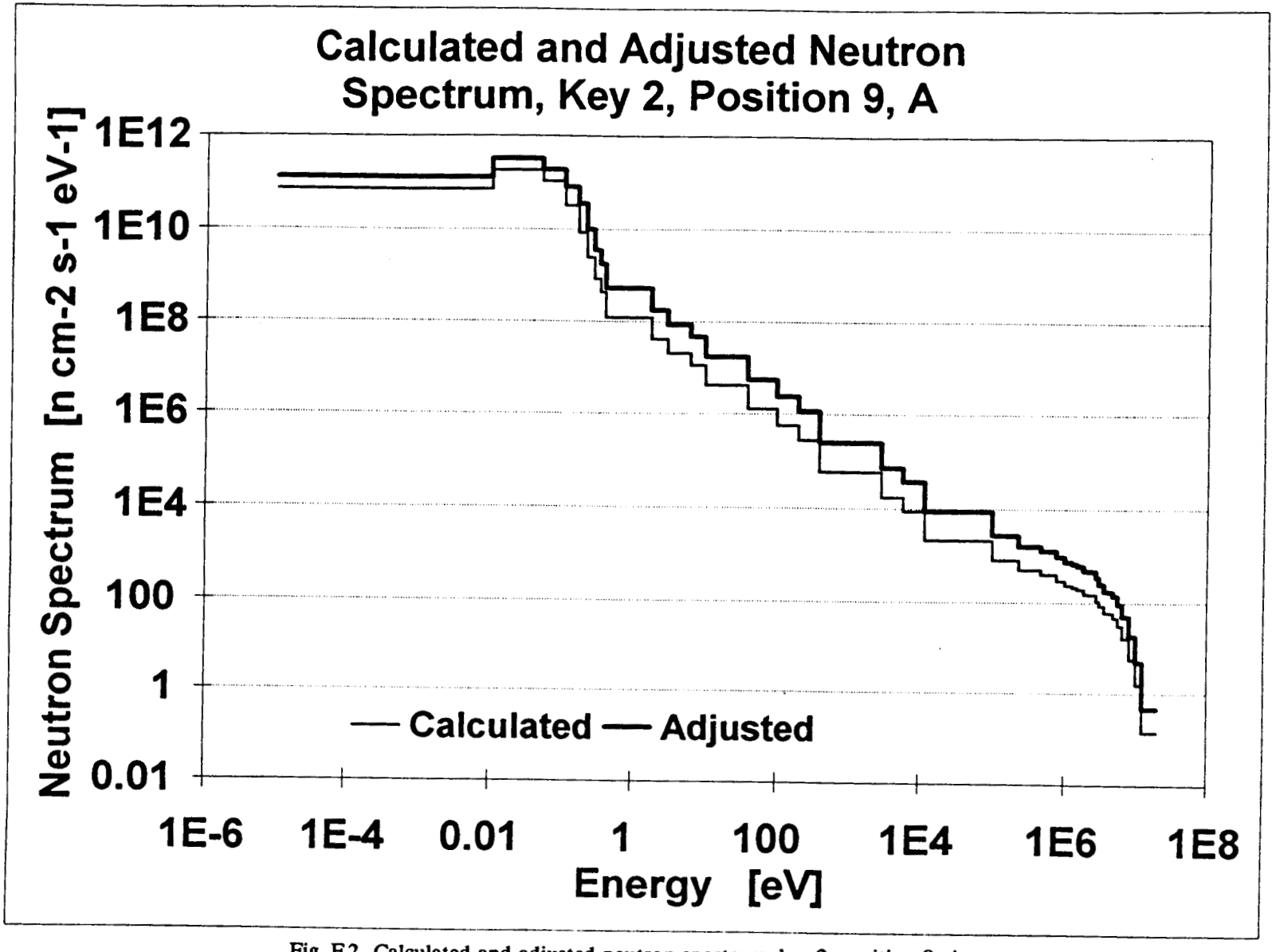

Fig. F.2 Calculated and adjusted neutron spectrum, key 2, position 9, A

APPENDIX G

RESULTS FOR KEY 4, POSITION 2

Table G.1 Calculated and adjusted irradiation parameters, key 4, position 2

	Calculated Value*	Calculated Std.%	Adjusted Value	Adjusted Std. %	Scale Fact.	Adj. Fact.	Adj./ Calc.
Slot D							
F > 1MeV	2.47E+08	± 38	2.43E+08	± 9	0.941	1.048	0.99
F > 0.1MeV	4.96E+08	± 38	4.91E+08	± 13	0.941	1.051	0.99
F < 0.4 eV	3.12E+10	± 139	9.99E+09	± 5	0.941	0.340	0.32
dpa/s	6.46E-13	± 68	4.42E-13	± 5	0.941	0.727	0.68
Slot J							
F > 1MeV	2.47E+08	± 38	3.10E+08	± 10	1.421	0.885	1.26
F > 0.1MeV	4.96E+08	± 38	6.43E+08	± 13	1.421	0.912	1.30
F < 0.4 eV	3.12E+10	± 139	2.33E+10	± 6	1.421	0.525	0.75
dpa/s	6.46E-13	± 68	6.66E-13	± 6	1.421	0.726	1.03
Slot B							
F > 1MeV	2.47E+08	± 38	3.16E+08	± 41	1.432	0.895	1.28
F > 0.1MeV	4.96E+08	± 38	6.54E+08	± 41	1.432	0.920	1.32
F < 0.4 eV	3.12E+10	± 139	2.50E+10	± 39	1.432	0.559	0.80
dpa/s	6.46E-13	± 68	6.90E-13	± 22	1.432	0.746	1.07
Slot A							
F > 1MeV	2.47E+08	± 38	4.30E+08	± 10	2.154	0.812	1.74
F > 0.1MeV	4.96E+08	± 38	9.05E+08	± 13	2.154	0.850	1.82
F < 0.4 eV	3.12E+10	± 139	7.20E+10	± 6	2.154	1.076	2.31
dpa/s	6.46E-13	± 68	1.29E-12	± 5	2.154	0.933	2.00
Slot ET							
F > 1MeV	2.47E+08	± 38	2.39E+08	± 10	1.037	0.936	0.97
F > 0.1MeV	4.96E+08	± 38	4.92E+08	± 13	1.037	0.956	0.99
F < 0.4 eV	3.12E+10	± 139	1.02E+10	± 6	1.037	0.314	0.33
dpa/s	6.46E-13	± 68	4.42E-13	± 5	1.037	0.659	0.68
Slot EM							
F > 1MeV	2.47E+08	± 38	3.14E+08	± 10	1.421	0.898	1.28
F > 0.1MeV	4.96E+08	± 38	6.51E+08	± 13	1.421	0.923	1.31
F < 0.4 eV	3.12E+10	± 139	2.26E+10	± 6	1.421	0.510	0.73
dpa/s	6.46E-13	± 68	6.66E-13	± 5	1.421	0.726	1.03
Slot EB							
F > 1MeV	2.47E+08	± 38	4.35E+08	± 10	2.077	0.850	1.77
F > 0.1MeV	4.96E+08	± 38	9.09E+08	± 13	2.077	0.882	1.83
F < 0.4 eV	3.12E+10	± 139	6.50E+10	± 6	2.077	1.003	2.08
dpa/s	6.46E-13	± 68	1.23E-12	± 5	2.077	0.918	1.91

Table G.1 (continued)

	Calculated Value*	Std.%	Adjusted Value	Std. %	Scale Fact.	Adj. Fact.	Adj./ Calc.
Slot FT							
F > 1MeV	2.47E+08	± 38	2.36E+08	± 10	1.049	0.914	0.96
F > 0.1MeV	4.96E+08	± 38	4.88E+08	± 13	1.049	0.937	0.98
F < 0.4 eV	3.12E+10	± 139	1.10E+10	± 6	1.049	0.336	0.35
dpa/s	6.46E-13	± 68	4.46E-13	± 5	1.049	0.658	0.69
Slot FM							
F > 1MeV	2.47E+08	± 38	3.03E+08	± 10	1.389	0.884	1.23
F > 0.1MeV	4.96E+08	± 38	6.28E+08	± 13	1.389	0.911	1.27
F < 0.4 eV	3.12E+10	± 139	2.33E+10	± 6	1.389	0.537	0.75
dpa/s	6.46E-13	± 68	6.56E-13	± 6	1.389	0.731	1.02
Slot FB							
F > 1MeV	2.47E+08	± 38	4.17E+08	± 10	2.047	0.827	1.69
F > 0.1MeV	4.96E+08	± 38	8.75E+08	± 13	2.047	0.862	1.76
F < 0.4 eV	3.12E+10	± 139	5.83E+10	± 6	2.047	0.913	1.87
dpa/s	6.46E-13	± 68	1.15E-12	± 5	2.047	0.868	1.78

* Units are neutron . cm^{-2}. s^{-1} for F > 1 MeV, F> 0.1 MeV, F > 0.4 eV, and s^{-1} for dpa rate (dpa/s).

Table G.2 Measured reaction rates, C/M, and A/M ratios, key 4, position 2

Reaction	M*	C/M	A/M
Slot D			
Al-27 (n,a) Na-24 [Bare]	8.333E-19	0.99	1.05
Ti-48 (n,p) Sc-48 [Bare]	3.374E-19	0.90	0.94
Ti-48 (n,p) Sc-48	3.191E-19	0.95	0.99
Cu-63 (n,a) Co-60 [Bare]	4.669E-19	0.98	0.98
Cu-63 (n,a) Co-60	4.332E-19	1.05	1.05
Ti-46 (n,p) Sc-46 [Bare]	6.684E-18	1.00	0.95
Ti-46 (n,p) Sc-46	6.220E-18	1.07	1.02
Fe-54 (n,p) Mn-54 [Bare]	2.926E-17	1.20	1.11
Fe-54 (n,p) Mn-54	3.153E-17	1.11	1.03
Ti-47 (n,p) Sc-47 [Bare]	8.127E-18	0.93	0.89
Ti-47 (n,p) Sc-47	7.619E-18	0.99	0.94
Fe-58 (n,g) Fe-59 [Bare]	9.525E-15	3.43	1.06
Sc-45 (n,g) Sc-46 [Bare]	2.167E-13	3.18	0.99
Sc-45 (n,g) Sc-46	7.903E-15	2.33	1.07
Slot A			
Ni-58 (n,p) Co-58 [Bare]	7.278E-17	0.62	1.03
Ni-58 (n,p) Co-58	7.370E-17	0.62	1.01
Co-59 (n,g) Co-60 [Bare]	1.980E-12	0.48	1.04
Co-59 (n,g) Co-60	1.426E-13	0.21	1.03
Slot B			
U-235 (n,f) Ba-140	5.644E-13	0.62	1.06
U-235 (n,f) Zr-95	5.287E-13	0.66	1.14
U-235 (n,f) Ru-103	5.433E-13	0.64	1.11
Slot J			
U-235 (n,f)	5.972E-13	0.58	1.05
Ni-58 (n,p) Co-58 [Bare]	5.506E-17	0.82	0.98
Ni-58 (n,p) Co-58	5.302E-17	0.86	1.02
Co-59 (n,g) Co-60 [Bare]	6.167E-13	1.54	1.06
Co-59 (n,g) Co-60	4.794E-14	0.61	1.17

Table G.2 (continued)

Reaction	M*	C/M	A/M
Slot ET			
Ni-58 (n,p) Co-58 [Bare]	4.145E-17	1.10	1.01
Ni-58 (n,p) Co-58	4.203E-17	1.08	1.00
Co-59 (n,g) Co-60 [Bare]	2.574E-13	3.70	1.08
Co-59 (n,g) Co-60	2.409E-14	1.22	1.19
Slot EM			
Ni-58 (n,p) Co-58 [Bare]	5.400E-17	0.84	1.02
Ni-58 (n,p) Co-58	5.491E-17	0.83	1.00
Co-59 (n,g) Co-60 [Bare]	6.108E-13	1.56	1.05
Co-59 (n,g) Co-60	4.643E-14	0.63	1.11
Slot EB			
Ni-58 (n,p) Co-58 [Bare]	7.652E-17	0.59	0.99
Ni-58 (n,p) Co-58	7.380E-17	0.61	1.03
Co-59 (n,g) Co-60 [Bare]	1.869E-12	0.51	1.02
Co-59 (n,g) Co-60	1.055E-13	0.28	1.03
Slot FT			
Ni-58 (n,p) Co-58 [Bare]	4.223E-17	1.08	0.98
Ni-58 (n,p) Co-58	4.051E-17	1.12	1.02
Co-59 (n,g) Co-60 [Bare]	2.713E-13	3.51	1.10
Co-59 (n,g) Co-60	2.787E-14	1.05	1.20
Slot FM			
Ni-58 (n,p) Co-58 [Bare]	5.612E-17	0.81	0.94
Ni-58 (n,p) Co-58	5.112E-17	0.89	1.03
Co-59 (n,g) Co-60 [Bare]	6.225E-13	1.53	1.05
Co-59 (n,g) Co-60	4.945E-14	0.59	1.11
Slot FB			
Ni-58 (n,p) Co-58 [Bare]	7.235E-17	0.63	1.00
Ni-58 (n,p) Co-58	7.079E-17	0.64	1.02
Co-59 (n,g) Co-60 [Bare]	1.596E-12	0.60	1.04
Co-59 (n,g) Co-60	1.168E-13	0.25	1.05

*Reactions per second per atom

Table G.3 Calculated and adjusted neutron group fluxes, key 4, position 2, slot J

Group	Group Upper Energy Boundary* [eV]	Neutron Group Fluence Rate Calculated**	Adjusted**
1	2.000E+07	5.520E+05	8.033E+05
2	1.271E+07	1.858E+06	2.659E+06
3	1.013E+07	5.141E+06	7.235E+06
4	8.072E+06	1.117E+07	1.310E+07
5	6.434E+06	1.065E+07	1.212E+07
6	5.523E+06	1.386E+07	1.549E+07
7	4.742E+06	1.490E+07	1.665E+07
8	4.071E+06	1.363E+07	1.547E+07
9	3.495E+06	1.668E+07	1.897E+07
10	3.000E+06	1.182E+07	1.523E+07
11	2.724E+06	4.116E+07	5.409E+07
12	2.038E+06	1.289E+07	1.700E+07
13	1.850E+06	1.718E+07	2.260E+07
14	1.655E+06	1.671E+07	2.198E+07
15	1.480E+06	2.182E+07	2.867E+07
16	1.282E+06	3.651E+07	4.778E+07
17	1.000E+06	3.967E+07	5.179E+07
18	7.653E+05	7.020E+07	9.141E+07
19	4.704E+05	7.372E+07	9.586E+07
20	2.297E+05	6.601E+07	9.390E+07
21	1.000E+05	1.205E+08	3.275E+08
22	1.202E+04	3.599E+07	9.783E+07
23	6.004E+03	3.677E+07	9.995E+07
24	3.000E+03	1.167E+08	3.173E+08
25	3.911E+02	4.298E+07	1.168E+08
26	1.978E+02	4.544E+07	1.235E+08
27	1.000E+02	6.854E+07	1.863E+08
28	3.817E+01	1.049E+08	2.853E+08
29	1.000E+01	4.094E+07	1.113E+08
30	6.178E+00	6.436E+07	1.750E+08
31	3.000E+00	5.223E+07	1.420E+08
32	1.770E+00	1.840E+08	5.000E+08
33	3.970E-01	3.543E+07	9.632E+07
34	3.300E-01	7.459E+07	2.028E+08
35	2.700E-01	2.310E+08	6.280E+08
36	2.150E-01	8.234E+08	2.238E+09
37	1.620E-01	3.471E+09	4.003E+09
38	1.040E-01	1.116E+10	6.757E+09
39	5.000E-02	1.404E+10	8.503E+09
40	1.000E-02	1.381E+09	8.364E+08
	1.000E-05***		

*Energy in eV
**Group fluxes in neutrons $cm^{-2}. s^{-1}$
***Lower energy boundary of 40th group

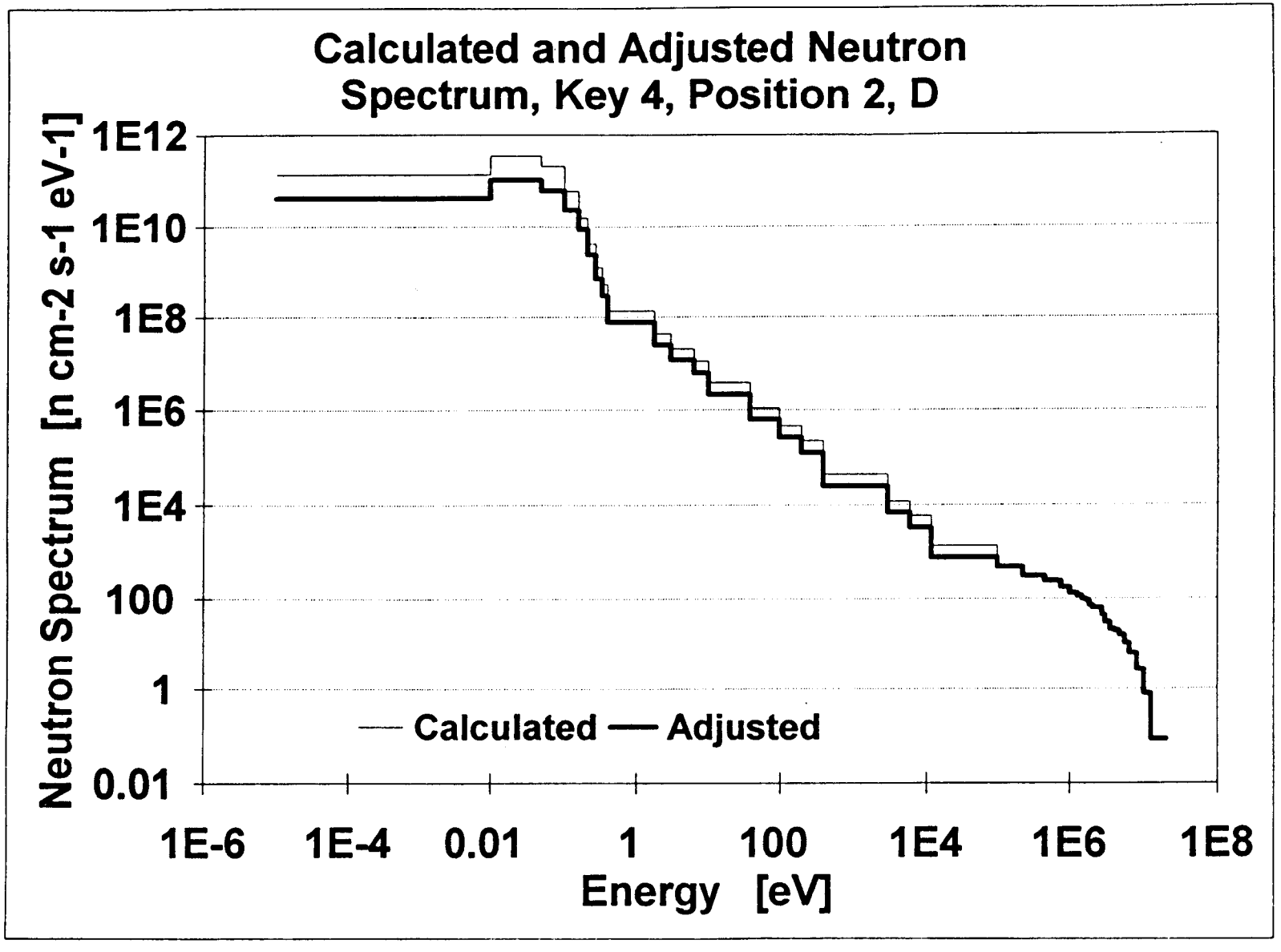

Fig. G.1 Calculated and adjusted neutron spectrum, key 4, position 2, D

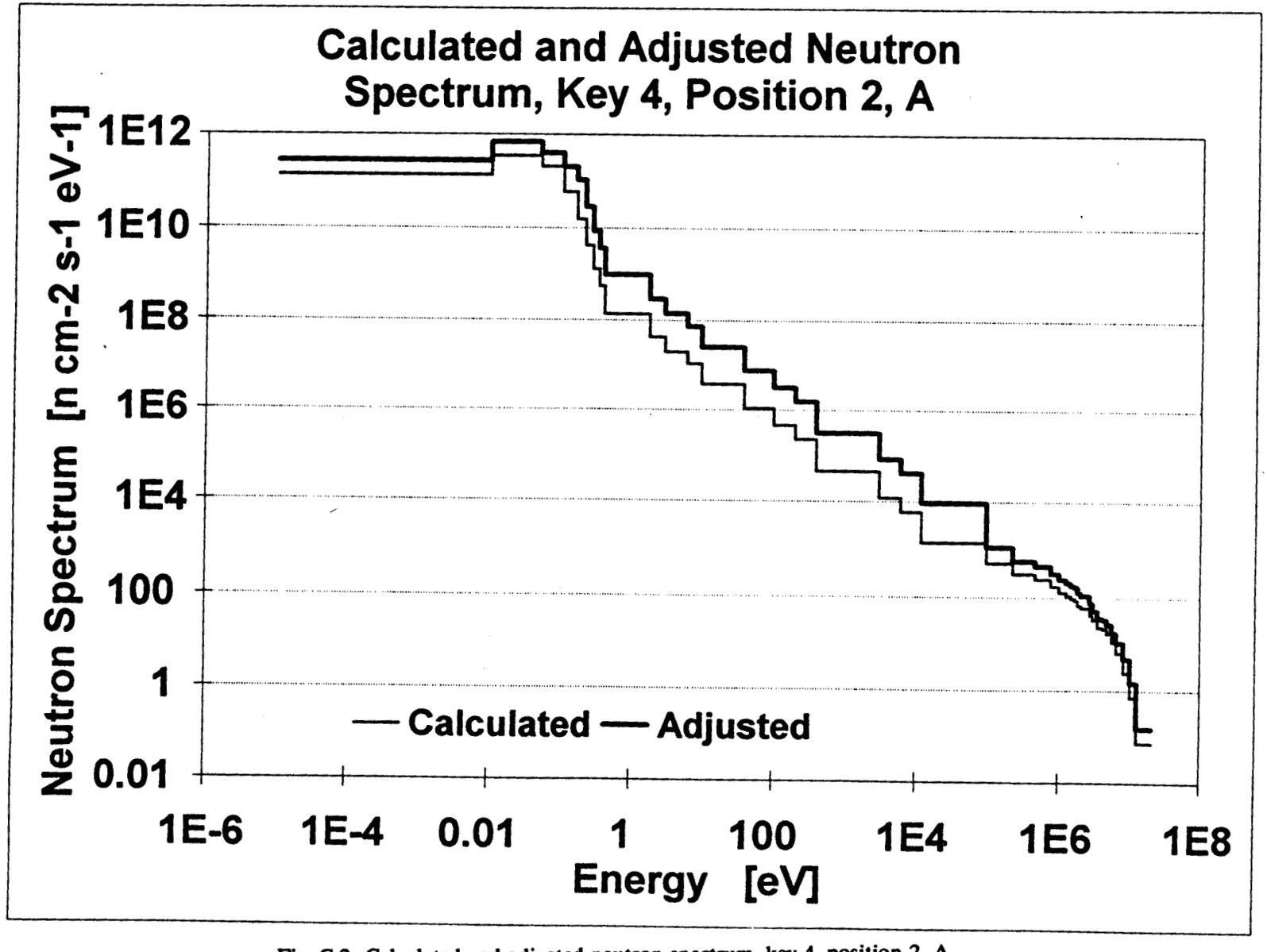

Fig. G.2 Calculated and adjusted neutron spectrum, key 4, position 2, A

APPENDIX H

RESULTS FOR KEY 4, POSITION 10

Table H.1 Calculated and adjusted irradiation parameters, key 4, position 10

	Calculated Value*	Calculated Std.%	Adjusted Value	Adjusted Std. %	Scale Fact.	Adj. Fact.	Adj./ Calc.
Slot D							
F > 1MeV	3.97E+08	± 38	2.95E+08	± 9	0.660	1.127	0.74
F > 0.1MeV	7.56E+08	± 38	5.68E+08	± 13	0.660	1.139	0.75
F < 0.4 eV	3.26E+10	± 139	1.11E+10	± 5	0.660	0.516	0.34
dpa/s	8.94E-13	± 55	5.34E-13	± 5	0.660	0.905	0.60
Slot J							
F > 1MeV	3.97E+08	± 38	4.09E+08	± 10	1.088	0.946	1.03
F > 0.1MeV	7.56E+08	± 38	8.05E+08	± 13	1.088	0.979	1.06
F < 0.4 eV	3.26E+10	± 139	2.75E+10	± 6	1.088	0.775	0.84
dpa/s	8.94E-13	± 55	8.62E-13	± 6	1.088	0.886	0.96
Slot B							
F > 1MeV	3.97E+08	± 38	3.90E+08	± 40	1.021	0.962	0.98
F > 0.1MeV	7.56E+08	± 38	7.66E+08	± 40	1.021	0.992	1.01
F < 0.4 eV	3.26E+10	± 139	2.64E+10	± 40	1.021	0.793	0.81
dpa/s	8.94E-13	± 55	8.22E-13	± 25	1.021	0.900	0.92
Slot A							
F > 1MeV	3.97E+08	± 38	6.00E+08	± 10	1.717	0.880	1.51
F > 0.1MeV	7.56E+08	± 38	1.20E+09	± 13	1.717	0.921	1.58
F < 0.4 eV	3.26E+10	± 139	8.01E+10	± 6	1.717	1.433	2.46
dpa/s	8.94E-13	± 55	1.64E-12	± 6	1.717	1.066	1.83
Slot ET							
F > 1 MeV	3.97E+08	± 38	2.78E+08	± 10	0.70	1.00	0.70
F > 0.1 MeV	7.56E+08	± 38	5.42E+08	± 13	0.70	1.03	0.72
F < 0.4eV	3.26E+10	± 139	1.16E+10	± 6	0.70	0.51	0.36
dpa/s	8.94E-13	± 55	5.19E-13	± 6	0.70	0.83	0.58
Slot EM							
F > 1 MeV	3.97E+08	± 38	3.76E+08	± 10	0.99	0.96	0.95
F > 0.1 MeV	7.56E+08	± 38	7.38E+08	± 13	0.99	0.99	0.98
F < 0.4eV	3.26E+10	± 139	2.56E+10	± 6	0.99	0.80	0.79
dpa/s	8.94E-13	± 55	7.94E-13	± 6	0.99	0.90	0.89

Table H.1 (continued)

	Calculated Value*	Std.%	Adjusted Value	Std. %	Scale Fact.	Adj. Fact.	Adj./ Calc.
Slot EB							
F > 1 MeV	3.97E+08	± 38	5.47E+08	± 10	1.53	0.90	1.38
F > 0.1 MeV	7.56E+08	± 38	1.09E+09	± 13	1.53	0.94	1.44
F < 0.4eV	3.26E+10	± 139	6.20E+10	± 6	1.53	1.25	1.91
dpa/s	8.94E-13	± 55	1.39E-12	± 6	1.53	1.02	1.55
Slot FT							
F > 1 MeV	3.97E+08	± 38	3.26E+08	± 10	0.82	1.00	0.82
F > 0.1 MeV	7.56E+08	± 38	6.37E+08	± 13	0.82	1.02	0.84
F < 0.4eV	3.26E+10	± 139	1.22E+10	± 6	0.82	0.45	0.37
dpa/s	8.94E-13	± 55	5.97E-13	± 6	0.82	0.81	0.67
Slot FM							
F > 1 MeV	3.97E+08	± 38	4.44E+08	± 10	1.17	0.96	1.12
F > 0.1 MeV	7.56E+08	± 38	8.72E+08	± 13	1.17	0.99	1.15
F < 0.4eV	3.26E+10	± 139	2.84E+10	± 6	1.17	0.75	0.87
dpa/s	8.94E-13	± 55	9.22E-13	± 6	1.17	0.88	1.03
Slot FB							
F > 1 MeV	3.97E+08	± 38	6.50E+08	± 10	1.81	0.91	1.64
F > 0.1 MeV	7.56E+08	± 38	1.29E+09	± 13	1.81	0.94	1.71
F < 0.4eV	3.26E+10	± 139	7.40E+10	± 6	1.81	1.26	2.27
dpa/s	8.94E-13	± 55	1.65E-12	± 6	1.81	1.02	1.85

* Units are neutrons . cm^{-2}. s^{-1} for F>1 MeV, F>0.1 MeV, F<0.4 eV, and s^{-1} for dpa rate (dpa/s).

Table H.2 Measured reaction rates, C/M, and A/M ratios, key 4, position 10

Reaction	M*	C/M	A/M
Slot D			
Al-27 (n,a) Na-24 [Bare]	1.102E-18	1.71	1.04
Ti-48 (n,p) Sc-48 [Bare]	4.474E-19	1.53	0.94
Ti-48 (n,p) Sc-48	4.161E-19	1.64	1.01
Cu-63 (n,a) Co-60 [Bare]	6.529E-19	1.57	0.98
Cu-63 (n,a) Co-60	6.119E-19	1.67	1.04
Ti-46 (n,p) Sc-46 [Bare]	9.345E-18	1.54	0.99
Ti-46 (n,p) Sc-C46	8.734E-18	1.65	1.05
Fe-54 (n,p) Mn-54 [Bare]	4.306E-17	1.57	1.05
Fe-54 (n,p) Mn-54	4.485E-17	1.50	1.01
Ti-47 (n,p) Sc-47 [Bare]	1.065E-17	1.33	0.91
Ti-47 (n,p) Sc-47	1.046E-17	1.36	0.93
Fe-58 (n,g) Fe-59 [Bare]	1.143E-14	2.95	0.99
Sc-45 (n,g) Sc-46 [Bare]	2.400E-13	2.97	0.99
Sc-45 (n,g) Sc-46	8.682E-15	2.37	1.05
Slot J			
U-235 (n,f)	6.980E-13	0.56	0.96
Ni-58 (n,p) Co-58 [Bare]	8.540E-17	1.01	0.96
Ni-58 (n,p) Co-58	7.895E-17	1.09	1.03
Co-59 (n,g) Co-60 [Bare]	7.508E-13	1.31	1.04
Co-59 (n,g) Co-60	5.326E-14	0.63	1.15
Slot B			
U-235 (n,f) Ba-140	5.232E-13	0.74	1.11
U-235 (n,f) Zr-95	5.651E-13	0.69	1.02
U-235 (n,f) Ru-103	5.475E-13	0.71	1.06
Slot A			
Ni-58 (n,p) Co-58 [Bare]	1.181E-16	0.73	1.01
Ni-58 (n,p) Co-58	1.169E-16	0.74	1.02
Co-59 (n,g) Co-60 [Bare]	2.261E-12	0.44	1.03
Co-59 (n,g) Co-60	1.507E-13	0.22	1.00

Table H.2 (continued)

Reaction	M*	C/M	A/M
Slot ET			
Ni-58 (n,p) Co-58 [Bare]	5.512E-17	1.57	1.01
Ni-58 (n,p) Co-58	5.574E-17	1.55	1.00
Co-59 (n,g) Co-60 [Bare]	3.133E-13	3.15	1.04
Co-59 (n,g) Co-60	2.489E-14	1.35	1.11
Slot EM			
Ni-58 (n,p) Co-58 [Bare]	7.839E-17	1.10	0.96
Ni-58 (n,p) Co-58	7.191E-17	1.20	1.04
Co-59 (n,g) Co-60 [Bare]	7.171E-13	1.37	1.03
Co-59 (n,g) Co-60	4.878E-14	0.69	1.06
Slot EB			
Ni-58 (n,p) Co-58 [Bare]	1.105E-16	0.78	0.99
Ni-58 (n,p) Co-58	1.054E-16	0.82	1.03
Co-59 (n,g) Co-60 [Bare]	1.756E-12	0.56	1.02
Co-59 (n,g) Co-60	1.145E-13	0.29	1.02
Slot FT			
Ni-58 (n,p) Co-58 [Bare]	6.628E-17	1.31	0.99
Ni-58 (n,p) Co-58	6.428E-17	1.34	1.02
Co-59 (n,g) Co-60 [Bare]	3.170E-13	3.11	1.07
Co-59 (n,g) Co-60	2.940E-14	1.15	1.13
Slot FM			
Ni-58 (n,p) Co-58 [Bare]	9.240E-17	0.94	0.96
Ni-58 (n,p) Co-58	8.599E-17	1.01	1.03
Co-59 (n,g) Co-60 [Bare]	7.844E-13	1.26	1.03
Co-59 (n,g) Co-60	5.774E-14	0.58	1.07
Slot FB			
Ni-58 (n,p) Co-58 [Bare]	1.343E-16	0.64	0.97
Ni-58 (n,p) Co-58	1.240E-16	0.70	1.04
Co-59 (n,g) Co-60 [Bare]	2.105E-12	0.47	1.02
Co-59 (n,g) Co-60	1.332E-13	0.25	1.02

*Reactions per second per atom

Table H.3 Calculated and adjusted neutron group fluxes, key 4, position 10, slot J

Group	Group Upper Energy Boundary* [eV]	Neutron Group Fluence Rate Calculated**	Adjusted**
1	2.000E+07	1.018E+06	8.997E+05
2	1.271E+07	4.031E+06	3.575E+06
3	1.013E+07	1.239E+07	1.102E+07
4	8.072E+06	2.601E+07	2.316E+07
5	6.434E+06	2.306E+07	2.105E+07
6	5.523E+06	2.727E+07	2.533E+07
7	4.742E+06	2.711E+07	2.518E+07
8	4.071E+06	2.205E+07	2.164E+07
9	3.495E+06	2.504E+07	2.473E+07
10	3.000E+06	1.743E+07	1.904E+07
11	2.724E+06	5.955E+07	6.589E+07
12	2.038E+06	1.881E+07	2.083E+07
13	1.850E+06	2.502E+07	2.763E+07
14	1.655E+06	2.406E+07	2.656E+07
15	1.480E+06	3.121E+07	3.438E+07
16	1.282E+06	5.300E+07	5.790E+07
17	1.000E+06	5.657E+07	6.111E+07
18	7.653E+05	1.030E+08	1.106E+08
19	4.704E+05	1.067E+08	1.149E+08
20	2.297E+05	9.266E+07	1.097E+08
21	1.000E+05	1.652E+08	3.942E+08
22	1.202E+04	4.817E+07	1.149E+08
23	6.004E+03	5.000E+07	1.193E+08
24	3.000E+03	1.579E+08	3.768E+08
25	3.911E+02	5.820E+07	1.389E+08
26	1.978E+02	6.196E+07	1.478E+08
27	1.000E+02	9.355E+07	2.232E+08
28	3.817E+01	1.433E+08	3.419E+08
29	1.000E+01	5.581E+07	1.332E+08
30	6.178E+00	8.758E+07	2.090E+08
31	3.000E+00	7.058E+07	1.684E+08
32	1.770E+00	2.343E+08	5.591E+08
33	3.970E-01	4.785E+07	1.142E+08
34	3.300E-01	9.270E+07	2.212E+08
35	2.700E-01	2.704E+08	6.451E+08
36	2.150E-01	9.198E+08	2.195E+09
37	1.620E-01	3.733E+09	4.492E+09
38	1.040E-01	1.174E+10	8.447E+09
39	5.000E-02	1.437E+10	1.034E+10
40	1.000E-02	1.383E+09	9.958E+08
	1.000E-05***		

*Energy in eV
**Group fluxes in neutrons $cm^{-2}. s^{-1}$
***Lower energy boundary of 40th group

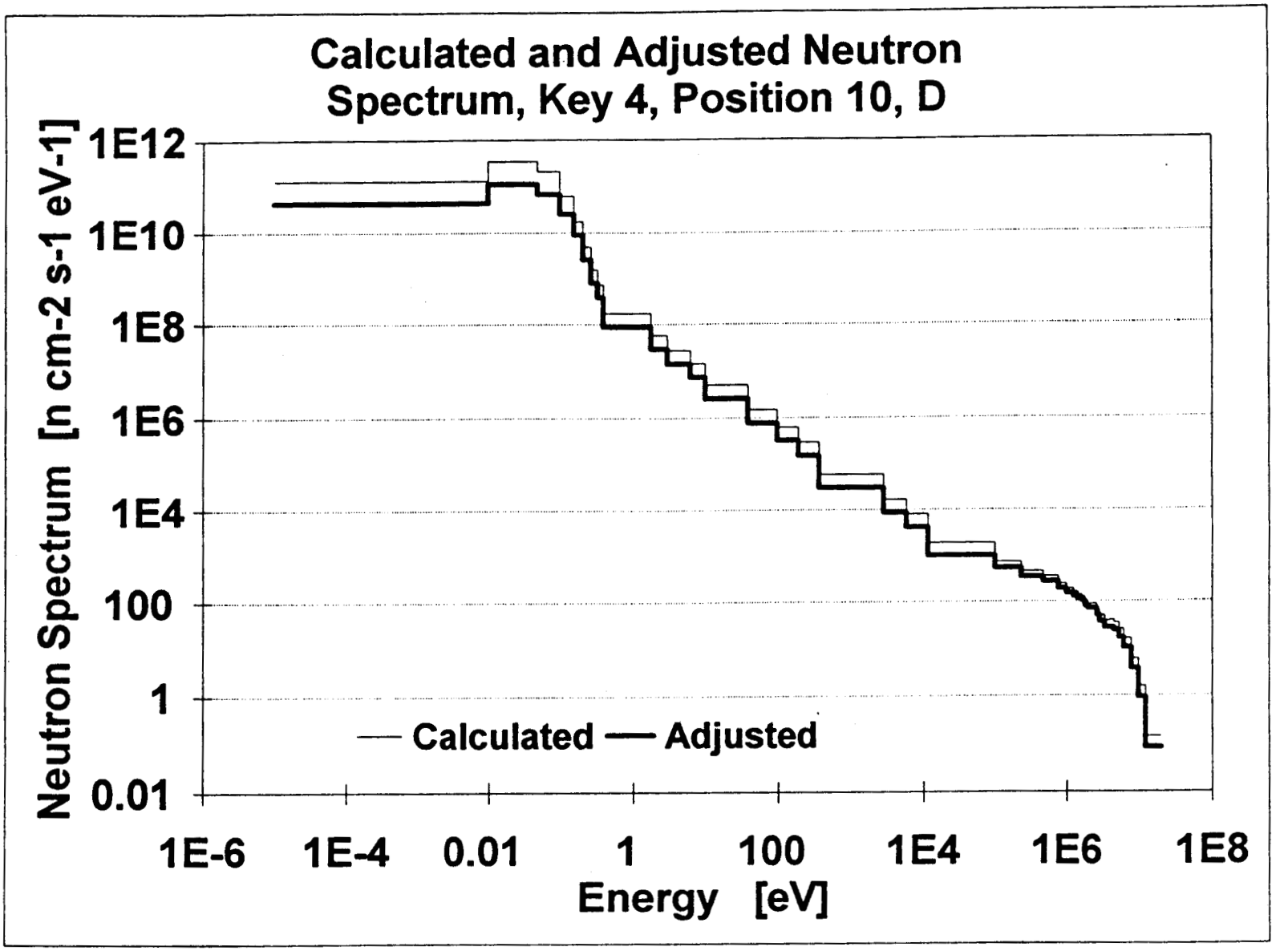

Fig. H.1 Calculated and adjusted neutron spectrum, key 4, position 10, D

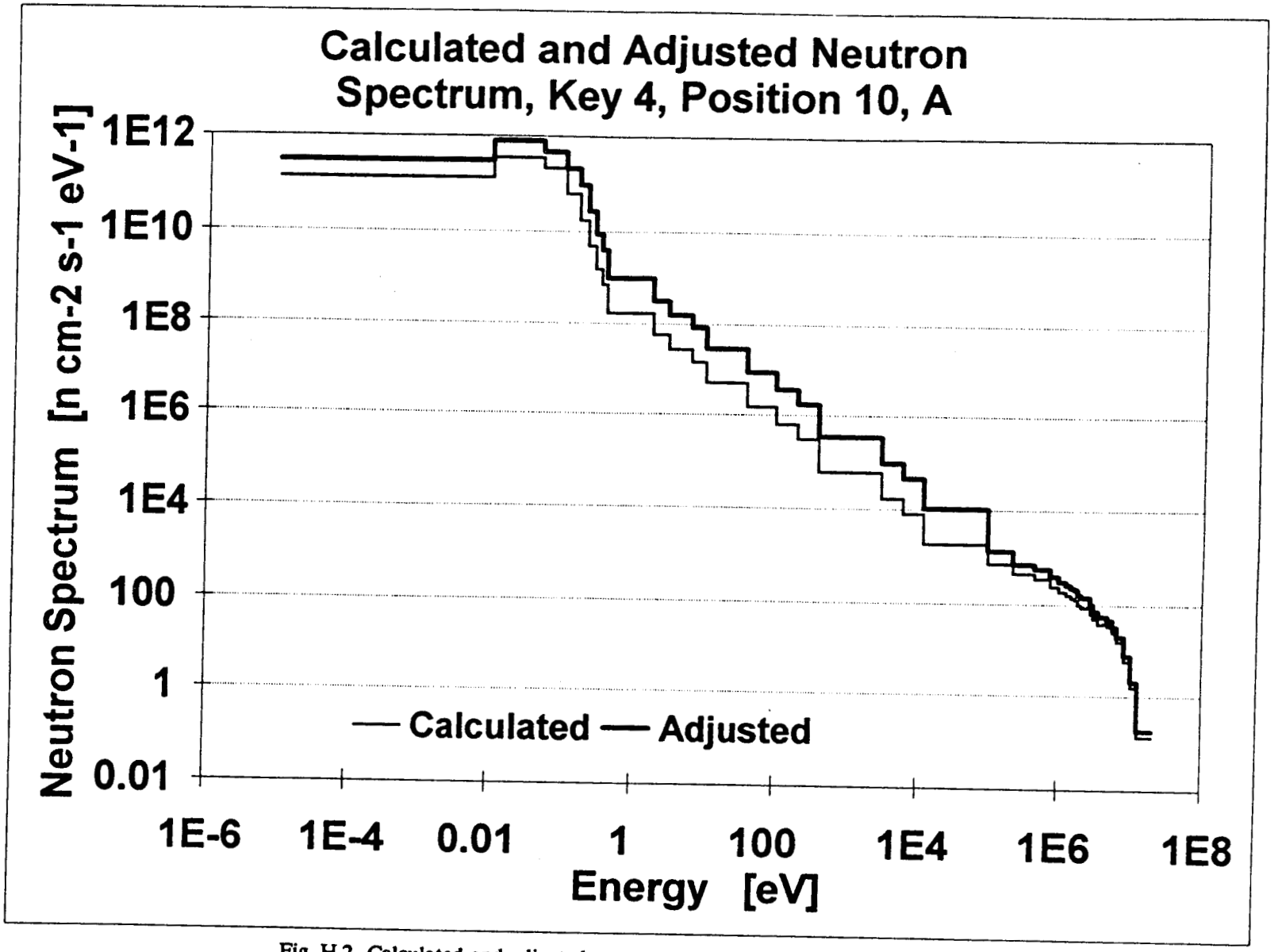

Fig. H.2 Calculated and adjusted neutron spectrum, key 4, position 10, A

APPENDIX I

SCHEMATIC OF DOS3 LOWER SPLIT HALF HOLDER
(PART 2-2 DWG. M-11511-OH-001-E-R1)
SHOWING SLOT NOMENCLATURE AND DOSIMETER LOADING ASSIGNMENT

ORNL-DWG 93M-14907

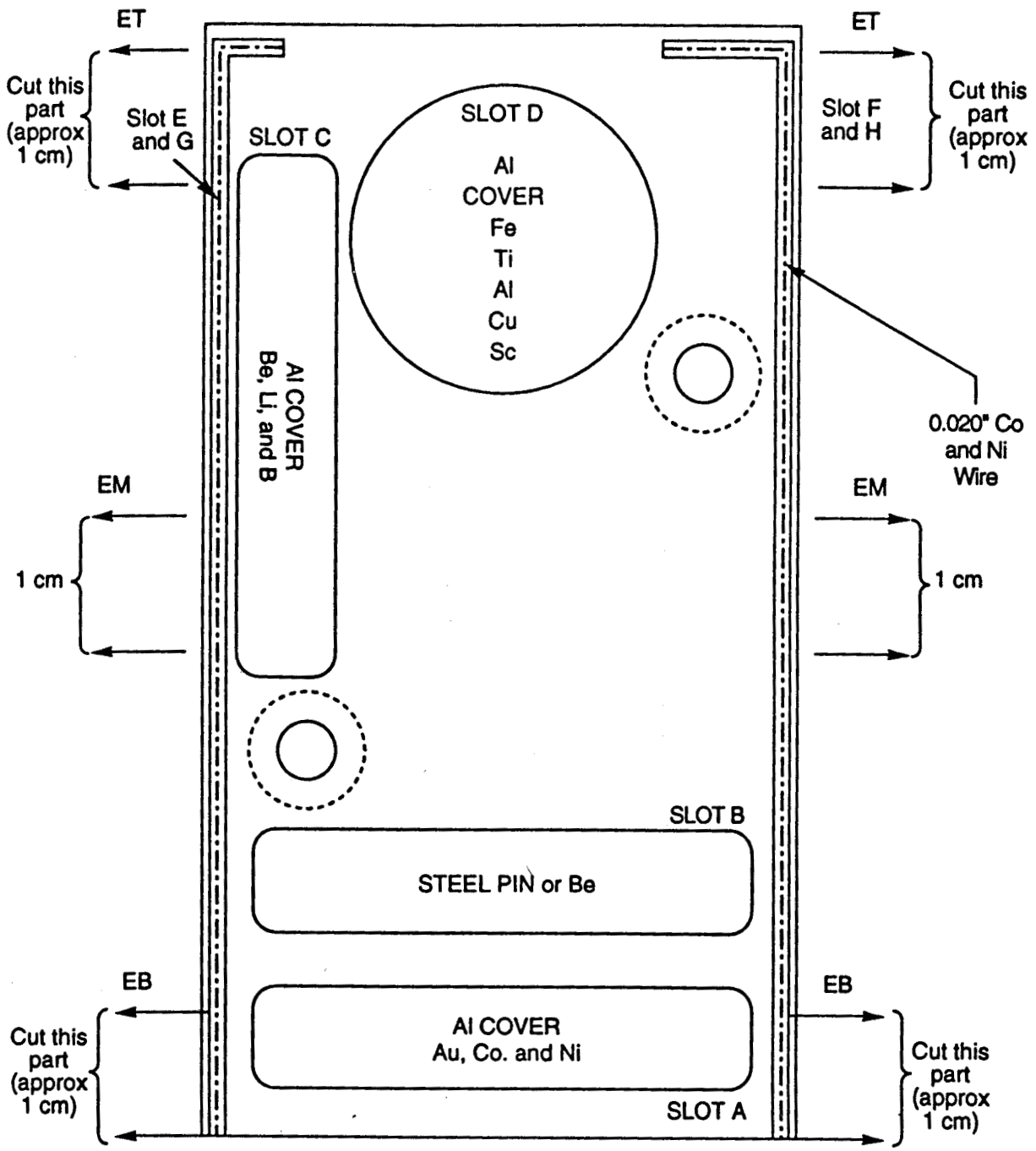

SCHEMATIC OF LOWER SPLIT HALF HOLDER

Fig. I. 1 Schematic of dosimetry capsule with slot locations

INTERNAL DISTRIBUTION

1. C. A. Baldwin
2. B. R. Bass
3. E. E. Bloom
4. J. A. Bucholz
5. R. D. Cheverton
6. W. R. Corwin
7. F. Dyer
8. K. Farrell
9. D. Glasgow
10. F. M. Haggag
11. Dennie Heatherly
12. G. Hirtz
13. R. Hobbs
14. R. L. Huddeleston
15. D. J. Ingersol
16. S. K. Iskander
17-21. F. B. K. Kam
22. L. K. Mansur
23. D. E. McCabe
24. J. G. Merkle
25. R. K. Nanstad
26. J. Pace
27. W. E. Pennell
28. C. E. Pugh
29-33. I. Remec
34-36. C. H. Shappert
37. R. E. Stoller
38. K. Thoms
39. J. A. Wang
40. R. M. Westfall
41. G. E. Whitesides
42. Central Research Library
43. ORNL Y-12 Research Library Document Reference Section
44-45. Laboratory Records Department
46. Laboratory Records, ORNL (RC)
47. ORNL Patent Office

EXTERNAL DISTRIBUTION

48. S. T. Byrne, ABB - Combustion Engineering, Windsor, CR 60695

49. Frank C. Cherney, Section Leader, USNRC, Office of Nuclear Regulatory Research, Mail Stop NL/S 302, Washington, D.C. 20555

50. B. J. Elliott, Nuclear Regulatory Commission, NRR/Div. of Engineering Technology, MS704, Washington, DC 20555

51. A. Fabry, CEN/SCK, Belgium, Reactor Physics Department, Boeretang 200, B-2400MOL, Belgium

52. Dr. Bogdan Glumac, Head, Reactor Physics Division, Reactor Center, Brine Jamova 39, 61111 Ljubljana, Slovenia

53. L. R. Greenwood, Pacific Northwest Laboratories, Mail Stop P7-22, P.O. Box 999, Richland, Washington 99352

54. J. Grundl, National Institute of Standards and Technology, Bldg. 235-A155, Gaithersburg, Maryland 20899

55. J. R. Hawthorne, Materials Engineering Associates, 9700B Martin Luther King, Jr. Highway, Lanham, MD 20706

56. C. A. Hrabal, USNRC, Office of Nuclear Regulatory Research, Mail Stop NL/S 302, Washington, D.C. 20555

57. Matt Hutmaker, NE44 Germantown, U. S. Department of Energy, Washington, D.C. 20585

58. R. E. Johnson, USNRC, Division of Engineering, Mail Stop NL S 314, Washington, D.C. 20555

59. N. P. Kadambi, USNRC, Mail Stop 8 D22, Washington, DC 20555

60. Mike Mayfield, USNRC, Division of Engineering, Mail Stop NL S 217 C, Washington, D.C. 20555

61. Jozef Stefan Institute, Library, Jamova 39, 61 111 Ljubljana, Slovenia

62. Dr. G. P. Marino, USNRC, Mail Stop NLS007, Washington, DC 20555

63. E. D. McGarry, National Institute of Standards and Technology, Bldg. 235-A155, Gaithersburg, Maryland 20899

64. Bill McLaughlin, National Institute of Standards and Technology, Bldg. 235-A155, Gaithersburg, Maryland 20899

65. Warren Minners, USNRC, Office of Nuclear Regulatory Research, Mail Stop NL/S 360, Washington, D.C. 20555

66. Joseph A. Murphy, U. S. Nuclear Regulatory Commission, Mail Stop NLS007, Washington, DC 20555

67. P. E. Norian, U. S. Nuclear Regulatory Commission, Mail Stop NLS314, Washington, DC 20555

68. Brian Oliver, Rockwell International, Rocketdyne Div., 6633 Canoga Ave., Canoga Park, California 91309

69. Frank Ruddy, Westinghouse Science & Technology Center, 1310 Beulah Rd., Bldg. 302, Rm. 201, Pittsburgh, Pennsylvania 15235

70. C. Z. Serpan, Jr., U. S. Nuclear Regulatory Commission, Division of Engineering, Mail Stop NLS217C, Washington, D.C. 20555

71. Al Taboada, USNRC, Division of Engineering, Mail Stop NL S 217 C, Washington, D.C. 20555

72. T. J. Walker, USNRC, Division of Engineering, Mail Stop NL S 217 C, Washington, D.C. 20555

73. John Williams, University of Arizona, Tucson, Arizona 85721

74-80. NRC/RES Division of Engineering, Washington, D.C. 20555

81. Ohio State University, Dept. of Metallurgical Engineering, Columbus, Ohio 43210-1179

82. University of Missouri-Rolla, Dept. of Nuclear Engineering, Rolla, Missouri 65401

83. Office of the Deputy Assistant Manager for Energy, Research, and Development, Department of Energy Oak Ridge Operations (DOE-ORO), P.O. Box 2008, Oak Ridge, Tennessee 37831-6269

84-87. Office of Scientific and Technical Information, P.O. Box 62, Oak Ridge, Tennessee 37831

88-216. Given distribution as shown in category RF (NTIS-10)

NRC FORM 335 (2-89) NRCM 1102, 3201, 3202

U.S. NUCLEAR REGULATORY COMMISSION

BIBLIOGRAPHIC DATA SHEET

(See instructions on the reverse)

1. REPORT NUMBER (Assigned by NRC, Add Vol., Supp., Rev., and Addendum Numbers, if any.)
NUREG/CR-6117
ORNL/TM-12484

2. TITLE AND SUBTITLE
Neutron Spectra at Different High Flux Isotope Reactor (HFIR) Pressure Vessel Surveillance Locations

3. DATE REPORT PUBLISHED

MONTH	YEAR
December	1993

4. FIN OR GRANT NUMBER
L2552

5. AUTHOR(S)
I. Remec,* F. B. Kam

6. TYPE OF REPORT

7. PERIOD COVERED *(Inclusive Dates)*

8. PERFORMING ORGANIZATION – NAME AND ADDRESS *(If NRC, provide Division, Office or Region, U.S. Nuclear Regulatory Commission, and mailing address; if contractor, provide name and mailing address.)*
Oak Ridge National Laboratory
Oak Ridge, TN 37831-6370

*Josef Sefan Institute
Ljubljana, Slovenia

9. SPONSORING ORGANIZATION – NAME AND ADDRESS *(If NRC, type "Same as above"; if contractor, provide NRC Division, Office or Region, U.S. Nuclear Regulatory Commission, and mailing address.)*
Division of Safety Issue Resolution
Office of Nuclear Regulatory Research
U.S. Nuclear Regulatory Commission
Washington, DC 20555-0001

10. SUPPLEMENTARY NOTES

11. ABSTRACT *(200 words or less)*

This project addresses the potential problem of radiation embrittlement of reactor pressure vessel (RPV) supports. Surveillance specimens irradiated at the High Flux Isotope Reactor (HFIR) at relatively low neutron flux levels (about 1.5E+8 $cm^{-2}. s^{-1}$) and low temperature (about 50°C) showed embrittlement more rapidly than expected. Commercial power reactors have similar flux levels and temperatures at the vessel support structures. The purposes of this work are to provide the neutron fluence spectra data that are needed to evaluate previously measured mechanical property changes in the HFIR, to explain the discrepancies in neutron flux levels between the nickel dosimeters and two other dosimeters, neptunium and beryllium, and to address any questions or peculiarities of the HFIR reactor environment.

12. KEY WORDS/DESCRIPTORS *(List words or phrases that will assist researchers in locating the report.)*
neutron spectra
High Flux Isotope Reactor (HFIR)
radiation embrittlement
reactor pressure supports
pressure vessel surveillance

13. AVAILABILITY STATEMENT
unlimited

14. SECURITY CLASSIFICATION
(This Page)
unclassified
(This Report)
unclassified

15. NUMBER OF PAGES

16. PRICE

NRC FORM 335 (2-89)